Iowa State University
Digital Repository

Graduate Theses and Dissertations | Graduate College

2011

Chemical Mechanical Paired Grinding

David Thomas Asplund
Iowa State University

Follow this and additional works at: http://lib.dr.iastate.edu/etd

Part of the Mechanical Engineering Commons

Recommended Citation
Asplund, David Thomas, "Chemical Mechanical Paired Grinding" (2011). *Graduate Theses and Dissertations*. 12233.
http://lib.dr.iastate.edu/etd/12233

This Thesis is brought to you for free and open access by the Graduate College at Iowa State University Digital Repository. It has been accepted for inclusion in Graduate Theses and Dissertations by an authorized administrator of Iowa State University Digital Repository. For more information, please contact digirep@iastate.edu.

Chemical Mechanical Paired Grinding

by

David Asplund

A thesis submitted to the graduate faculty
in partial fulfillment of the requirements for the degree of
MASTER OF SCIENCE

Major: Mechanical Engineering

Program of Study Committee:
Abhijit Chandra, Major Professor
Ashraf Bastawrsos
Gap Kim

Iowa State University
Ames, Iowa
2011

Copyright © David Asplund, 2011. All rights reserved

TABLE OF CONTENTS

LIST OF FIGURES iv

LIST OF TABLES vi

ABSTRACT vii

Chapter 1 Introduction & Literature Review 1
- 1.1. CMP Machine Development 2
  - 1.1.1 First Generation Polishers 3
  - 1.1.2 Second Generations Polishers 4
  - 1.1.3 Third Generation Polishers and Beyond 6

Chapter 2 CMPG Concept and Background 12
- 2.1. Defect Mitigation via Minimization of Maximum Force 13
- 2.2. Effective Planarization via Profile Driven Determination of Force Gradient 14
- 2.3. Robustness via Homogenization 16

Chapter 3 Construction of Prototype CMPG Machine 18
- 3.1. Framework & Supporting Assemblies 18
  - 3.1.1 Machine Frame 18
  - 3.1.2 Upper Stage Frame 19
  - 3.1.3 Vertical Guide Assembly 19
  - 3.1.4 Mounting Table 19
- 3.2. Gimbal Assembly 20
- 3.3. Motorized Assemblies 21
  - 3.3.1 Actuator Assembly 21
  - 3.3.2 Table Motor Assembly 21
  - 3.3.3 Stage Assembly 22
- 3.4. Enclosure and Slurry Dispenser 23
  - 3.4.1 Slurry Dispenser Assembly 23
  - 3.4.2 Enclosure 24
- 3.5. Future Components 24

Chapter 4 Experimental Setup, Procedure, & Testing Methodology 32
- 4.1. Experimental Setup 32
  - 4.1.1 Consumables 32
    - 4.1.1.1 Wafers 32
    - 4.1.1.2 Slurry 33
    - 4.1.1.3 Polishing Wheels 34
- 4.2. Calibration 34
  - 4.2.1 Load Cell Calibration 34
    - 4.2.1.1 Resolution 35
    - 4.2.1.2 Accuracy 35
  - 4.2.2 Vertical Actuator 36
- 4.3. Experimental Procedure 36
- 4.4. Data Analysis Procedure 38

4.4.1 Load Cell Analysis 39
4.4.1.1 Nominal Load Error Bar 40
4.4.2 Material Removal Height 40
4.4.2.1 Removal Depth Error Bars 41
4.4.3 Surface Waviness & Roughness 42
4.4.4 Surface Profile Comparison 43

Chapter 5 Testing Results 51
5.1. Load vs Material Removal Depth 51
5.2. Dwell Time vs Material Removal Depth 52
5.3. 50nm Silica Slurry - Load vs Material Removal Depth 54
5.4. Medium Density Wheel - Load vs Material Removal Depth 56
5.5. Relative Velocity vs Material Removal Depth 58
5.6. Worn Wheel - Load vs Material Removal Depth 59
5.7. Profile Comparison 61
5.7.1 Low Density Wheel Profile Comparison 61
5.7.2 Medium Density Wheel Profile Comparison 62
5.7.3 Dwell Time Profile Comparison 62
5.8. Full Wafer Test 62

Chapter 6 Conclusion 78

Bibliography 80

Appendix 85

ACKNOWLEDGEMENTS 89

LIST OF FIGURES

Figure 1-1 Rotary Polisher 9
Figure 1-2 Multi-wafer Polisher 9
Figure 1-3 Sequential Rotational Polisher 10
Figure 1-4 Linear Polisher 10
Figure 1-5 Orbital Polisher 11
Figure 1-6 Web Polisher 11
Figure 2-1 CMPG Platform 17
Figure 2-2 Surface Profile Comparison of Control Strategies 17
Figure 3-1 Physical Prototype & CAD Rendering of CMPG Machine 25
Figure 3-2 Motion of CMPG Machine 25
Figure 3-3 Machine Frame 26
Figure 3-4 Upper Stage Frame 26
Figure 3-5 Vertical Guide Assembly 27
Figure 3-6 Mounting Table 27
Figure 3-7 Gimbal Assembly 28
Figure 3-8 Actuator Assembly 28
Figure 3-9 Table Motor Assembly 29
Figure 3-10 Stage Assembly 29
Figure 3-11 Slurry Dispenser Assembly 30
Figure 3-12 Enclosure 30
Figure 3-13 Block Diagram of Labview Program Used To Control The Prototype ... 31
Figure 3-14 Front Panel of Labview Program Used To Control The Prototype 31
Figure 4-1 Illustration of 6" Wafer Setup 44
Figure 4-2 Illustration of 1.5" Wafer Setup 44
Figure 4-3 Electrical Noise With Equipment Power Off 45
Figure 4-4 Electrical Noise With Equipment Power On 45
Figure 4-5 Electrical Noise With Equipment Power On Then Off 46
Figure 4-6 Load Cell Calibration 46
Figure 4-7 Vertical Actuator Calibration 47
Figure 4-8 Example Of Load Cell Data From A Test 47
Figure 4-9 Results of Wafer Analyzed using ZYGO 48
Figure 4-10 Low Pass Waviness: Un-Polished Wafer 48
Figure 4-11 Low Pass Waviness: 4mmx1mm Un-Polished Wafer 49
Figure 4-12 Back Plot with 4mmx1mm Area Removed to Demonstrate Area Analyzed for Low Pass Waviness 49
Figure 4-13 High Pass Roughness: 1.41mmx1.06mm Un-Polished Wafer 50
Figure 4-14 Profile of a Vertical Cross Section 50
Figure 5-1 Load vs Material Removal Depth 65
Figure 5-2 Low Pass Waviness: Load vs Material Removal Depth 65
Figure 5-3 High Pass Roughness: Load vs Material Removal Depth 66
Figure 5-4 Dwell Time vs Material Removal Depth 66
Figure 5-5 Low Pass Waviness: Dwell Time vs Material Removal Depth 67

Figure 5-6 High Pass Roughness: Dwell Time vs Material Removal Depth 67
Figure 5-7 50nm Silica Slurry - Load vs Material Removal Depth 68
Figure 5-8 Zygo Results for 50nm Silica Slurry @ 13.6N 68
Figure 5-9 Low Pass Waviness: 50nm Silica Slurry - Load vs Material Removal Depth 69
Figure 5-10 High Pass Roughness: 50nm Silica Slurry - Load vs Material Removal Depth 69
Figure 5-11 Medium Density Wheel - Load vs Material Removal Depth 70
Figure 5-12 Low Pass Waviness: Medium Density Wheel - Load vs Material Removal Depth 70
Figure 5-13 High Pass Roughness: Medium Density Wheel - Load vs Material Removal Depth 71
Figure 5-14 Relative Velocity vs Material Removal Depth 71
Figure 5-15 Low Pass Waviness: Relative Velocity vs Material Removal Depth 72
Figure 5-16 High Pass Roughness: Relative Velocity vs Material Removal Depth 72
Figure 5-17 Worn Pad - Load vs Material Removal Depth 73
Figure 5-18 Low Pass Waviness: Worn Pad - Load vs Material Removal Depth 73
Figure 5-19 High Pass Roughness: Worn Pad - Load vs Material Removal Depth 74
Figure 5-20 Profile Comparison of Load w/ Low Density Wheels 74
Figure 5-21 Profile Comparison of Load w/ Medium Density Wheels 75
Figure 5-22 Profile Comparison of Dwell Time 75
Figure 5-23 Wafer Waviness: Top Down View 76
Figure 5-24 Wafer Waviness: Isometric View 76
Figure 5-25 High Pass Roughness: 6” Polished Wafer 77

LIST OF TABLES

Table 1 Results Data 85

ABSTRACT

Chemical Mechanical Planarization (CMP) is a polishing process that planarizes a surface at both a local and global scale. The multi scale planarization capabilities of CMP are used extensively in the fabrication of Integrated Circuits (IC). Though a relentless reduction of feature scales have driven a continual refinement of the CMP process, defectivity levels remain problematic in current CMP processes.

Chemical Mechanical Paired Grinding is a new planarization method, developed at Iowa State University, designed to provide a marked defect reduction at feasible and economic operational conditions. Proposed is a method of planarization that utilizes insights from the operational principals of polishing and grinding by combining the strengths of fixed abrasive grinding with those of free abrasive polishing while avoiding their drawbacks. Key features of the proposed CMPG method includes: Defect Mitigation via Minimization of Maximum Force, Effective Planarization via Profile Driven Determination of Force Gradient, and Robustness via Homogenization.

Presented in this thesis is a review of past and present CMP machines, the background and conceptual development of CMPG, and the construction and testing of a prototype CMPG machine. The construction of the prototype CMPG machine, built as a proof of concept, is thoroughly documented as it exists at its current juncture of development. A set of tests that parameterize the process parameters and consumables are analyzed. The analysis provides a characterization of the planarization capabilities of the prototype CMPG machine.

CHAPTER 1 INTRODUCTION & LITERATURE REVIEW

Chemical Mechanical Planarization (CMP) is a critical polishing technology used extensively throughout the semiconductor industry. Over $3 billion was spent on CMP equipment and materials in 2008 alone (Moinpour, 2008). The capital expenditures and critical status of CMP stem from the superior planarization it delivers at both a global and local scale. At a local scale, features less than a tenth of a micron will be planarized by CMP with near atomic precision while maintaining a global within wafer uniformity of 6%. Though CMP has known solutions for current and future flatness requirements as laid out by the International Technology Roadmap for Semiconductors (ITRS), surface defects including shattered and continuous scratches remains a problem and requires excessive and costly remedies to prevent abrasive particle agglomeration, excessive particle filtration and extreme operational conditions. The ITRS states that research is required for new planarization methods and materials that reduce defects and overall cost of producing Integrated Circuits (IC) (INTERNATIONAL ROADMAP COMMITTEE, 2010).

Chemical Mechanical Paired Grinding is a new planarization method, developed at Iowa State University, designed to provide a marked defect reduction at feasible and economic operational conditions. The proposed method utilizes insights from the operational principals of polishing and grinding by combining the strengths of fixed abrasive grinding with those of free abrasive polishing while avoiding their drawbacks. Key features of the proposed CMPG method includes:

Defect Mitigation via Minimization of Maximum Force, Effective Planarization via Profile Driven Determination of Force Gradient, and Robustness via Homogenization.

The objective of this thesis is to document the construction of a prototype CMPG machine and investigate its characteristics and performance.

The thesis layout is as follows. A literature review of the current state of the art in CMP machine development is presented in this chapter. An overview of the CMPG concept and background are presented in Chapter 2. Construction of the prototype CMPG machine is presented in Chapter 3. The experimental setup, procedure, and testing methodology are presented in Chapter 4. Detailed examination of the testing results is presented in Chapter 5.

1.1. CMP Machine Development

CMP is a hybrid of chemical etching and free abrasive polishing that smoothes a surface by selectively removing material from the peaks of surface asperities faster than the valleys (Brown, 1987)(LANDIS H, 1992)(Steigerwald J. M., 2000)(Steigerwald J., 1997)(Li, 2007)(Oliver, 2004). The three most important components of this process are: polishing pads, slurry, and abrasive particles suspended in the slurry (though recently systems sans slurry or abrasives have been developed (Velden, 2000)(Kondo S., 2000)). Figure 1-1 shows a standard layout of these components in a simple and familiar rotary design. The pad rotates or translates across the surface of a wafer transporting fresh slurry via internal pores or grooves which also carry abraded surface material away from the work zone. Slurry is dispensed onto the polishing pad in a quantity sufficient to flood the pad so

slurry can spread across the contact interface of the pad and wafer. The slurry is a chemical solution that is tailored to selectively passivate the upper layer of the wafer. Suspended in the slurry are abrasive particles that mechanically abrade material from the passivated layer of the wafer.

CMP was used primarily by the optics industry until the 1980s when IBM optimized the process for use in IC (LANDIS H, 1992). Once optimized, the continual miniaturization of line widths in IC justified the cost of CMP over cheaper alternatives used in semiconductor fabrication. This resulted in a rapid expansion of the demand for CMP products and allowed equipment manufacturers to produce standalone polishers designed to the exacting standards of semiconductor fabrication (Zantye P., 2004).

1.1.1 First Generation Polishers

The first generation of polishers date back to the 60's (Regh J., 1971) and were simple rotary polishers that had a large pad and a single wafer carrier that each rotated about its respective axis. Slurry was deposited near the center of the pad and upstream of the carrier to allow centrifugal force to spread it evenly across the pad. An example of this design can be seen in Figure 1-1 Rotary Polisher. The primary advantage of these systems was their simplicity which provided a low barrier of entry into the nascent field of CMP. Subsequent designs, and even alternative technologies at the time, would reveal that the simplicity of the first generation came with a high Cost Of Ownership (COO). The pads used in the rotary design were relatively large and would generate inconsistent Material Removal Rates (MRR)

after moderate usage. Confronted with an intolerable variation in process parameters, frequent replacement of the pad was required which carried with it additional downtime. The large pads also required the deposition of substantial amounts of slurry to ensure flooding of the entire pad surface. The flooded pad would provide adequate slurry flow to the wafer-pad interface, but would also cause slurry to build up on the leading edge of the carrier resulting in poor slurry utilization (Bibby T., 2000).

1.1.2 Second Generations Polishers

Though CMP was the premier planarization technique, it was also the bottleneck in most semiconductor production lines. The second generation of polishers addressed this by evolving the design of CMP machines to accommodate greater throughputs. One method of increasing throughput that had been investigated long before the advent of CMP (Cronkhite P., 1973) was the simultaneous polishing of numerous wafers on a single polishing pad. Increasing the number of wafers per polishing pad drastically increases the throughput of a system with a negligible increase in consumable costs. The drawing in Figure 1-2 Multi-waf er Polish er(Torbert W., 1990) is of a multi-carrier planarizer equipped with four sub carriers (labeled '24' in the drawing) that each hold a wafer (labeled '26') which mount to one of the four carriers (labeled '18') and are lowered into position against the rotary platen (labeled '14'). The increased throughput of a multi-wafer per pad system does come with a few disadvantages however. There is a chance that a wafer could shatter during the course of polishing, showering jagged

fragments onto the pad effectively destroying every other wafer along with it. The multitude of carriers also complicates pad loading making a uniform pressure distribution difficult if not impossible to achieve if the carriers are loaded asymmetrically. Both of these drawbacks will decrease the actual yield rate below the ideal yield rate of a production line, but will be more than offset by the increased throughput compared to a traditional, single headed polisher.

Another implementation still common in systems today is the use of sequential polishers. The design involves simultaneous processing of a single wafer at each platen of the machine. This type of approach is a natural fit for multi-step CMP techniques. An exploded view of one possible sequential rotational system is shown Figure 1-3 (Somekh, 1999). A common multi-step process for a sequential system would first polish the wafer on a platen with high MRR that removes the bulk of the material, followed by a subsequent polish on a platen optimized for planarization, and finished on a platen with a gentle MRR designed to buff out any superficial defects the first two platens may have created. Multi-step arrangements of this kind would require careful process control to ensure each step completes in approximately the same amount time or the slowest step will create a bottleneck the others. There is also the concern that a defect in one of the pads would destroy multiple wafers before an outgoing wafer could be examined. This adds the additional complication of figuring out which pad is defective once a defect has been identified. Downtime may also be an issue in sequential systems that employ a multi-step process since a failure of any one tool will shut down operation across the entire machine.

1.1.3 Third Generation Polishers and Beyond

The innovations made in previous generations focused on increasing throughput with slight progress made in process control. However, increasingly stringent planarization goals began to tax the ability of process engineers to generate acceptable yield levels with existing equipment. With a sufficient level of throughput achieved from previous advancements, the third generation of polishers focused on refining the more subtle aspects of the CMP process. Various innovative implementations were devised that each provided their own unique advantage in controlling process parameters while maintaining or exceeding productivity levels established by previous generations.

The linear polisher works like a belt sander by placing the pad in tension between two rollers and pressing the wafer against it. A linear polisher uses novel pad architecture that allows CMP polishing pad materials to be used in the construction of a flexible belt that can be drawn linearly across the wafer at very high and uniform speeds. Figure 1-4 is a representation of a continuous belt linear polisher. In this system the slurry is applied upstream of the wafer. The wafer is held against the pad above a rigid platen which may contain a fluid bearing capable of controlling the pressure distribution across the wafer face (Pant A., 1998). Superior MRR uniformity is achieved when the wafer is held with low down force and allowed to rotate gently within the carrier. An alternate implementation of the linear polisher uses a reciprocating belt rather than a continuous belt in concert with lateral motion of the carrier that effectively creates orbital motion between the pad and the wafer (Krusell W., 2002). Linear polishers are particularly useful at oxide CMP but

due to an incompatibility with multi platen systems lack the flexibility to perform multi step CMP process, like Cu CMP(Dyer, 2005).

Orbital polishers are similar to traditional polishers except for the platen which has exchanged rotational motion for orbital motion about the carrier head. This subtle, but important, distinction allows the orbital polisher to polish at similar or higher relative speeds, with greater MRR uniformity, and with a smaller tool profile (occupies less factory floor space) than its traditional counterpart. A platen that orbits the carrier has the advantages of reduced susceptibility to run-out, easier pad to replacement, and the unique ability to apply slurry directly to the wafer which greatly increases slurry utilization. The slurry is fed up through holes in the platen that are aligned with holes in the pad that allow the slurry both ingress into the pad and access across the interface via a pattern of flow facilitating grooves in the pad. Care must be taken to prevent these grooves from creating helical wear patterns on the wafer (this is often accomplished by adding an arbitrary motion to the orbiter). Figure 1-5 is an example of an orbital polisher that orbits its platen about a rotating carrier head. Alternate, but equally viable, implementations of an orbiting polisher have the carrier orbiting atop a large rotary platen (Shendon, 1999), have a carrier orbiting atop a linear polisher (Adams J., 2002), and have both the carrier and the platen performing orbiting motion (Lee K., 2001).

Web polishers utilize a pad that is advanced from a roll.. Since the pad remains stationary relative motion is produced exclusively by the carrier which rotates and translates producing an orbital motion. Greater control of the MRR is capable when carrier motion is carefully controlled to maintain equal velocities

across all points on the wafer. This control can be further enhanced in systems that eschew rotational motion for a pneumatic interface that allows local pressure control of the wafer face (Tucker, 2004). A drawing of a web polisher is shown in Figure 1-6. The significant advantage of web polishers comes from the incremental advancement of fresh pad material to the wafer face. This is especially useful for pad materials that wear out quickly and would otherwise cause intolerable downtime from the pad replacements. Though slurries are commonly used in this design, there are equally common variants of web polishers that contain an abrasive embedded within the pad itself (Goetz, 2001)(Shon-Roy, 2000). Web tools hold a distinct advantage over other designs in tool utilization claiming continuous production times of up to a week before it needs to be re-qualified (Bonner B., 2008).

Each CMP method has been developed for a specific issue. The first generation CMP machines use a simple design to provide adequate process control, albeit at high cost of ownership. The second generation CMP machines sacrifice efficiency and simplicity for greater productivity. The third generation CMP machines regain some of the efficiency lost in the second generation as well as expanding process controls at the cost of greater complexity. Though each generation has been a step forward for IC fabrication, none of the methods developed have focused on the reduction of defects. CMPG is the first method designed specifically to reduce defects at economic operating conditions.

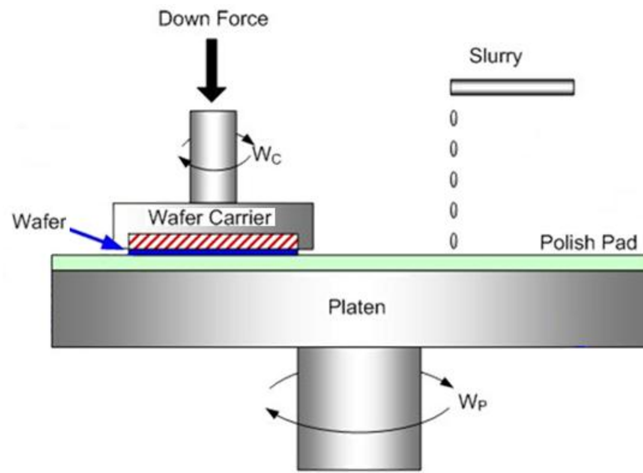

Figure 1-1 Rotary Polisher

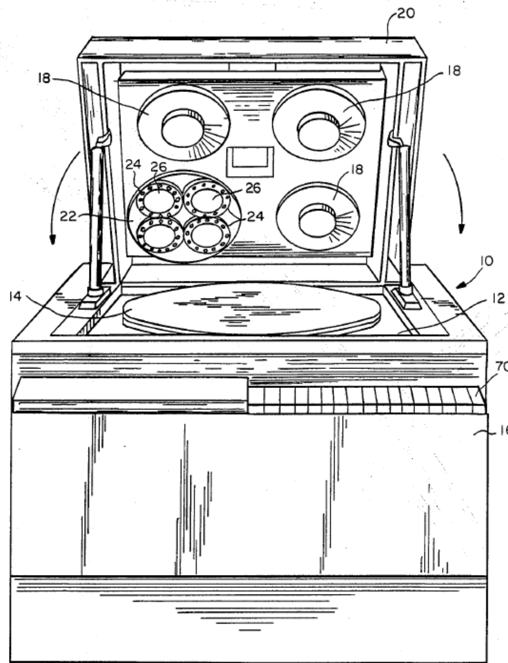

Figure 1-2 Multi-wafer Polisher

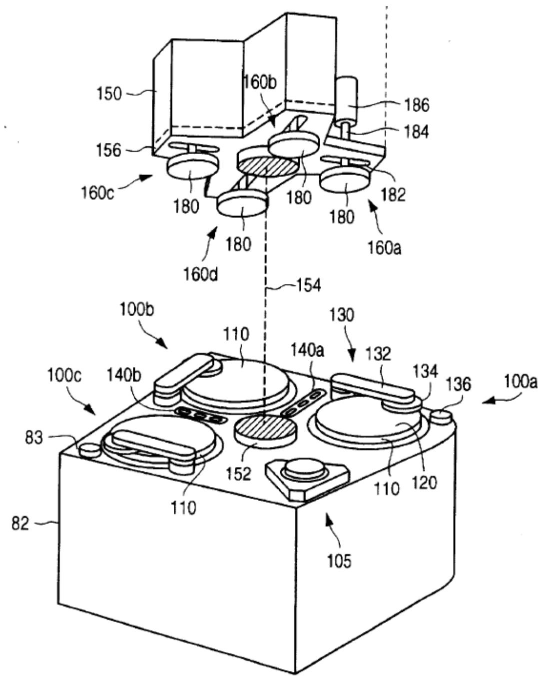

Figure 1-3 Sequential Rotational Polisher

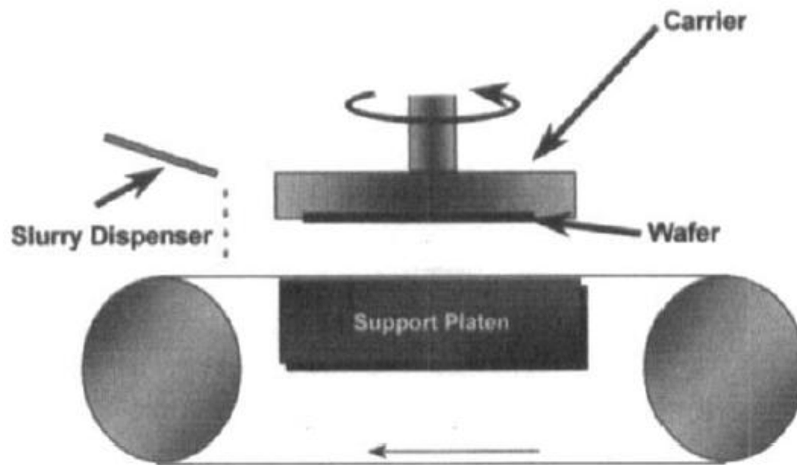

Figure 1-4 Linear Polisher

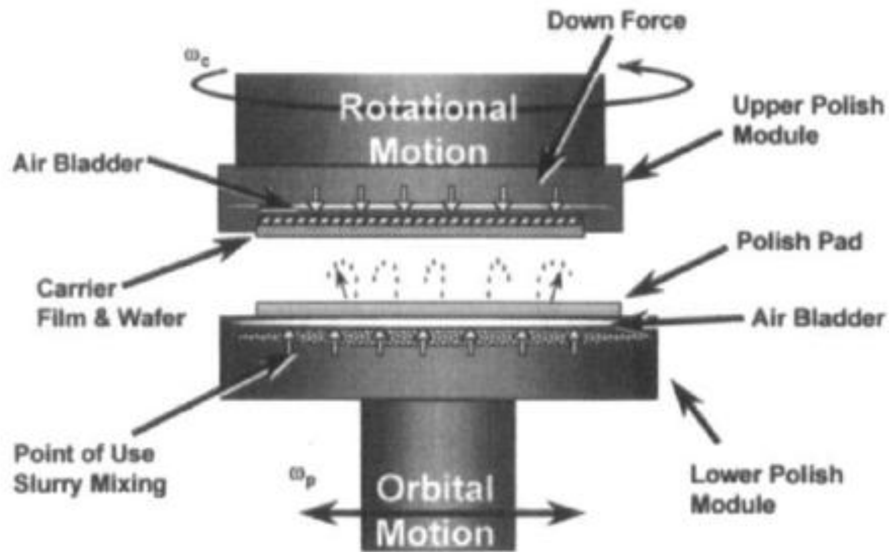

Figure 1-5 Orbital Polisher

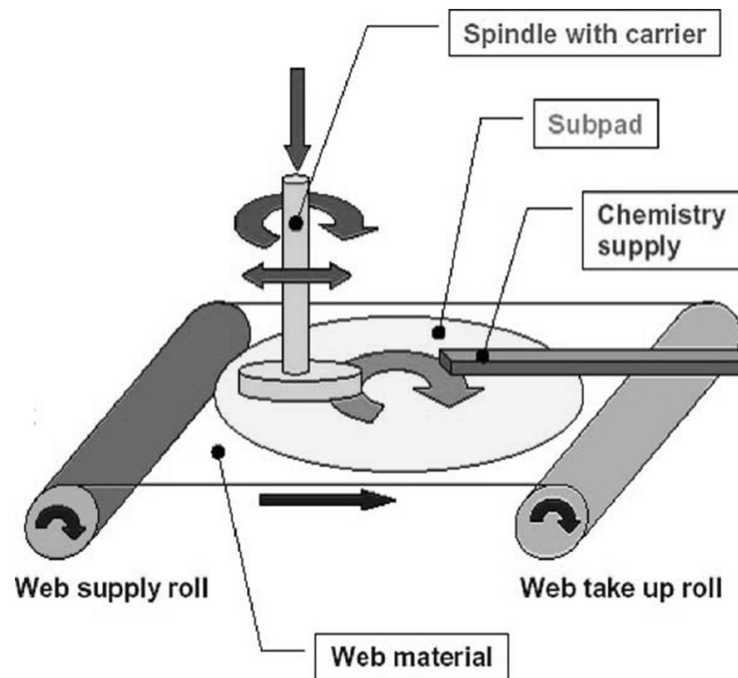

Figure 1-6 Web Polisher

CHAPTER 2 CMPG CONCEPT AND BACKGROUND

CMP is expensive both in terms of upfront capital, costing millions of dollars for a single CMP machine, and cost of operation due to use of consumables like pads and slurry which occupied 11% of the budget for all materials related to semiconductor manufacturing in 2006 (Moinpour, 2008). Due to progressively shrinking feature sizes which are currently as small as 16nm, CMP is also mired by defectivity concerns at a multiplicity of length scales. Though reliability of the CMP process remains a primary goal, meeting the year over year goal of a 29% reduction of the cost-per-function has the semiconductor industry attempting to reduce defectivity levels from all possible angles (INTERNATIONAL ROADMAP COMMITTEE, 2010).

CMPG utilizes insights from the operational principals of polishing and grinding by combining the strengths of fixed abrasive grinding with those of free abrasive polishing to provide a marked defect reduction at feasible and economic operational conditions. Figure 2-1 outlines the goals of the synergistic combination of platforms into a single CMPG platform. Key features of the proposed CMPG method includes: Defect Mitigation via Minimization of Maximum Force, Effective Planarization via Profile Driven Determination of Force Gradient, and Robustness via Homogenization. These features are physically implemented via a counter-gimbaled base and high frequency on-demand pulsation of paired grinding wheels.

2.1. Defect Mitigation via Minimization of Maximum Force

Grinding has historically been a less expensive operation to implement than polishing. Though there are examples grinders attempting to parlay this economic advantage into the CMP process (Yoshio, 2000), commercial CMP machines rely exclusively on polishing due to the pre-requisite levels of roughness and planarization expected in IC fabrication (Bastawros, 2003). The primary distinction between polishing and grinding is the stiffness of the polishing media used (Li, 2007). Polishers use elastic media that sever bonds on a molecular level ejecting nanometer sized clusters (Steigerwald J., 1997). Conversely, grinders have rigid media that propagate cracks through a work piece abrading micron sized particles from the lattice of the substrate. The cracks created during grinding leave subsurface damage that can sap a surface of 70% of its strength. Modeling efforts by Chandra et al (Chandra A., 2000)(Qu W., 2000) have identified the maximum force/grit as a key variable of subsurface damage and minimization of force/grit as a productive avenue of subsurface damage mitigation. Processes like ductile regime grinding have long been known to induce plastic chip removal in brittle materials via low force/grit levels (Bifano T., 1991), but the high machine stiffness ductile machine grinders require makes them very expensive and still don't limit subsurface damage to levels acceptable in IC fabrication.

CMPG capitalizes on the insights gleaned from the investigation into minimization of force/grit by applying the insights to errant particles that plague polishing processes with surface damaging micro-scratches (Chandra, 2004). This is accomplished by incorporating the wafer platen into a gimbal and replacing the

polishing *pad* with a pair of diametrically opposed polishing *wheels*. Large particles that get trapped between the wafer and one of the polishing wheels will produce a net torque that rotates the gimbal away from the offending particle effectively minimizing the force it can transfer to the surface. By optimizing the dynamics of the gimbal to respond to the acute forces created by errant particles, a defect-mitigating maximum-force-minimization is realized at low cost since implementing the gimbal does not require a stiff frame.

2.2. Effective Planarization via Profile Driven Determination of Force Gradient

A wide range of studies on the CMP process have been reported. For example, previous work investigated MRR (Komanduri, 1996)(Evans C.J., 2003) and the effects of the pad and slurry properties (Bastawros A. F., 2002) on the process. Wang et al. (Wang, 2005) introduced the effects of pad wear and its evolution in an effort to extend the pad response model developed by Bastawros et al. (Bastawros A. F., 2002), and Luo and Dornfeld (Luo, 2003) to assess the propensity of scratching. It is also well known that the slurry gradually evolves with time, with and even without continued processing, and that there is a strong correlation between slurry evolution and the generation of scratches on the finished wafers. In the physics and colloidal chemistry communities a variety of modeling efforts as well as experimental investigations (Lin, , 1989,)(Lin, 1990) of slurry agglomeration have been reported. There also exists a wide body of literature where the interactions between mechanical and chemical evolutions of slurry properties have been investigated (Komulski, 2001) (Che, 2005). Recently, Saka et al (Saka, 2010) have also investigated the roles of pad hardness and friction coefficient on scratching.

Scratches are currently a major source of yield deterioration since current CMP processes can be expected to produce around 40 critical scratches per wafer (INTERNATIONAL ROADMAP COMMITTEE, 2010). Understanding the root causes of scratches and eliminating them will provide a boost to yield.

Utilizing insights from such modeling activities have to the development of control algorithms that predict the optimum process parameters to apply to a specific location on a wafer depending on the surface profile at that location. The control algorithms can reduce variations in step height (Kadavasal M., 2005) or scratch propensity (Chandra A., 2008). To employ these algorithms however, a process must be able to apply zonal control since the optimal parameters will vary depending on the surface profile located within a die. Figure 2-2 Surface Profile Comparison of Control Strategies is a graph of the theoretical difference in step height an effective control strategy can have on step height. The large polishing pads used in conventional CMP have very limited zonal control and are better suited to providing uniform conditions across an entire wafer. CMPG however, calls for the use of polishing wheels, which are in contact with a fraction of the wafer at any time, that are capable of high frequency on-demand pulsation, which controls the force applied by the wheels to the wafer, enabling an unprecedented level of zonal control in a CMP process. The zonal control combined with the control algorithm allows the CMPG to use profile driven determination of force gradient.

2.3. Robustness via Homogenization

An advantage of conventional CMP is it can maintain a uniform set of process parameters across a large surface area. Though this advantage can be seen as a disadvantage when optimal conditions vary across the surface of a wafer as is the case during over-polish, the resultant suboptimal surface profile created by the uniformity still falls within satisfactory limits of planarization. However, when optimal conditions across an entire wafer are exactly the same , as is often the case after a film that is equal in thickness across the entirety of a wafer needs to be removed, uniformity must be maintained to planarize a surface down to its target profile.

The process parameters on a rotary CMP machine aren't actually uniform at any instant during planarization since the relative velocity and pressure will vary depending on the location from the center of the wafer. The wafer is rotated however, and the rotation will create a homogenizing effect on the average process parameters applied to any point on a wafer. Linear polishers, for example, apply a true uniform velocity field across a wafer but they also have pressure variations at the leading and trailing edges. This is ameliorated by rotating the wafer within its carrier which homogenizes the average conditions seen across the wafer. It is essential to the robustness of a process that a specific set of process parameters can be selected from a large range of possible values and be applied with a repeatable and reliable uniformity to a wafer

CMPG utilizes the insight that robustness via homogenization is the economical and effective method applying uniform conditions across the entirety of a wafer. CMPG realizes this by inducing rotation about two orthogonal axes.

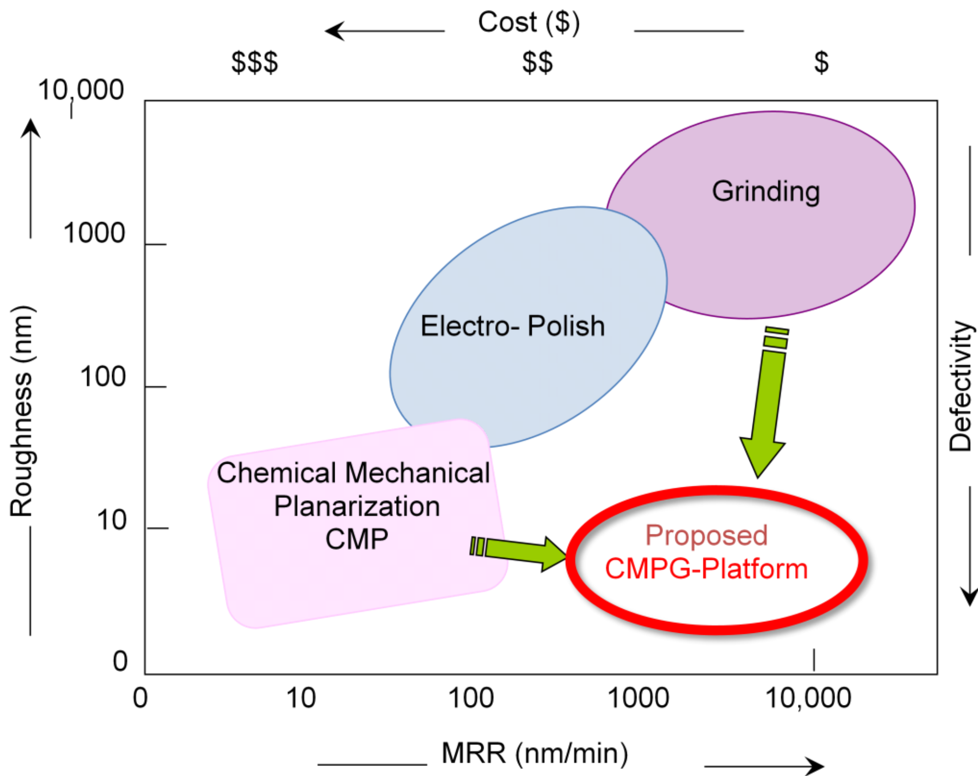

Figure 2-1 CMPG Platform

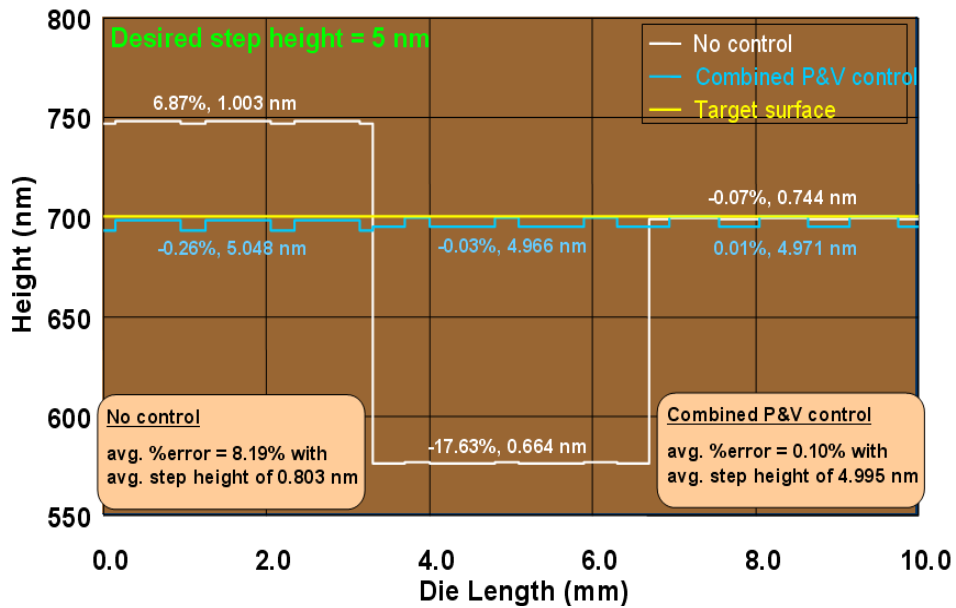

Figure 2-2 Surface Profile Comparison of Control Strategies

CHAPTER 3 CONSTRUCTION OF PROTOTYPE CMPG MACHINE

The three key features of CMPG require a unique combination of untested machine design. To prove this design was feasible a prototype was constructed as a proof of concept. This chapter documents the construction of the prototype with an explanation of critical assemblies and control systems. The prototype and its CAD rendering can be seen in Figure 3-1 Physical Prototype & CAD Rendering. Figure 3-2 is an illustration of the motion of the core components of the CMPG machine. Construction of the prototype CMPG machine began in 2007 and has taken place entirely within the laboratories at Black Engineering of Iowa State University.

3.1. Framework & Supporting Assemblies

3.1.1 Machine Frame

Construction of the prototype began with the Machine Frame. The Machine Frame provides a rigid base that supports all other components in the assembly. The use of 2x2 square steel tubing welded together to form a cube that provides a base of satisfactory stiffness. In addition to the twelve segments that comprise the cube, there are four segments of cross bracing that provide additional stiffness but serve primarily as the mounting location of most other components. Welded to the bottom two cross bracings are four legs that affix to the Mounting Table. An engineering drawing of the Machine Frame can be seen in Figure 3-3 Machine Frame.

3.1.2 Upper Stage Frame

The Upper Stage Frame is a sturdy mount for the Lateral Stage while facilitating smooth vertical translation. It holds the Lateral Stage between the two squared tubes with a five inch gap and below the row of Stage Mounting Plates. The frame can be moved up and down via an Actuator Bolting Plate that is welded to the center Stage Mounting Plate. The Actuator Bolting Plate bolts to a Vertical Actuator that lifts and lowers the Upper Stage Frame and everything mounted to it. The four Linear Bearings located at either end of the square tubes spaced 28.44" apart ensures a smooth vertical motion by coupling to four Vertical Guides. An engineering drawing of the Upper Stage Assembly can be seen in Figure 3-4.

3.1.3 Vertical Guide Assembly

The Vertical Guide Assembly is a guide for the Upper Stage Frame. The guides ensure the Upper Stage Frame and all other parts mounted to it do not drift laterally when lifted or lowered or imparted with any lateral displacement force. There are four guides, each with a vertically oriented stainless steel rod that couple to the four linear bearings of the Upper Stage Frame. Figure 3-5 is an engineering drawing of the Vertical Guide Assembly.

3.1.4 Mounting Table

The Mounting Table is itself mounted to the Machine Frame. The Mounting Table has four legs welded to the bottom of it. These four legs are inserted into the four receiving legs welded to the bottom of the Machine Frame. Once inserted, a series of pre-drilled holes present in the legs of both the frame and the table allow a

mounting pin to be inserted through each matching leg set. Once a pin has been inserted into all four sets the Mounting Table is securely fastened in place. The Mounting Table is the mounting platform for the Gimbal Assembly. A drawing of the Mounting Table can be seen in Figure 3-6. The hole in the middle of the table allows the Table Motor to enter from beneath and couple to the Gimbal Table mounted above.

3.2. Gimbal Assembly

The Gimbal Assembly is mounted to the Mounting Table. The Gimbal Assembly contains the gimbal mechanism which holds the wafer during polishing. The gimbal is designed to rotate when the polishing wheels apply a net torque, thus balancing the nominal load beneath each of the polishing wheels. The assembly mounts to the Mounting Table via a Thrust Bearing. The thrust bearing allows the entire assembly to rotate and is mounted to the bottom of the Gimbal Table. The Gimbal Table has a broached keyway that couples to the Table Motor. Bolted to the top the Gimbal Table are two Gimbal Legs. The Gimbal Legs couple to the Gimbal Ring which is the first component of the actual gimbal mechanism. The Gimbal Ring is coupled to the Gimbal legs via a Collared Bolt inserted through a Plastic Bushing. The Gimbal Ring is in turn coupled to the Platen, which is the disc the wafer is secured to during polishing. A Collared Bolt and Plastic Bushing are also used to couple the Gimbal Ring to the Platen. The Collared Bolt and Plastic Bushing are item 5 and 4 respectively as seen in Detail A and Detail B of Figure 3-7. There are also four sets of shocks coupled to the Platen. The shocks control the rotational dynamics of the gimbal mechanism.

3.3. Motorized Assemblies

3.3.1 Actuator Assembly

The Actuator Assembly contains the Vertical Actuator which is an in-line actuator with an 8" stroke and NEMA 23 stepper motor from Ultra Motion. The Vertical Actuator lifts and lowers the Upper Stage Frame. The assembly is located atop the Machine Frame. It mounts to the frame via four U-Bolts that tighten against the Actuator Mounting Plate. The Vertical Actuator is inserted through a Plastic Spacer. Since the Vertical Actuator would sit too close to the Upper Stage Frame if mounted directly to the Actuator Mounting Plate, the Plastic Spacer allows the actuator to utilize its full range of motion by elevating it 10".

The Vertical Actuator is driven by a 'PDO 5580 Step Motor Driver' from Applied Motion Products. The driver receives control signals from a host computer running Labview. Labview is used as a virtual instrument which has back end code, called a Block Diagram which can be seen in Figure 3-13, and a Front Panel which contains a graphical user interface an operator can use to send a specific set of command instructions. The top left block of the Front Panel seen in Figure 3-14 is used to command the Vertical Actuator.

3.3.2 Table Motor Assembly

The Table Motor Assembly contains the Table Motor which is a 154W brushless motor from MCG. The Table Motor couples to the Gimbal Table via a broached keyway. The Table Motor is used to rotate the Gimbal Assembly at a specified velocity or to hold a commanded position. The motor is secured in place

via a Table Motor Plate and two Table Motor Brackets. The Table Motor Plate is secured to the four legs welded to the bottom of the Machine Frame. The Table Motor Assembly can be seen in Figure 3-9. Note that the Table Motor has a 5:1 reducer mounted to it in its current configuration. It's the reducer that protrudes up through the Mounting Table and couples to the Gimbal Table.

The Table Motor is driven using a 'Xenus XTL' amplifier from Copley Controls. The amplifier is sent control signals from Labview which an operator can command using the bottom right block of the Front Panel in Figure 3-14.

3.3.3 Stage Assembly

The Stage Assembly mounts to the underside of the Upper Stage Frame. The Stage Assembly contains the Lateral Stage, Load Cells, Wheel Motors, and Polishing Wheels.

The Lateral Stage is a 30" two carriage bi-slide powered by a NEMA 34 motor from Velmex. The carriages, annotated as item 2 in Detail B of Figure 3-10, are located symmetrically about the middle of the rail and always move an equal and opposite distance when the rail rotates. The Lateral Stage is driven by a 'VXM Stepping Motor Controller' from Velmex. The controller is commanded via the bottom left block of the Front Panel in Figure 3-14.

Mounted to the carriages of the Lateral Stage are the Load Cells which are single point bending beam 20 kg capacity load cells from Loadstar Sensors. The Load Cells and Load Cell Mounting Bracket are annotated as item 5 and 4 respectively in Figure 3-10. The Load Cells transduce the load applied to the

polishing wheels into a measureable signal recorded by the data acquisition system. Readings from the Load Cell are automatically saved though they can also be viewed in real time via the top right block of the Front Panel in Figure 3-14.

Mounted to the Bottom of the Load Cell is the Wheel Motor Bracket and Wheel Motor. The Wheel Motors are 481W brushless motors from MCG. Attached to the shaft of each Wheel Motor is an Arbor that holds the Polishing Wheel. The Arbor is designed to reduce the dead zone between the wheels as much as possible. The dead zone is a consequence of a pair of wheels that meet in the center of a wafer but cannot actually polish directly at the center. The Wheel motor is annotated as item 3 in Figure 3-10.

3.4. Enclosure and Slurry Dispenser

3.4.1 Slurry Dispenser Assembly

The Slurry Dispenser Assembly mounts to the top cross bracing of the Machine Frame. The Slurry Dispenser Assembly contains the Slurry Dispenser. The Slurry Dispenser reserves all necessary slurry required for polishing and dispenses it at an appropriately metered rate. The dispenser is bolted to a Dispenser Mounting Plate. The Dispenser Mounting Plate is connected to four U-Bolts that are secured to the Machine Frame. The Slurry Dispenser has a plastic tube that leads from the nozzle of the dispenser to the screw hole of the Motor Bracket that is positioned directly above the Polishing Wheels. There are two Slurry Dispenser Assemblies, one for each Polishing Wheel. The dispenser is metered via

a needle valve and a solenoid. The Slurry Dispenser Assembly can be seen in Figure 3-11.

3.4.2 Enclosure

The Enclosure is not part of the CMPG machine but it is required to safely perform tests when using slurry. Though slurry is a necessary part of CMPG, it is potentially hazardous if not disposed of properly. The Enclosure has a floor made of HDPE and has channels that run down into the center of the Enclosure. At the center of the floor is a floor drain that is attached to a tube that runs out the side of the enclosure and into a floor drain located within the Laboratory. The Enclosure has two walls and two doors that allow access to the machine. The walls and doors are made of Lexan. The floor boards that run along the bottom of the Enclosure are also made of HDPE.

3.5. Future Components

At the time of this thesis' writing, the prototype is lacking components that would fully utilize the three key features of CMPG. Despite the absence of polishing wheels capable of high frequency pulsation and a gimbal with customizable dynamics, testing of the prototype in its current form has significant data to offer. Though testing has been performed constantly throughout the development cycle to ensure functionality of components as they are added, the tests evaluated in this thesis represent a thorough evaluation of the prototype and its capabilities at its current development juncture. Results will be used directly in the future development of prototype construction and modeling efforts.

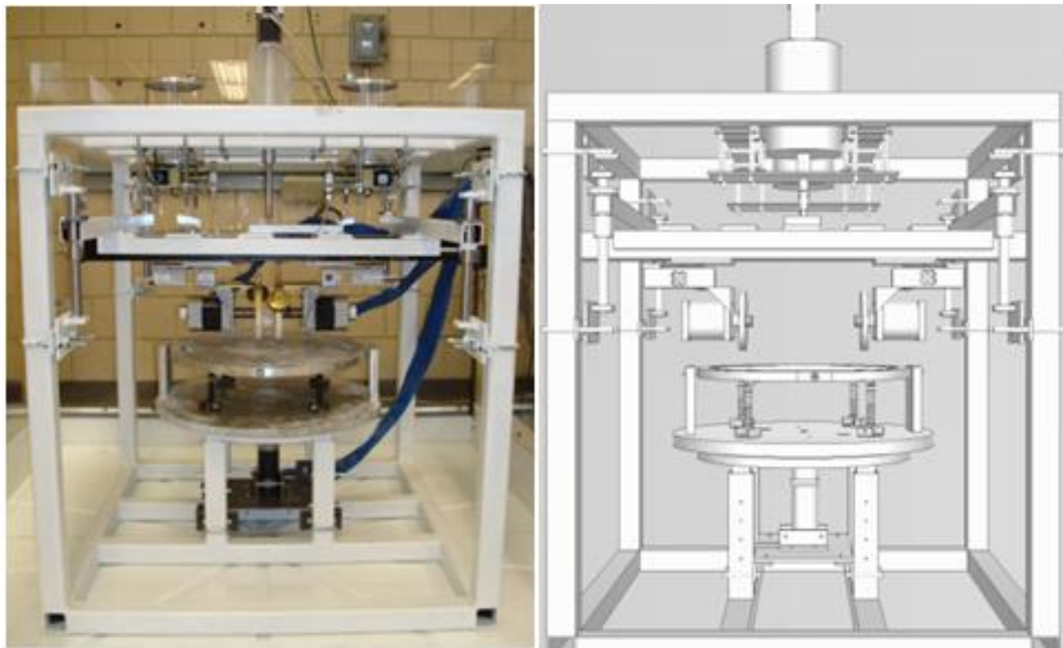

Figure 3-1 Physical Prototype & CAD Rendering of CMPG Machine

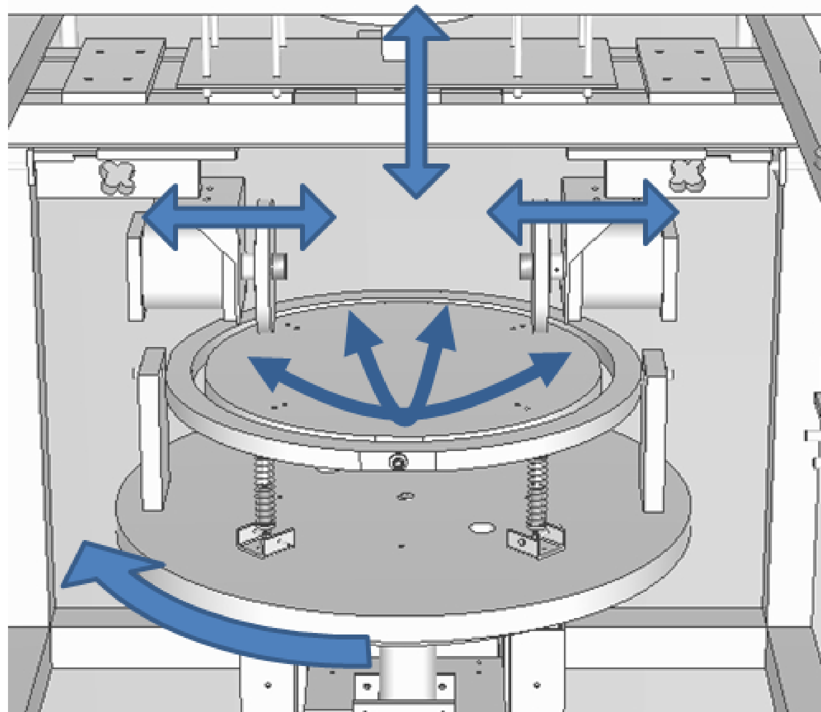

Figure 3-2 Motion of CMPG Machine

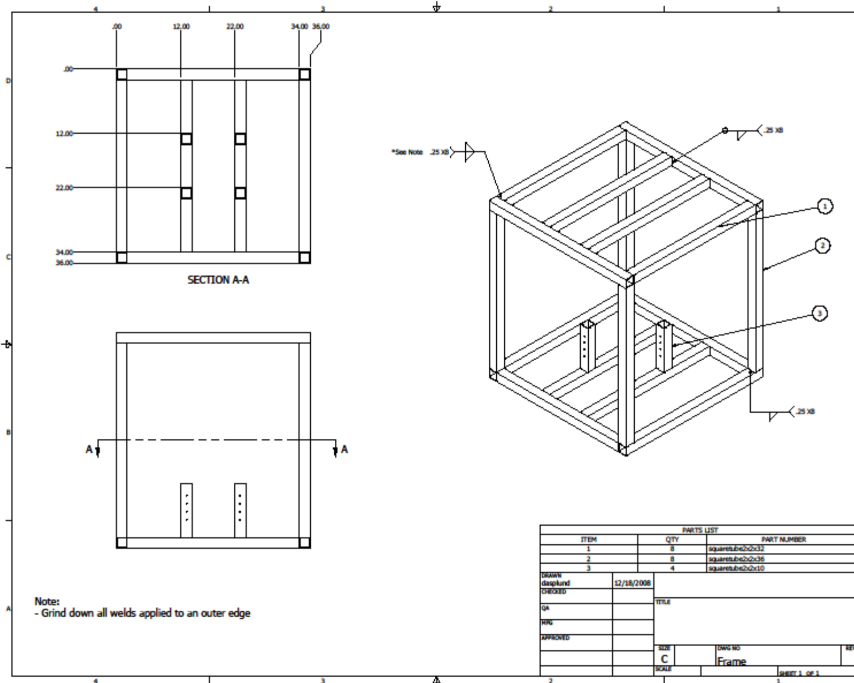

Figure 3-3 Machine Frame

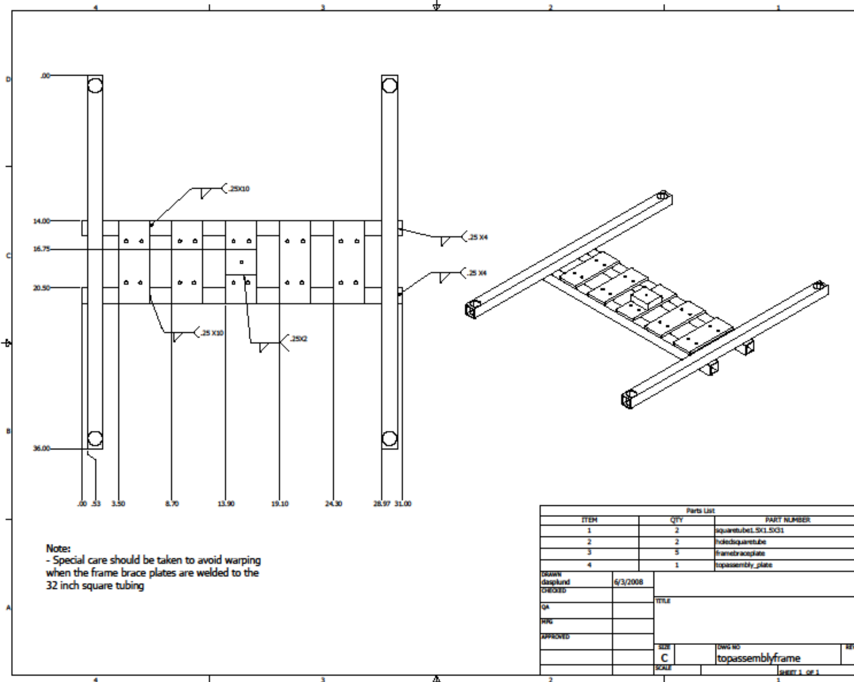

Figure 3-4 Upper Stage Frame

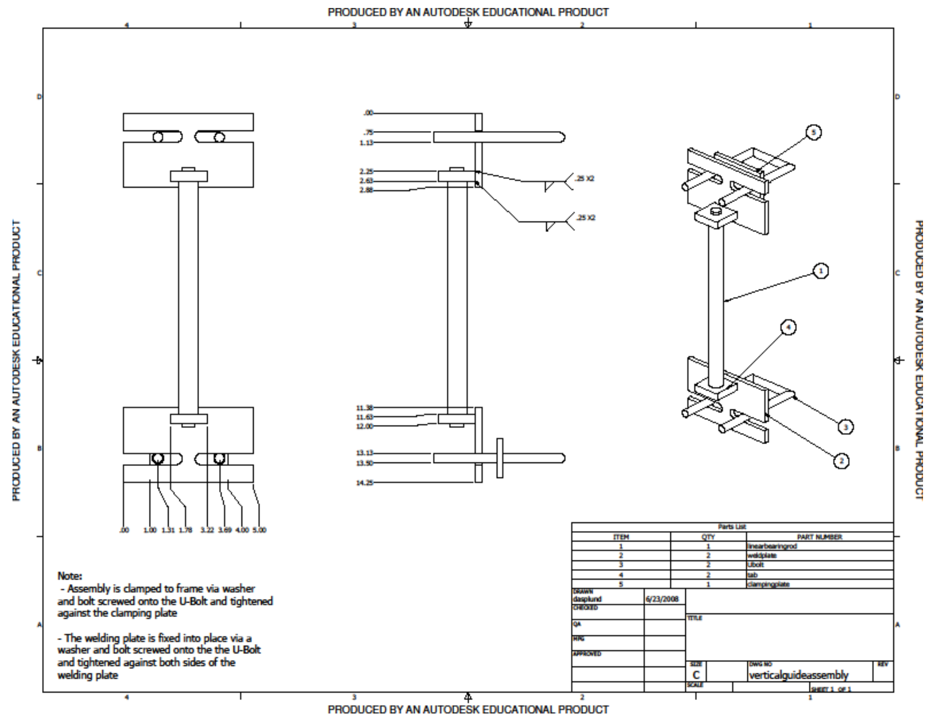

Figure 3-5 Vertical Guide Assembly

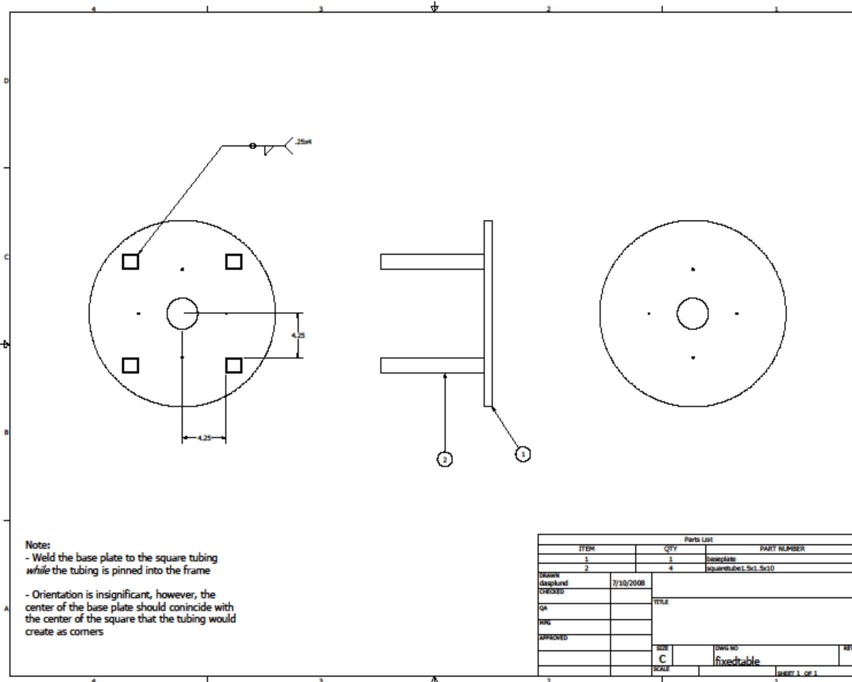

Figure 3-6 Mounting Table

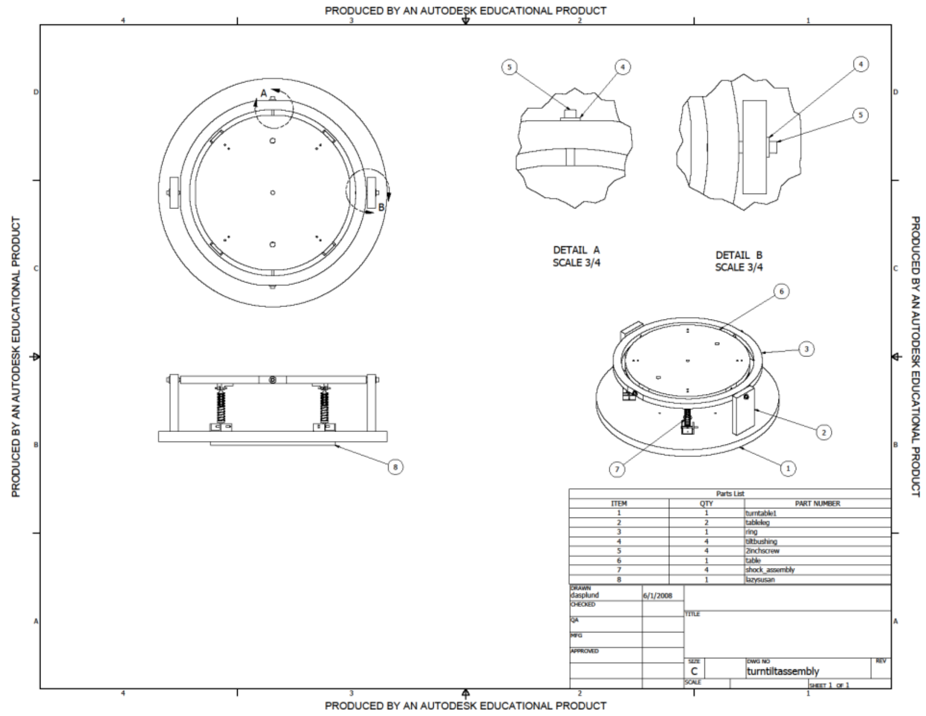

Figure 3-7 Gimbal Assembly

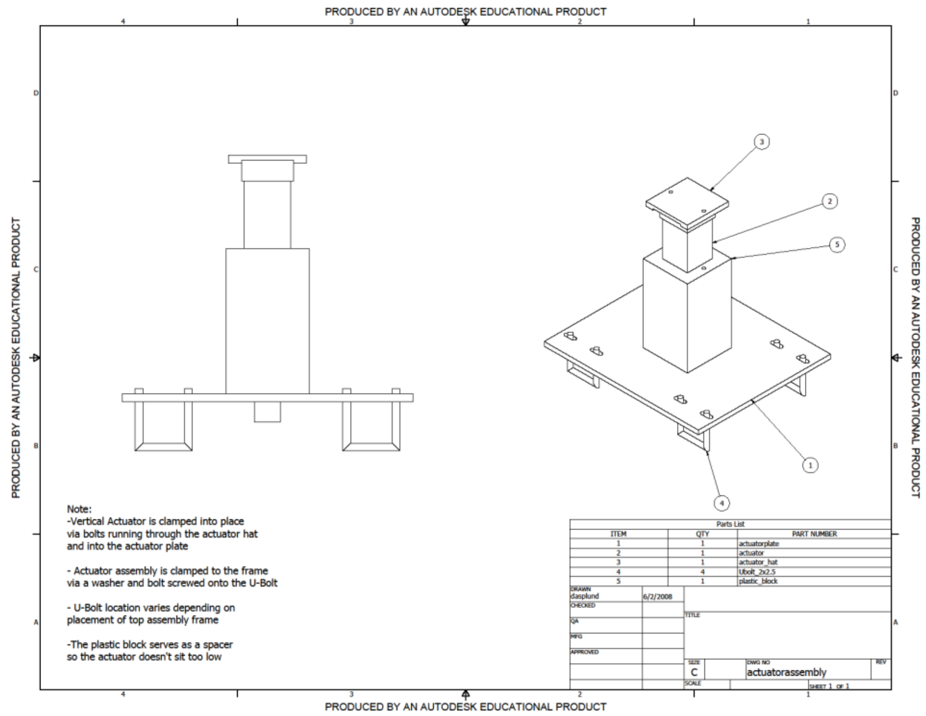

Figure 3-8 Actuator Assembly

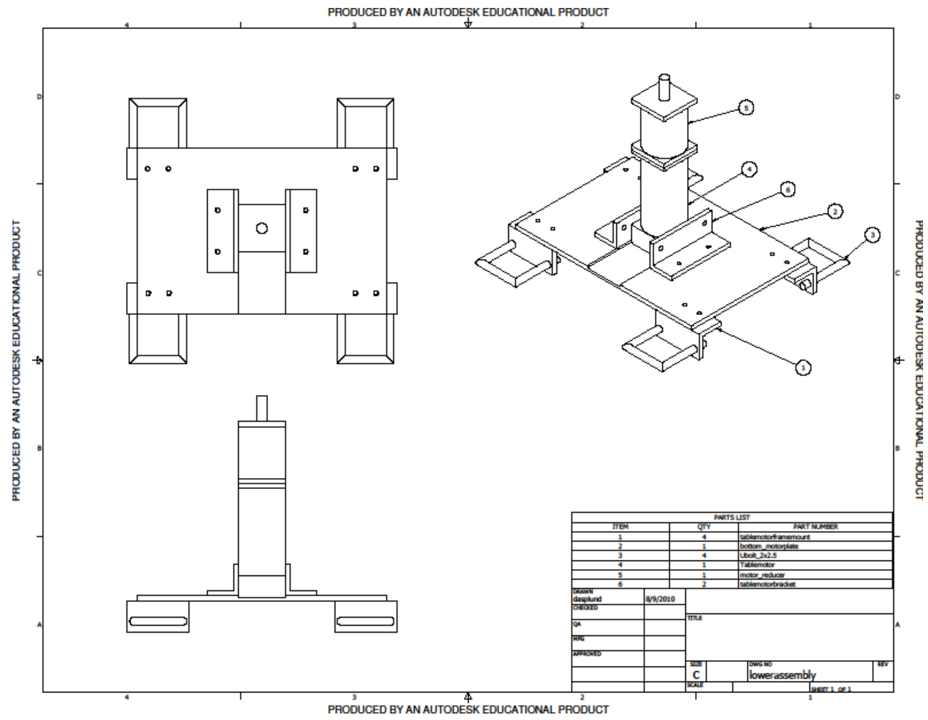

Figure 3-9 Table Motor Assembly

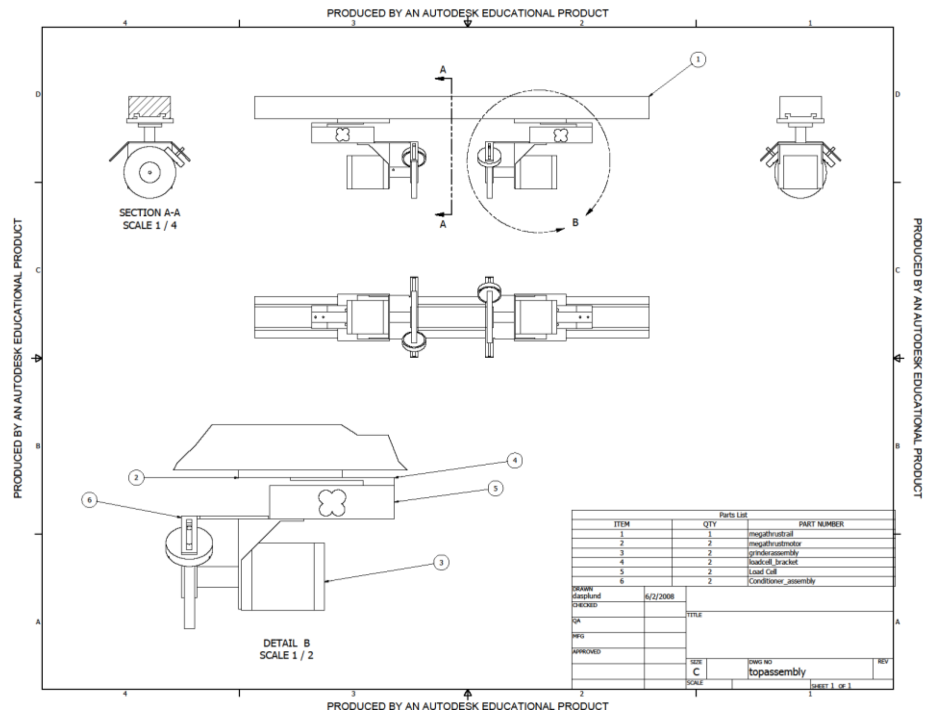

Figure 3-10 Stage Assembly

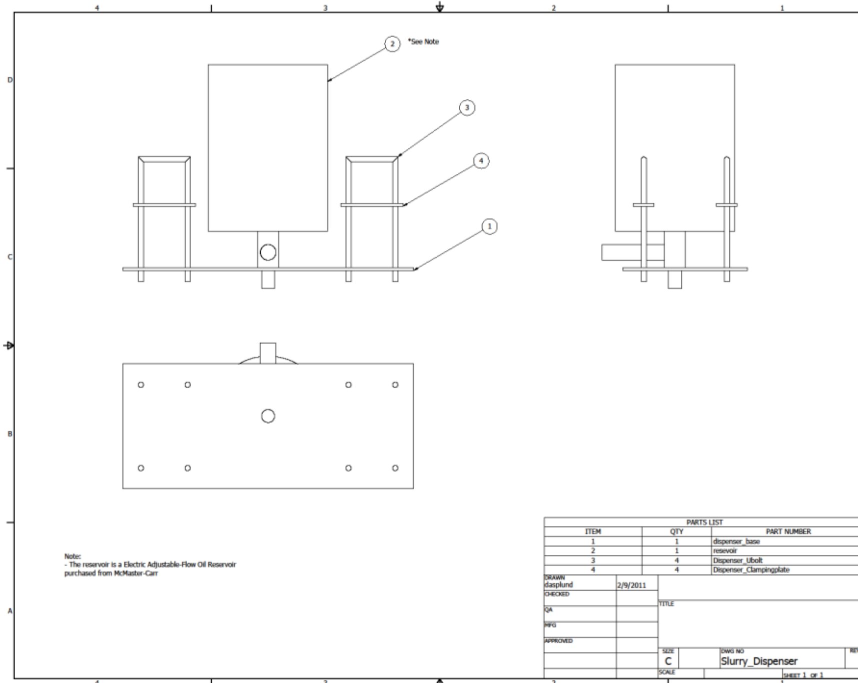

Figure 3-11 Slurry Dispenser Assembly

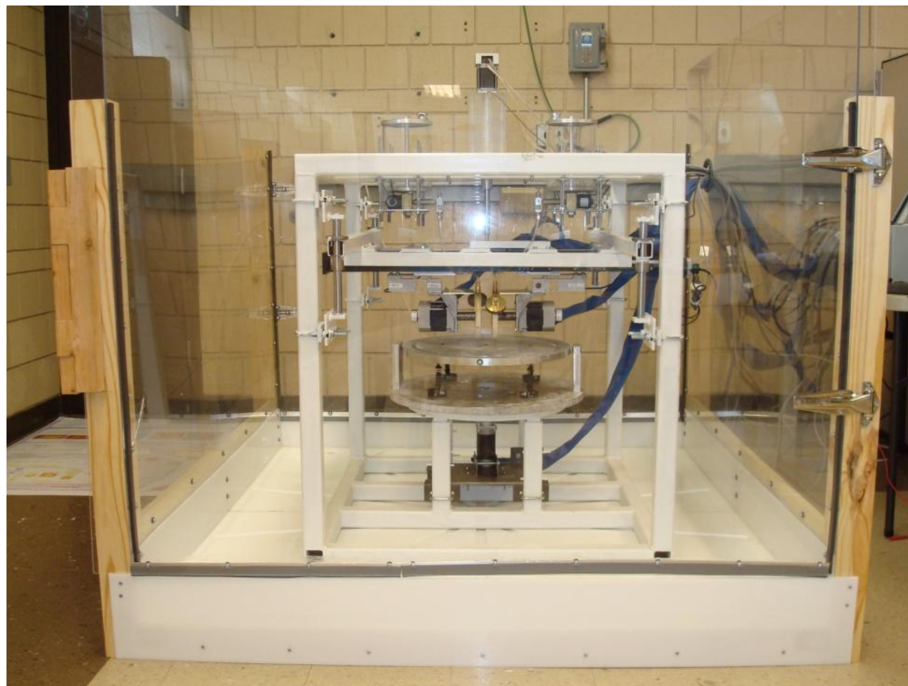

Figure 3-12 Enclosure

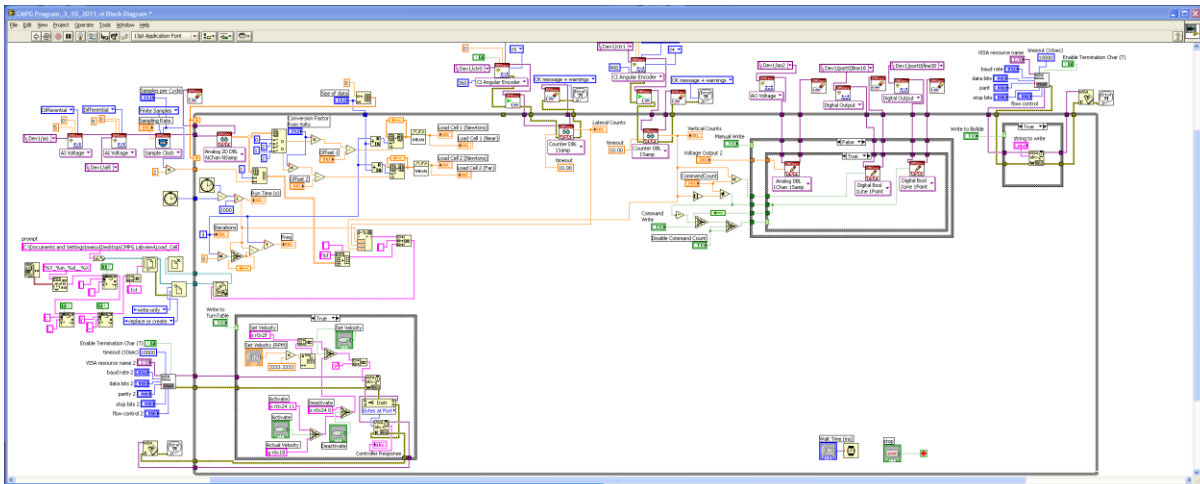

Figure 3-13 Block Diagram of Labview Program Used To Control The Prototype

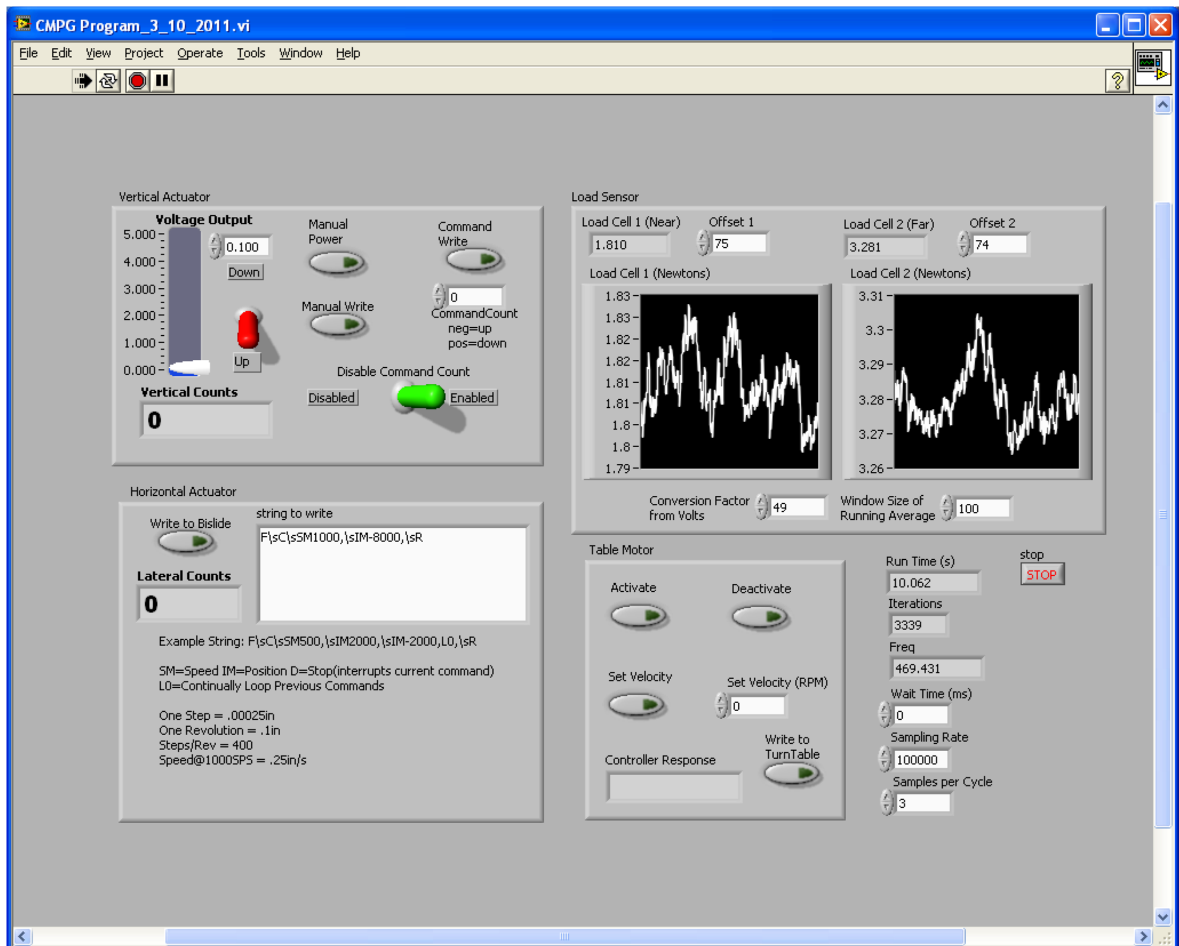

Figure 3-14 Front Panel of Labview Program Used To Control The Prototype

CHAPTER 4 EXPERIMENTAL SETUP, PROCEDURE, & TESTING METHODOLOGY

4.1. Experimental Setup

An experimental parameterization of consumables and process parameters is performed to determine the capabilities of the prototype. The consumables used are aluminum wafers, soft and hard polishing wheels, and high and low MRR slurries. The process parameters varied across tests are the relative velocity between the wheel and the wafer, the nominal load between the wheel and the wafer, the dwell time of a wheel on the testing region of a wafer. An additional test evaluating the effect of previously used polishing wheels is also performed.

4.1.1 Consumables

4.1.1.1 Wafers

The wafers are made of 6061 aluminum that has been machined into either 1.5” or 6” diameter discs. The aluminum wafers have been pre-polished on one side by the supplier. All test polishing is performed on the side that has been pre-polished. The pre-polished aluminum has very low surface roughness at short wavelengths. The global planarity of the pre-polished surface is poor, showing a significantly high level of waviness at longer wavelengths. The waviness and roughness of the pre-polish is quantified in Section 4.4.3. In the tests examined in this thesis there is only one test that uses a 6” wafer. All other tests use a pair of 1.5” wafers. Figure 4-1 Illustration of 6" Wafer Setup is an illustration of the setup

for a 6" wafer. In this configuration the wheels may start at the outer edge or the middle of the wafer and slowly move laterally towards or away from each other. The platen rotates in the 6” configuration. The polish is completed when the wheels meet at the center or reach the edge of the wafer. The entire wafer is polished in this configuration. Figure 4-2 is the setup for 1.5" wafers. Two wafers are polished in this configuration. The left wheel would start at the inner or outer edge of the left wafer and the right wheel would start at the inner or outer edge of the right wafer. The wheels would then move laterally toward or away from each other while the polishing wheels rotate but the platen remains stationary. The polish is complete when each wheel meets the other side of its respective wafer. Only a channel through the middle of the wafer is polished in this configuration. In either configuration the wafers are secured to the platen using a high stiffness double sided tape.

4.1.1.2 Slurry

Most test runs use highly aggressive slurry that contains alumina particles one micron in diameter. The high Material Removal Rate (MRR) of the alumina slurry produces a surface topography that can be interpreted through the background noise inherent in every test. In all tests using the alumina slurry the slurry is diluted from with DI in an 8:1 ratio of DI to slurry. Low MRR slurry containing .05 micron diameter silica particles is used as a point of comparison in a few of the test runs. The silica slurry is used is not diluted. All slurries are mixed vigorously before use to ensure a homogenous mixture. All slurries used are purchased from Eminess.

4.1.1.3 Polishing Wheels

The polishing wheels are made of an impregnated felt and are purchased from Spartan Felts. The wheels are 5" in diameter and of either a low or medium density. The wheels have a .5" arbor hole in the center of the wheel for mounting of the wheel to the arbor. Most tests use the low density polishing wheels, though a run of tests are made using the medium density wheels as a point of comparison. The wheels are always soaked in DI water for 24 hours before a test. All test runs begin with fresh polishing wheels with the exception of the test run that purposely uses ‘worn’ polishing wheels as a point of comparison.

4.2. Calibration

4.2.1 Load Cell Calibration

Calibration of the load cells is twofold. First a base level of electrical noise is established to determine the minimum resolution a reading can be taken at. The second aspect of calibration uses a 200 gram weight to establish overall accuracy of the load cells.

The yellow and green lines running through each of the load cell charts are running averages of the data points for cell 1 and 2 respectively. A running average of 100 data points is used in all instances a running average is presented. All tests had a sampling rate of 400 Hertz so the running average would reflect all data gathered in the last quarter second.

4.2.1.1 Resolution

The active component of the load cells transduce load via a resistive mechanism, essentially a strain gauge mounted to the top of the load cell. The active component is not completely shielded from electrical interference and components like the polishing motors will alter the resolution of the load cells when power is flowing through them. Figure 4-3 shows a chart of the readings collected from the load cells when none of electrical components are powered on. Figure 4-4 is a chart of the load cells after all electrical components are powered on but not engaged (meaning they have power flowing through them but have not been commanded to move). It is clear from visual inspection that load cell readings are noticeably less precise when other compnents are active. Specifically the data from Figure 4-3 has a standard deviation of 0.079 and 0.096 for load cell 1 and 2 respectively while the data from Figure 4-4 has a standard deviation 1.733 and 0.698 for load cell 1 and 2 respectively. It's unclear why load cell 1 is noisier than 2 but the effect on resolution is drastic. Figure 4-5 is a chart of load cell 1 and 2 when the power is turned off halfway through the test.

4.2.1.2 Accuracy

The accuracy of the load cells are gauged using a 200 gram weight placed on top of each polishing wheel after the wheels have been mounted to the motor. The weight is placed on the wheel to simulate the loading that would occur during a test. Figure 4-6 shows a chart of the load cells when the 200 gram weight was placed first on the wheel connected to cell 2 then removed and placed on wheel of cell 1. The test was performed while all other electrical components were off. The mean value

recorded by the load cells while the weight was on the wheel compared to the values when it was off shows a difference of 1.92N and 1.90N for cell 1 and 2 respectively. Since a 200 gram weight is the equivalent of 1.96N load cells 1 and 2 appear to be off by 2% and 3% respectively.

4.2.2 Vertical Actuator

Before a test could begin the Vertical Actuator needs calibration. This is required since the displacement of the Vertical Actuator determines the nominal load applied to the wafer by the polishing wheels. To ensure the correct load is applied during a test the wheels are positioned over the center of the wafers and lowered slowly down until the load cells indicate the wheels are pressing against the wafer with the desired load. Once the desired load is reached the Vertical Actuator is raised a standard number of counts (an encoder attached to the Vertical Actuator is wired into the host computer and displayed on the Front Panel), usually 100 counts, and then held there until the test starts. Once the test starts the Vertical Actuator can be lowered back down the pre-determined number of counts to return to the desired load. Figure 4-7 is a chart of the Vertical Actuator being calibrated by moving it in increments to see what load will occur at a specific displacement. The Vertical Actuator needs to be calibrated every time the wheels are taken off and put back on.

4.3. Experimental Procedure

Step 1: Soak the Wheels

Every test used either low or medium density polishing wheels. Regardless of the wheel type used, all wheels were soaked for a minimum of 24 hours in DI water before a test.

Step 2: Prepare Consumables

The consumables used in each test were a pair of polishing wheels, aluminum wafers, and a polishing slurry. First the aluminum wafers would be placed on the platen in the arrangement shown in Figure 4-2. Then the wheels would be removed from the DI water, placed in the arbors, and mounted to the wheel motors. The wheels were then spun for five minutes to expel the excess water. Once the wheels are in place the slurry can be deposited into the slurry dispensers. The slurry must be first diluted if so required, then stirred before depositing into the dispensers. Once the slurry is in, the wheels are given a run in time before polishing begins, meaning the wheels are spun at a low speed while the slurry is fed to them so they become saturated with slurry.

Step 3: Process Parameters Initialized

Labview and Pro Motion (the program that runs the polishing motors) are opened and the values the specific tests calls for are uploaded before the test is begun. The Lateral Stage moves the wheels to the edge of their respective wafers. The Vertical Actuator would be calibrated in this step if not already done in a previous test.

Step 4: Initiate Polish

The wheels are commanded to begin spinning at the specified speed and the slurry dispensers are activated. Once the wheels and slurry are active Labview is

activated and Load Cell data is collected for the remainder of the test. Once Labview is active the Vertical Actuator is lowered into position. Once the Vertical Actuator is in position the Lateral Stage is commanded to move the wheels 2" across the wafers at a specified speed.

Step 5: End Polish

Once the Lateral Stage has moved 2" the Vertical Actuator is raised back up into its initial position. Once raised back up a minimum of fifteen seconds are allowed to transpire before the Labview program is deactivated which concludes the gathering of Load Cell data. After Labview is deactivated the slurry dispensers and wheels are turned off.

Step 6: Clean Wafers

Once the polish has concluded the aluminum wafers are removed from the Platen. Care is taken to preserve the side and direction the wafer is mounted in. The wafers are washed with DI water and wiped gently with latex gloves to remove abraded material and slurry. Once clean the wafers are placed in wafer holders which have the details of the testing conditions written on the back to preserve the testing parameters experienced by the wafer.

4.4. Data Analysis Procedure

Analyzing the results of a test occurs in two discrete segments. First the load cell data is analyzed to determine what load was actually applied to the wafer during testing. The other portion of data analysis uses an interferometer to create a profile

of the surface to determine the depth of the channel that has been polished into the wafer. The interferometer is also used to determine the roughness of the wafer.

4.4.1 Load Cell Analysis

Once polishing has completed the txt file created by Labview is renamed using a naming convention that allows wafers and data files to be correlated with one another. After the file is renamed, the file is loaded into Matlab. Matlab converts the text file into a series of charts that can be visually inspected. Figure 4-8 is a chart of load cell data from a test. There are a few aspects of this chart common among all other tests. The upward slope that occurs from around 30 second to 100 comes from the wheels not yet being completely on the wafers. This is because the wheels start at the edge of the wafer and are slowly dragged laterally across the wafer by the Lateral Stage. From about 120 to 170 seconds the wheel is completely on top of the wafer. From about 170 to 250 seconds the wheels begin to fall off the other wide of the wafer thus the load decreases. When the wheels have translated completely the side of the wafer the Vertical Actuator is raised back up as indicated by the green line in Figure 4-8. Once the actuator is back in its initial position the wheels are allowed to rotate for an minimum of fifteen seconds so a zero load reading can be ascertained. An average value of the zero load reference section is compared to the average value of the 120-170 second portion of the test. The difference between the zero load section and the section with the wheels entirely on top of the wafer is used as the nominal load value for that test. The data shown in Figure 4-8 gives a difference of 14.21N and 20.55N for load cell 1 and 2 respectively.

4.4.1.1 Nominal Load Error Bar

Graphs are presented in Chapter 5 that plot the nominal load from a test run against a relevant variable. The nominal load for each individual test has a margin of error. The error is represented by the error bars. The span of the error bars for load is based on the standard deviation of the running average of the load. Only the load cell data gathered during the period when the wheels are completely on the wafer are used to calculate the standard deviation. This corresponds to approximately the middle third of the polishing time starting when the vertical actuator is completely down and ending when the actuator is lifted up. The standard deviation of the moving average from 120 to 170 seconds as shown in Figure 4-8 is 1.75 and .95 for cell 1 and 2 respectively. The span of the error bars is equal to two standard deviations of the running average of the load.

4.4.2 Material Removal Height

The polishing wheels leave a channel in the wafers. The channels are deeper at their center and shallow at their edge. Often the edge has little to no discernable amount of material removed and is at the same level as the un-polished portions of the wafer. To determine the depth of the channels a profilometer is used. The profilometer is an interferometer produced by the ZYGO Corporation. Figure 4-9 is an example of the results from the interferometer which has profiled a wafer after testing. The top left portion of Figure 4-9 is the Back Plot and is a false color top view of the wafer that alters the color of the pixel to show its relative depth. The bottom left portion of Figure 4-9 is the Surface Profile. The Surface Profile shows

the cross sectional view of the lines cut across the back plot. In Figure 4-9 there are two lines that cut across each other perpendicularly. The green line on the Surface Profile shows the cross section of the line that cuts horizontally across the back plot and the blue line is the vertical line. By placing the vertical line across a point of the wafer that was polished when the wheels were exclusively on top of the wafer and not hanging off the sides an accurate depth reading can be taken from the deepest point of the channel. Using tools within the program the vertical slice on the Back Plot seen as the blue line in the Surface Profile of Figure 4-9 can be seen to read 27 micrometers from the upper edges of the channel to the bottom of the channel.

4.4.2.1 Removal Depth Error Bars

The error bars for the removal depth are based on data range rather than standard deviation. The data point for removal depth of any test is the average of three cross sectional slices taken perpendicular to the channel. The three slices are taken at different points in the region of the channel where the polishing wheel was not hanging off the edge of the wafer. This region is the middle third of the wafer, approximately 12mm wide. The error bar reflects the variation in depth within this region. The variation is quantified by taking the difference of the max and min of the center 10 mm (reducing the sampling width by 2mm ensures data outside of the intended region is not unintentionally included) of Surface Profile that corresponds to the horizontal slice through center of the channel in the Back Plot. This is seen as the green line in the Surface Profile of Figure 4-9 which has a 10mm center region

with a max of -19.4μm and a min of -23.1μm producing a data range of 3.7μm. The removal depth error bar for this data point would have a span of 3.7μm.

4.4.3 Surface Waviness & Roughness

The waviness and roughness of the wafers is determined using the same interferometer used to determine removal depth.

Waviness is defined as the Root Mean Square (RMS) of the surface when filtered using a low pass Fast Fourier Transformation (FFT) with a cutoff wavelength of 100μm. The low pass waviness of an unpolished 1.5" wafer can be seen in Figure 4-10. All low pass waviness data presented in this thesis is produced from a 4mm x 1mm area with a pixel resolution of 35.34μm. The same unpolished wafer shown in Figure 4-10 is analyzed over a 4mmx1mm area in Figure 4-11. When analyzing polished wafers the 4mmx1mm area always places the 4mm dimension within the middle 10mm of the lateral length and the 1mm dimension in the center of the channel vertically. Figure 4-12 is the Back Plot of Figure 4-9 if a 4mmx1mm area were removed from portion of the channel that is sampled for low pass waviness.

Roughness is defined as the RMS of the surface when filtered using a high pass FFT with a cutoff wavelength of 500μm. All high pass roughness is taken over a 1.41mm x 1.06mm area with a pixel resolution of 2.207μm. Figure 4-13 shows the high pass roughness of an unpolished wafer.

4.4.4 Surface Profile Comparison

In addition to analyzing the depth of the profiles created by the polished channels the shape of the profiles are analyzed as well. The shape of the profile is analyzed using the Surface Profile produced by the ZYGO interferometer. Once an appropriate sample has been selected a single vertical slice is made on the Back Plot. The single vertical slice shows up on the Surface Profile as a cross sectional profile of the wafer through the slice. Figure 4-14 is an example of the Surface Profile of Figure 4-9 if only a single vertical slice were made through the Back Plot. The process is repeated on two different samples ensuring that the distance and height scale are exactly the same when saving the data from a Surface Profile. Once gathered, the three profiles are overlaid on one another. A direct comparison of the profiles can then be made to determine the affect of the test variable on the shape of the profile.

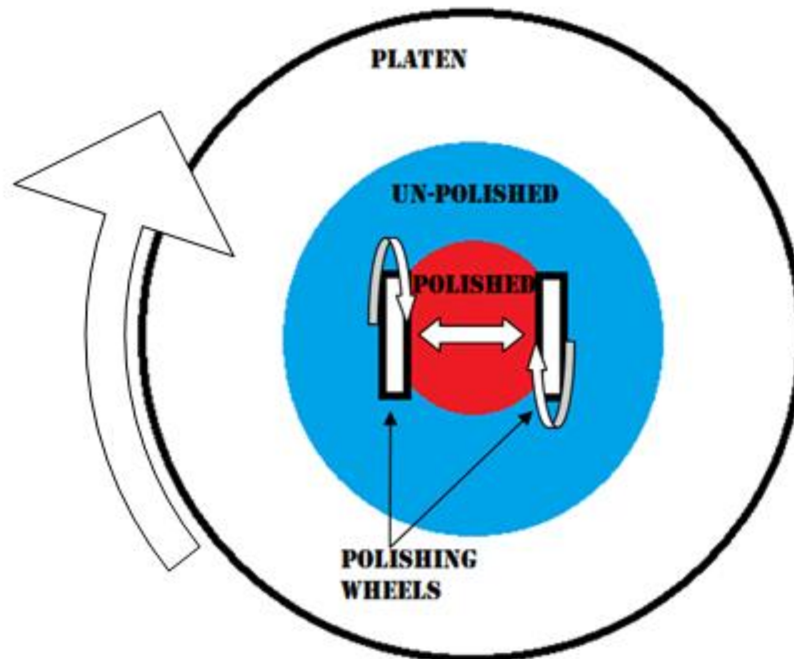

Figure 4-1 Illustration of 6" Wafer Setup

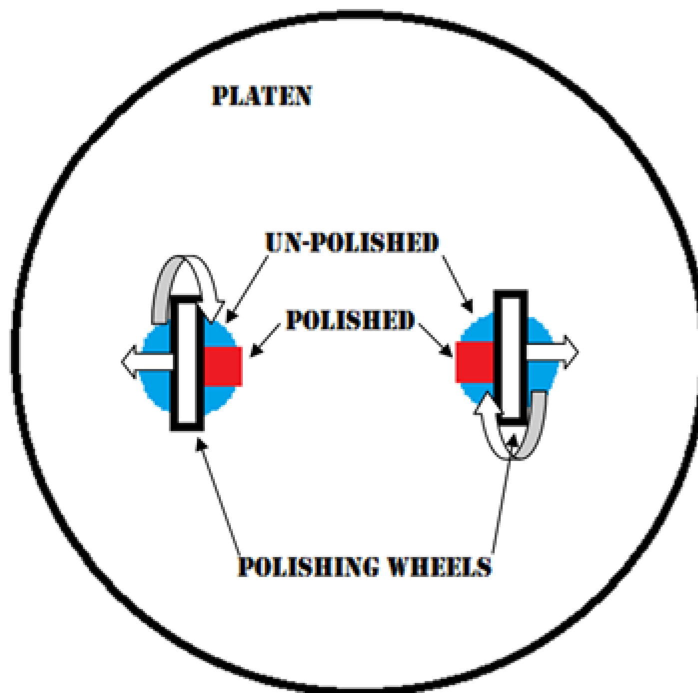

Figure 4-2 Illustration of 1.5" Wafer Setup

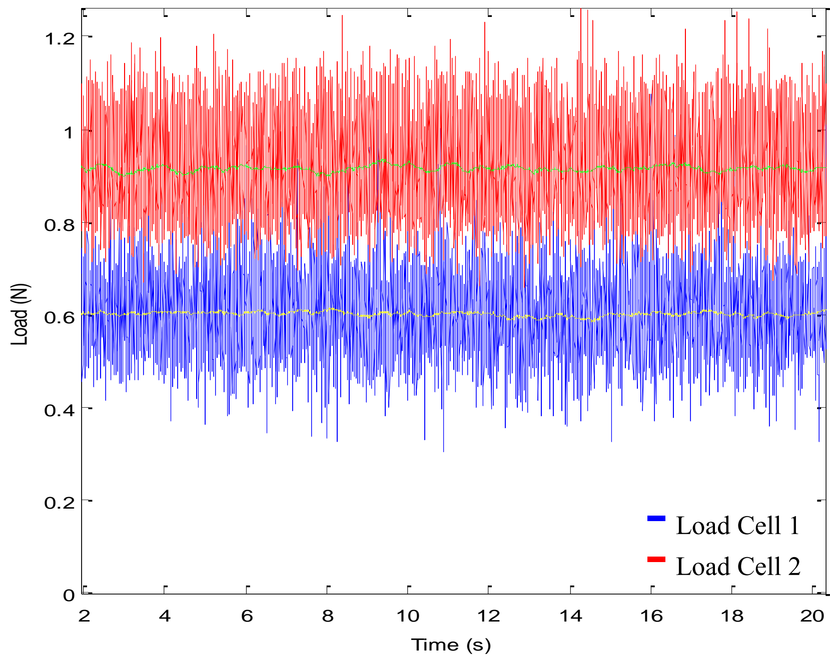

Figure 4-3 Electrical Noise With Equipment Power Off

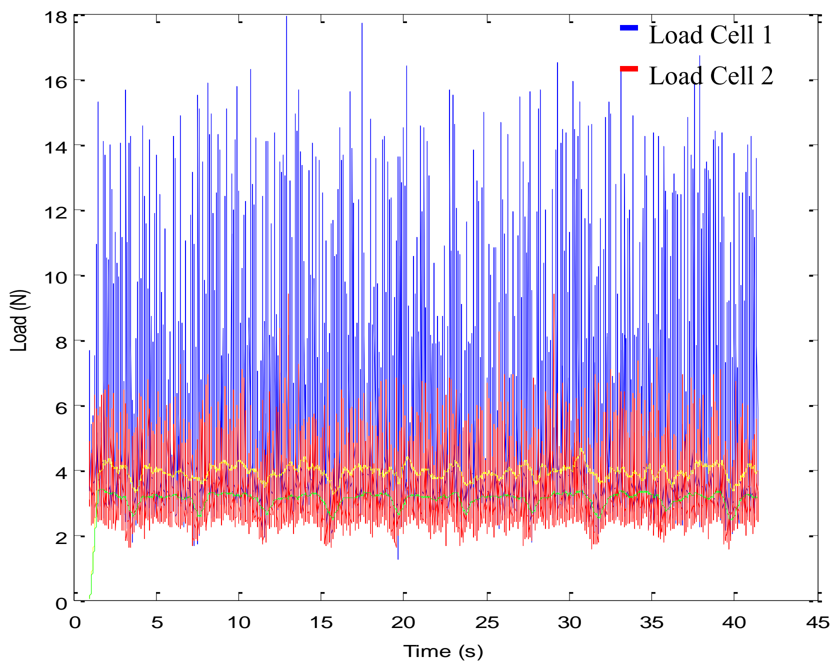

Figure 4-4 Electrical Noise With Equipment Power On

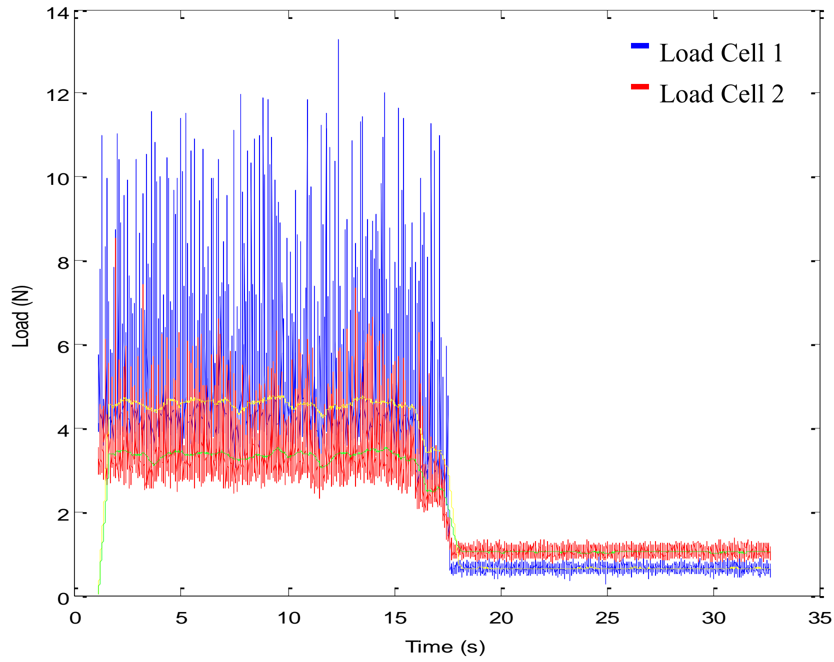

Figure 4-5 Electrical Noise With Equipment Power On Then Off

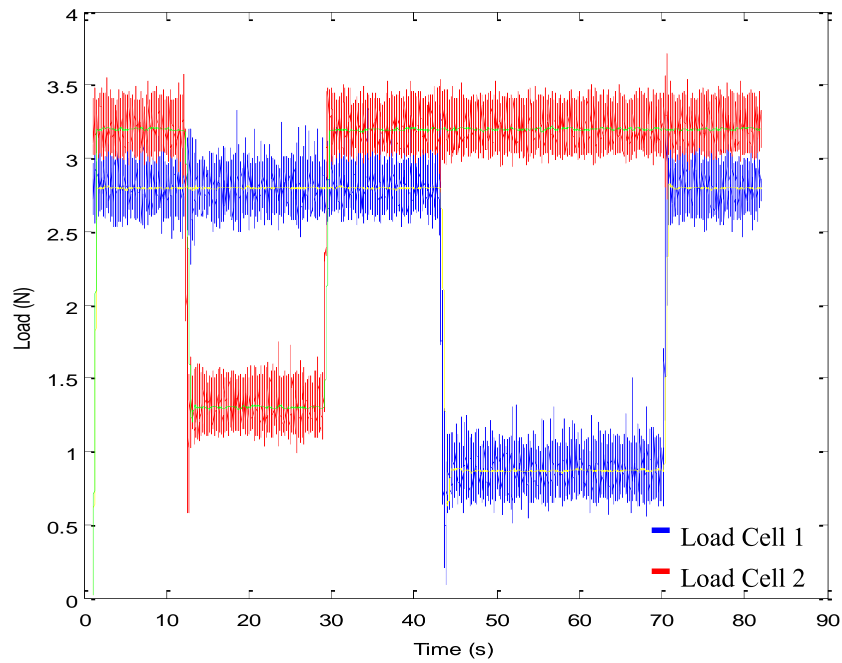

Figure 4-6 Load Cell Calibration

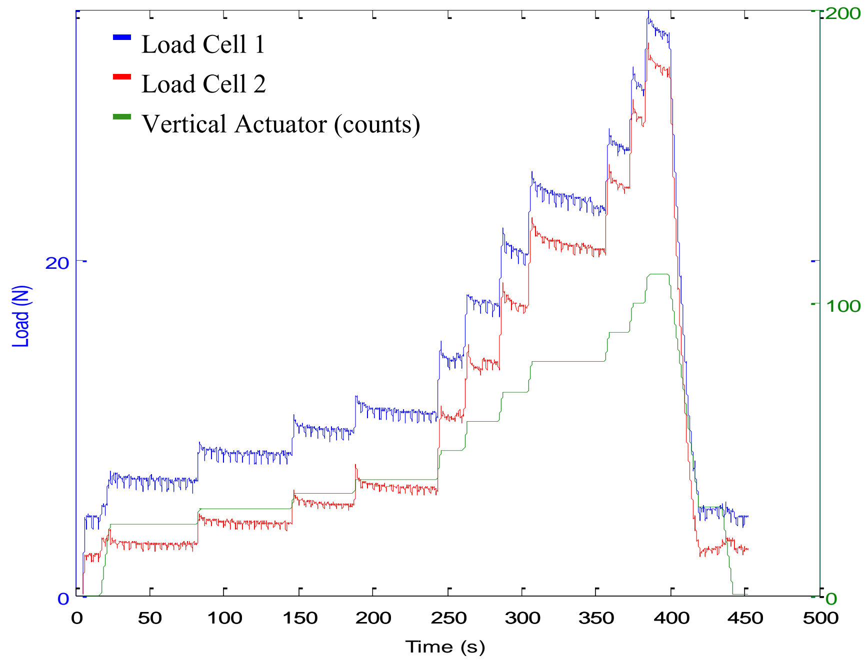

Figure 4-7 Vertical Actuator Calibration

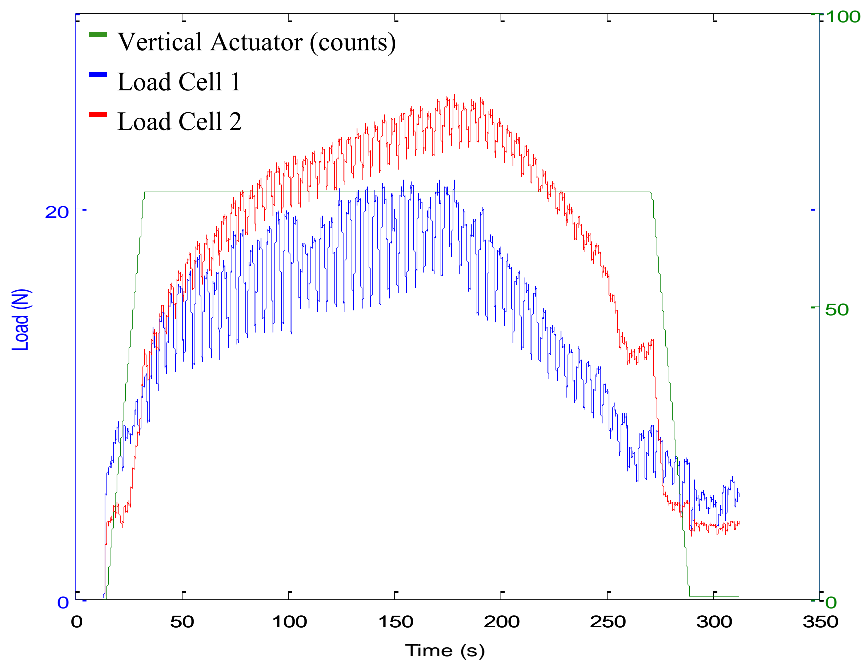

Figure 4-8 Example Of Load Cell Data From A Test

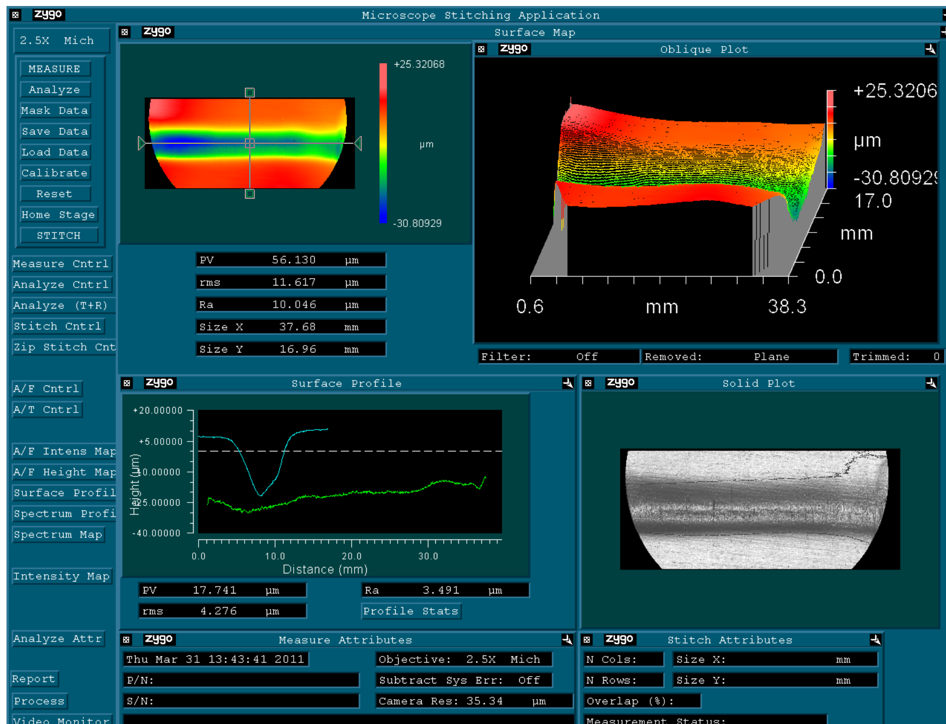

Figure 4-9 Results of Wafer Analyzed using ZYGO

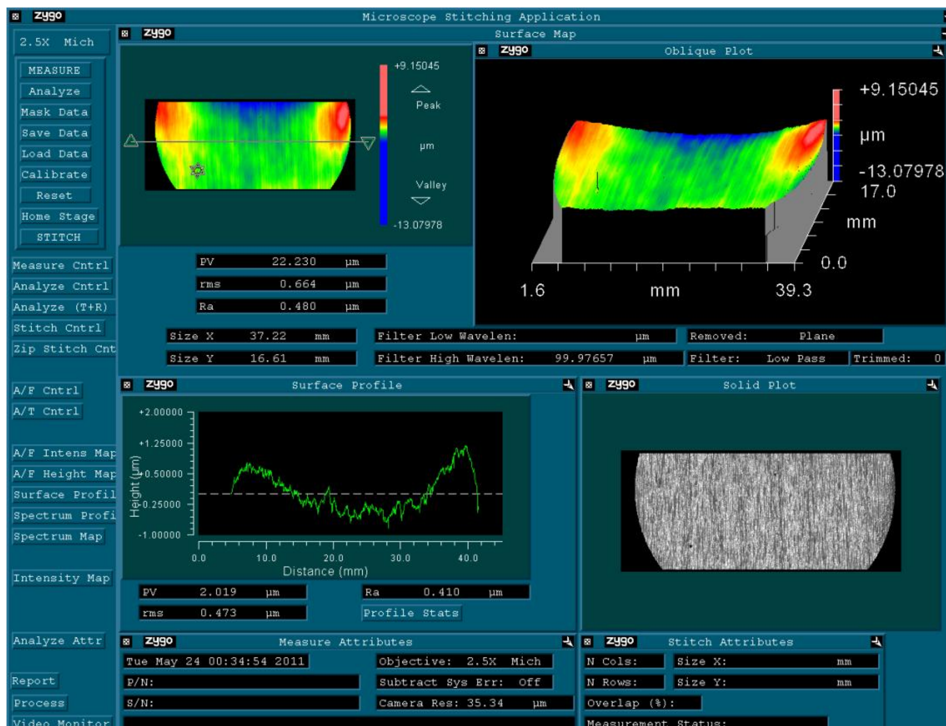

Figure 4-10 Low Pass Waviness: Un-Polished Wafer

Figure 4-11 Low Pass Waviness: 4mmx1mm Un-Polished Wafer

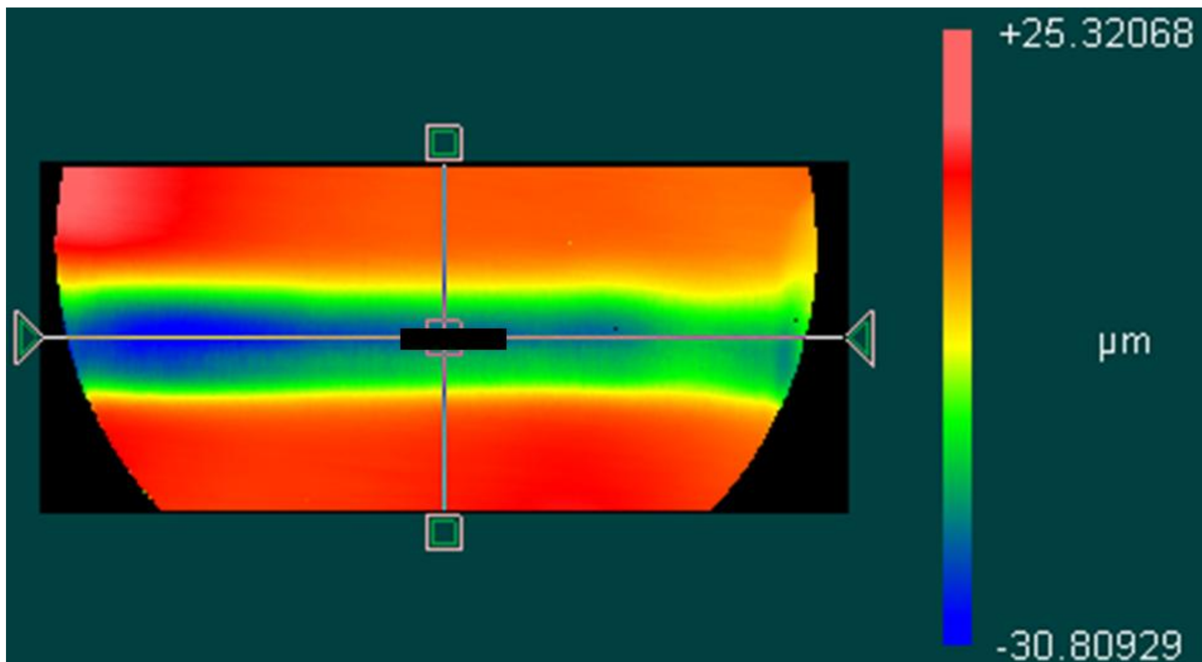

Figure 4-12 Back Plot with 4mmx1mm Area Removed to Demonstrate Area Analyzed for Low Pass Waviness

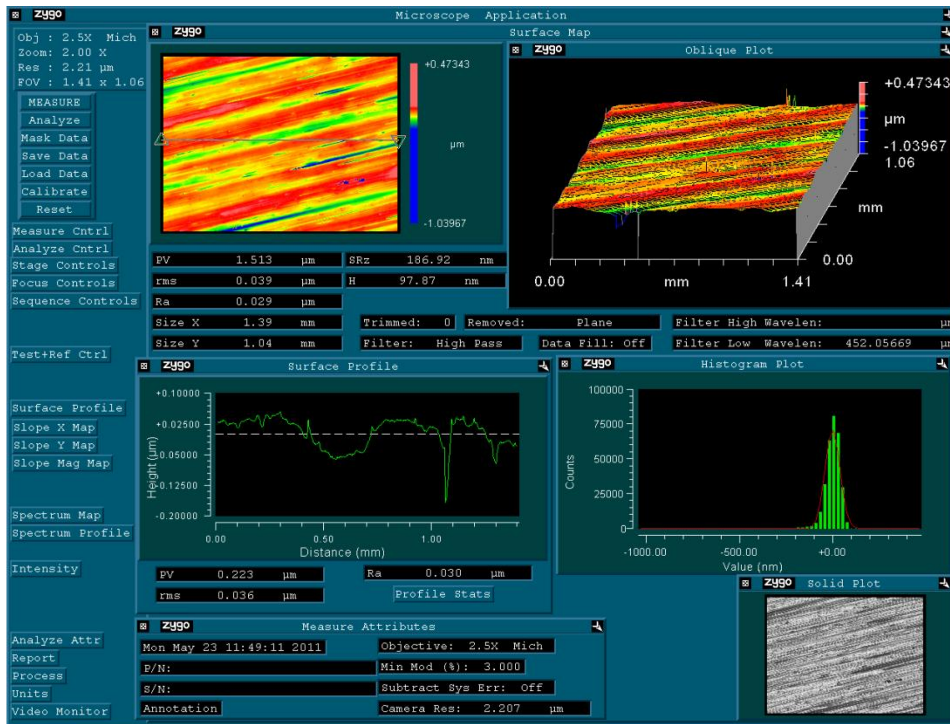

Figure 4-13 High Pass Roughness: 1.41mmx1.06mm Un-Polished Wafer

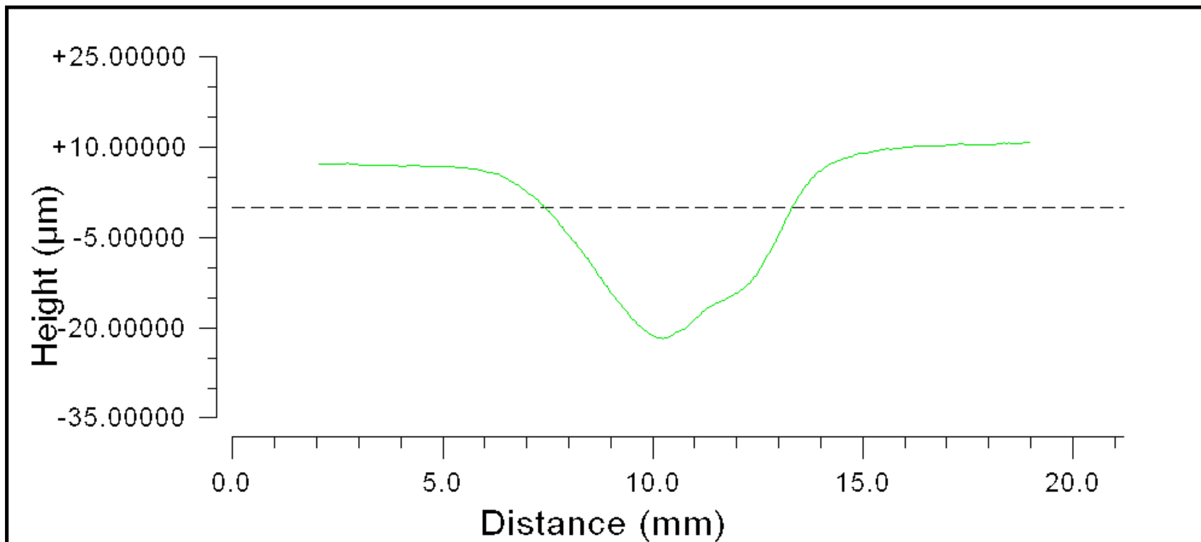

Figure 4-14 Profile of a Vertical Cross Section

CHAPTER 5 TESTING RESULTS

Testing of the prototype CMPG machine is conducted to determine the capabilities of the machine at its current juncture of development. The objective of the testing is to determine the effect consumables and process parameters have on the Material Removal Rate (MRR) and planarization. To determine the effects, consumables and process parameters are parameterized from test to test. Contrary to a typical CMP process which would polish an entire wafer, the tests are performed primarily on 1.5" wafers as described in Section 4.1.1.1. The resulting channel that is polished into the 1.5" wafers has a depth which is used as a proxy for MRR. Results will use the material removal depth or surface RMS as the dependent variable for all the charts examined in this chapter. All data presented in the charts can be found in Table 1 Results Data in the Appendix.

5.1. Load vs Material Removal Depth

The first test run varies the load applied to the polishing wheels. The process parameters and consumables used in this test run and the results they generate are used as the standard against which other tests are compared.

A relative velocity of 3.32 m/s and a dwell time 60.5 seconds are maintained through the test run. The 1µm alumina slurry and low density polishing wheels are used. The wafers used are pre-polished 1.5" aluminum wafers. Eight wafers were polished at eight different loads ranging from 4.6 N to 20.1 N. The results from the eight wafers are charted in Figure 5-1. A linear trend line has been overlayed on the

chart as a visual guide, but should not be interpreted as an inferred linear relationship.

Load is used as a corrollary of pressure and pressure been shown to have a strong effect on MRR. A directly proportional relationship can be seen between load and material removal depth. The directly proportional relationship adheres to the expected trend. The expectation of a direct proportionality comes from the increase in number of actively polishing abrasive particles that occurs when pressure is increased. Though there are exceptions to this if the polishing media is extremely stiff, the increase in active particles is caused by the deformation of the wheel. The deformation, rather than pressing harder against the particles already in contact, will place more of the wheel fibers into contact with the wafer increasing the actual contact area. Since the actual contact area is the region where the abrasive particles are actively polishing the increase translates into a greater removal of material.

An examination of waviness and roughness, as seen in Figure 5-2 Low Pass Wav iness: Load v s Material Remov al Dep th and Figure 5-3 respectively, indicates that niether has a strong relationship with load under the specificed test conditions. The test conditions produced a range of waviness and roughness values that varied from 143µm-351µm and 57µm-248µm respectively.

5.2. Dwell Time vs Material Removal Depth

This section analyzes the results of a test run that varies the dwell time of the polishing wheels vs material removal depth. Dwell time is the amount of time the

wheels are in contact with any point in the polishing region. Assuming the wheels are a constant width and translate at a constant speed, the dwell time is determined by dividing the width of the wheel by the lateral translation speed.

A relative velocity of 3.32 m/s and a load of 20-27N are maintained through the test run. The 1μm alumina slurry and low density polishing wheels are used. The wafers used are pre-polished 1.5" aluminum wafers. Nine wafers were polished at five different dwell times ranging from 14.1-127.0 seconds. The results from the nine wafers are charted in Figure 5-4. A linear trend line has been overlayed on the chart as a visual guide.

Though dwell time has been shown to have subtle effects on MRR, its affects are primarily implicated in total material removed, not the rate at which it's removed. Indeed, it can be intuitively expected that the longer a polishing process takes place the greater the volume of material removed becomes. Figure 5-4 confirms a directly proportional relationship, of greater significance however is an apparent linear relationship. If the relationship was not linear it would imply that a drastic change in polishing conditions occurs *during* polishing. As alluded to previously, the MRR can be expected to change slightly during a polish due to aspects of the CMP process like particle size distribution or surface topography whose states are in perpetual evolution while a polish is in progress. The effect of evolutionary aspects on the MRR is expected to be slight however and would prove troublesome if shown to manifest at the conditions used in these tests. The relationship does maintain the appearance of linearity however and further reinforces expected similarities between CMPG and standard CMP models.

An examination of waviness and roughness, as seen in Figure 5-5 and Figure 5-6 respectively, indicates that niether has a strong relationship with dwell time under the specificed test conditions. The test conditions produced a range of waviness and roughness values that varied from 177μm-366μm and 131μm-325μm respectively.

5.3. 50nm Silica Slurry - Load vs Material Removal Depth

A low MRR slurry containing 50nm silica particles rather than the highly aggressive 1μm alumina slurry is used in a run of tests. The 50nm silica slurry is tested on four wafers with a different load applied to each wafer.

A relative velocity of 3.32 m/s and a dwell time of 60.5 seconds are maintained through the test run. The 50nm silica slurry and low density polishing wheels are used. The wafers used are pre-polished 1.5" aluminum wafers. The results from the four wafers are charted in Figure 5-7. A linear trend line has been overlayed on the chart as a visual guide, but should not be interpreted as an inferred linear relationship.

The type of slurry used in a CMP process has a greater effect on the MRR than any other condition. In a production enviroment a wafer may be polished first with a high MMR slurry to remove the bulk of a film and then followed up with a polish that uses a finishing slurry which has a low MRR that can more preciesly remove the remainder of the material and produce a smother surface when finished. The 50nm silica slurry is an example of a low MRR slurry that is used in a finishing step and has been tested as a point of comparison. The chart in Figure 5-7

indicates that material removal depth is independent, perhaps even inversely proportional, of load in the presence of this low MRR slurry. The independence of the two variables deviates from the expected trend. It is expected that material removal depth is directly proportional to load regardless of slurry used. The likely culprit of the deviation is a lack of precision inherent in the testing methodology rather than true departure from standard CMP models. A large source of noise in the testing can be attributed to the waviness of the wafers. The factory pre-polish produces a very smooth surface free of high frequency roughness but fails to globally planarize the wafer leaving a high roughness at longer wavelengths. The waviness is apparent in the Zygo results for wafer tested at 13.6N seen in Figure 5-8. The region above and below the polished channel appears to vary in height as much or more than the deviation in height between the edge and valley of the channel. The waviness of the wafer would drastically alter readings if the removal depth measurements are taken from the global peak or valley of the wafer. Though the noise introduced by the waviness is present in all the tests, the use of high MRR slurry in other test runs produced results with amplitudes that rose sufficiently above the noise. The low MRR 50nm silica slurry does not produce a material removal depth great enough to make conclusions on the relationship between load and MRR.

An examination of waviness and roughness, as seen in Figure 5-9 and Figure 5-10 respectively, indicates that niether has a strong relationship with load under the specificed test conditions. The test conditions produced a range of waviness and roughness values that varied from 52μm-106μm and 31μm-51μm respectively. As

expected, the smaller abrasive size produced smoother surface than any of the other test condtions.

5.4. Medium Density Wheel - Load vs Material Removal Depth

A medium density polishing wheel rather than a low density wheel is used in a run of tests. The medium density wheels are tested on eight wafers with a different load applied to each wafer.

A relative velocity of 3.32 m/s and a dwell time of 60.5 seconds are maintained through the test run. The 1μm alumina slurry is used. The wafers used are pre-polished 1.5" aluminum wafers. Eight wafers are polished at eight different loads ranging from 14.1-127.0N. The results from the nine wafers are charted in Figure 5-11. A linear trend line has been overlayed on the chart as a visual guide, but should not be interpreted as an inferred linear relationship.

The density of the wheels is used as a corrollary of stiffness. The stiffness of a polishing media has been shown to affect MRR. The relationship between MRR and stiffness comes from the interatction between the polishing media and the abrasive particles. Abrasive particles are actively removing material if they are trapped between the polishing media and the wafer. This only occurs in the real contact area. It is presumed that the polishing wheels, similar to polishing pads used in standard cmp, will deform if a higher load is applied to them increasing the real contact area. If a pad is extremely stiff however, applying a greater load may not increase the contact area, but instead increase the load applied to the particles already in contact with the wafer. Though the MRR would increase directly with an

increase in load in either case, the initial MRR of an extremely stiff pad would be lower than a pad with low stiffness due to the drastically reduced contact area. Figure 5-11 shows that material removal depth is directly proportional to load with the use of a medium density polishing wheel. Shown on the same graph are the results of load variation if polished under the same conditions but with a low density wheel. At the loads the medium density wheels were tested, a consistently greater material removal depth was produced than those created at equal loads using a low density wheel. The greater material removal depth produced by the medium density wheel suggests that greater stiffness is indicitive of an increase in bulk material stiffness. The increase in bulk stiffness is presumed to create a smaller contact area, but produce a greater actual contact area thus increasing the MRR. Figure 5-11 also suggests that the rate at which the contact area increases with load, and consequently material removal depth, is higher for a medium density polishing wheel than a low density polishing wheel.

Alternatively, the presumed increase in MRR may be an artifact of the testing methodology. It is possible that the overall MRR, or rate of reduction of film thickness across an entire, may be approximately equal to a low density wheel. This would be a consequence of the difference in contact area. In the context of a channel, the smaller area is moot since only the depth is examined. In the context of an entire wafer however, the higher MRR in the smaller contact area may remove an equal volume across an entire wafer as the low density wheel which has a lower MRR but a larger contact area. There is currently insufficient data to determine if

this is the case. Further research is need to determine the precise effect wheel density has on MRR.

An examination of waviness and roughness, as seen in Figure 5-12 and Figure 5-13 respectively, indicates that niether has a strong relationship with load under the specificed test conditions. The test conditions produced a range of waviness and roughness values that varied from 269µm-564µm and 81µm-434µm respectively. A rough comparison of the range of values to the test conditions using a low density wheel indicate the use of high density wheel produces high values of wavieness and roughness. Further testing is required before a conclusion regarding the affect of wheel density on surface topography can be reached.

5.5. Relative Velocity vs Material Removal Depth

The run of tests examined in this section varies the relative velocity at which each wafer is polished.

A load nominal load in the range of 19.1-20.1N is used through the test run. The 1µm alumina slurry and low density polishing wheels are used. The wafers used are pre-polished 1.5" aluminum wafers. Five wafers were polished at five different relative velocities ranging from 1.33-3.99 m/s.. The results from the five wafers are charted in Figure 5-14. A linear trend line has been overlayed on the chart as a visual guide, but should not be interpreted as an inferred linear relationship.

Velocity and pressure are identified as the two main process parameters. Presenton's Equation in fact recognizes only pressure and velocity and attributes

everything else to a coefficient. Thus it is unsurprising to see that velocity has been shown to have a direct effect on MRR. Counter intuitively, Figure 5-14 shows that material removal depth is independent of relative velocity. Though the volume of material removed by any one particle does not increase with relative velocity, a higher relative velocity raises the number of abrasive particles brought into the contact area that become active which is expected to raise the MRR. It is suspected that the prototype employs a slurry delivery system that does not deliver and adequate amount of slurry to the polishing wheels. If the contact area is not saturated with slurry the increase in relative velocity will not correlate with the increase in abrasive particles brought to the contact area. Further testing with a slurry dispensing system that floods the conact area with slurry is required before a relationship between relative velocity and material removal depth can be established.

An examination of waviness and roughness, as seen in Figure 5-15 and Figure 5-16 respectively, indicates that niether has a strong relationship with velocity under the specificed test conditions. The test conditions produced a range of waviness and roughness values that varied from 146μm-259μm and 94μm-138μm respectively.

5.6. Worn Wheel - Load vs Material Removal Depth

A set of low density polishing wheels that have performed a total of 725 seconds of polishing are used rather than a fresh wheel. Following the conclusion of a previous test, the wheels were removed from the machine, rinsed gently with DI

water, dried for a week at STP, and then soaked per the standard 24 hour minimum in DI water All other test procedures remain identical to those of every other test.

A relative velocity of 3.32 m/s is maintained through the test run. The 1µm alumina slurry is used. The wafers used are pre-polished 1.5" aluminum wafers. Four wafers were polished at four different loads ranging from 15.5-20.7N. The results from the four wafers are charted in Figure 5-17 Worn Pad - Load vs Material Removal Depth. A linear trend line has been overlayed on the chart as a visual guide, but should not be interpreted as an inferred linear relationship.

The use of worn pads explores the variation in MRR that occurs between wafers when polished on the same machine. Standard CMP machines use pads that become glazed and lose the rough surface topography necessary to achieve the high MRR expected in a commercial environment. Though pad conditioners re-introduce roughness into the pad after it has been glazed, a gradual increase in stiffness also occurs as the pad is compressed over numerous polishing cycles. The increase in stiffness was presumed to cause the medium density polishing wheels to increase their actual contact area, but a polishing pad generally decreases its actual contact area as stiffness increases since it can no longer conform to the topography of the wafer. Figure 5-17 Worn Pad - Load vs Material Removal Depth shows a directly proportional relationship between material removal depth and load in the presence of a worn polishing wheel. An increase in the material removal depth similar to that seen with a medium density wheel suggests that the wheel has stiffened as a result of previous use. The apparent increase in MRR as wheel stiffness increases may be a consequence of one of the key features of CMPG.

However, it is more likely that the difference in effects produced by stiffness is a consequence of the polishing media used. Specifically, the use of a fibrous polishing wheel on the CMPG machine rather than the cellular polishing pads found on standard CMP machines.

An examination of waviness and roughness, as seen in Figure 5-18 and Figure 5-19 respectively, indicates that niether has a strong relationship with load under the specificed test conditions. The test conditions produced a range of waviness and roughness values that varied from 104μm-271μm and 165μm-333μm respectively.

5.7. Profile Comparison

A comparison of the profile of the channel polished across each wafer under different test conditions is analyzed. The profile of the channel at different loads using a low density wheel, the profile of the channel at different loads using a medium density wheel, and the profile of the channel at different dwell times are analyzed.

5.7.1 Low Density Wheel Profile Comparison

The low density wheel created a profile that does not appear to change shape considerably at high loads. The comparison of the profiles can be seen in Figure 5-20. The soft pads create an asymmetric profile that has a steeper wall on the left side which where the wheel enterse than the right side which is where the wheel exits.

5.7.2 Medium Density Wheel Profile Comparison

The medium density wheel created a profile that changes shape at high loads. The comparison of profiles can be seen in Figure 5-21. The steepness of the entering side increases rapidly with an increase in load. The right side of the channel, which is the exiting side, has a ‘hump’ that becomes increasingly pronounced as the load increases. An increase in the density/stiffness would presumably make the ‘hump’ more pronounced than is currently seen.

5.7.3 Dwell Time Profile Comparison

The profile comparison of tests with different dwell times produced profiles that do not change shape drastically between tests. The profile comparison can be seen in Figure 5-22. The profiles appear relatively symmetric at all dwell times. The symmetry may not hold if the same tests are repeated using medium density wheels instead of low density wheels.

5.8. Full Wafer Test

All the tests analyzed in sections 5.1 through 5.7 have been based on the results of the channel polished into a 1.5” wafer. During those tests the table was locked so it could not rotate. The final test of the CMPG machine rotates the table during polishing so the entire surface of a 6” wafer can be polished.

The 6” wafer is made of the same pre-polished aluminum as the 1.5” wafers. The 1µm alumina slurry and medium density polishing wheels are used for the test. Though the relative velocity was not constant since the wafer has a different speed depending on its radius from the center of table, an approximate relative velocity of

3.32 m/s can be assumed since the polishing wheels provide the majority of the relative motion. A nominal load of 14N was maintained through the entirety of the test. The dwell time varies from approximately 7 seconds at the outer edge to 14 seconds at the region 1.5” from the center.

The inner 1.5” radius region of the wafer remains unpolished. An unpolished region at the center of the wafer is a necessary consequence of using paired wheels. Though the radius of the region can smaller than 1.5”, a large unpolished region is useful as a point of comparison for measurement purposes.

The variation in dwell time from the outer edge to the inner regions was expected to create a discernable difference in material removed. An examination of the wafer provided inconclusive results due to the greater waviness of a 6” wafer than a 1.5” wafer. As seen in Figure 4-10 the waviness of the 1.5” is around 2-3μm. The 6” wafers are too large to create an edge to edge profile on the ZYGO interferometer so a Computerized Measurement Machine (CMM), which have an accuracy of ±1μm, is used instead. Figure 5-23 and Figure 5-24 indicate the 6” wafers have a waviness 30μm to 40μm in amplitude. Additionally, the shape of the wafer can be convex, concave, saddle shaped as seen in Figure 5-24 or a number of other ineffable shapes. The variation in shape and amplitude of the wafers render a meaningful measurement of material removal beyond the capabilities of the available measurement techniques. The same can be said of a low pass measurement of waviness.

A high pass measurement of roughness can still be taken from the polished wafer regardless of waviness. The ZYGO image seen in Figure 5-25 has an RMS of

72nm and is a representative result of the high pass roughness at any polished portion of the 6” wafer. The RMS varied from 60nm-90nm but was primarily between 70nm-80nm. Readings at different radii and orientations relative to the grain were taken but no discernable trend emerged. Ten points randomly selected at different points of the wafer gave an average RMS of 69.6nm. The high pass average of 69.6 is still higher than the unpolished RMS of 39nm shown in Figure 4-13 but is lower than all other roughness data points taken from the 1.5” wafers.

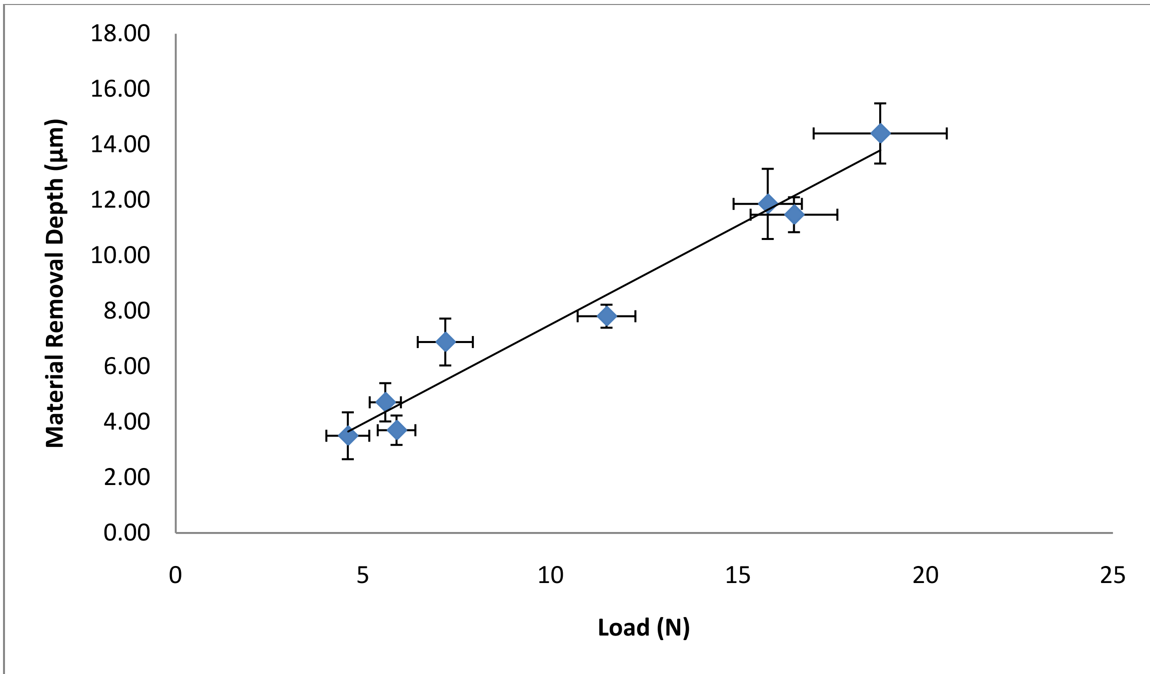

Figure 5-1 Load vs Material Removal Depth

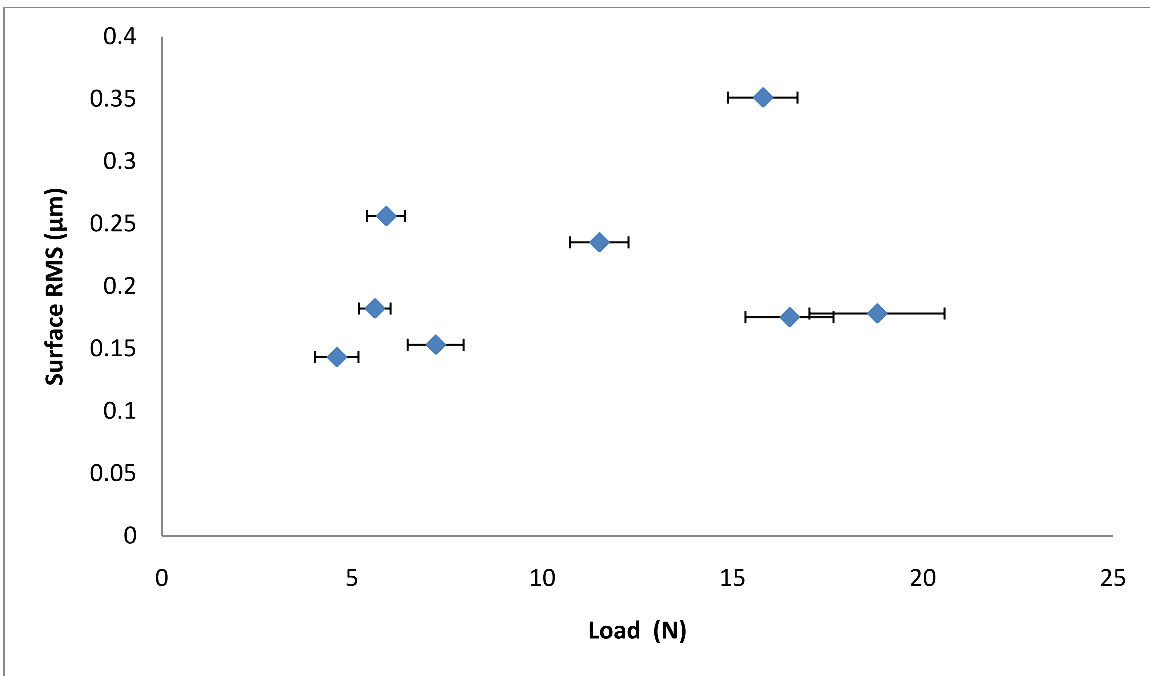

Figure 5-2 Low Pass Waviness: Load vs Material Removal Depth

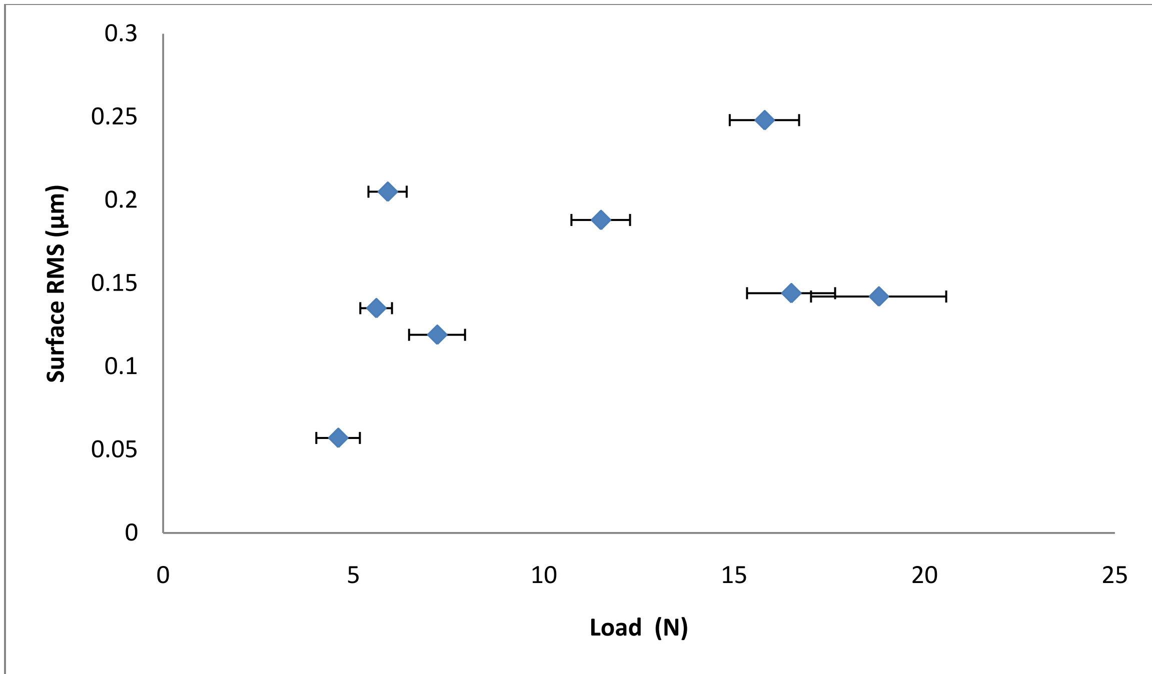

Figure 5-3 High Pass Roughness: Load vs Material Removal Depth

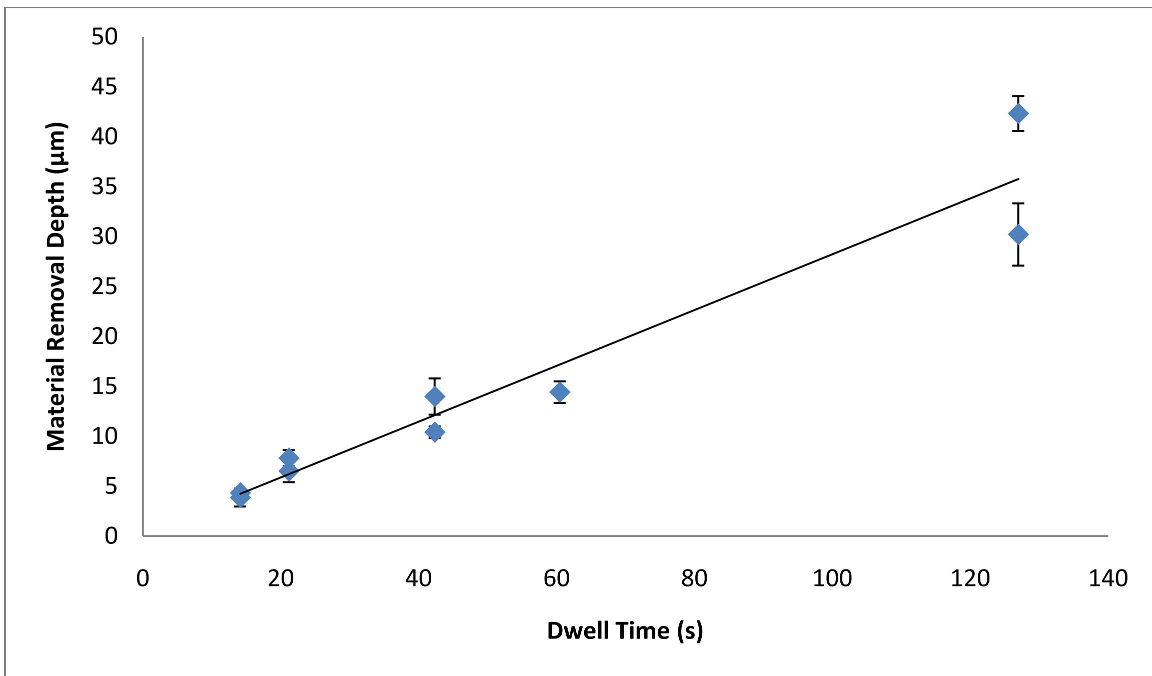

Figure 5-4 Dwell Time vs Material Removal Depth

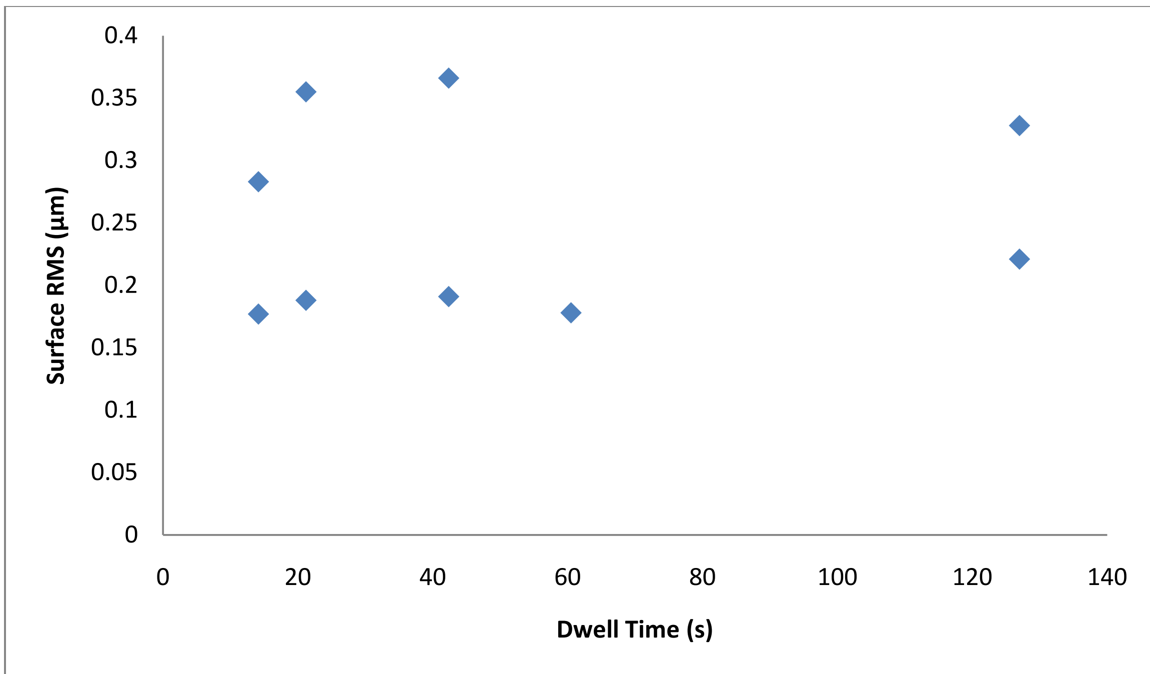

Figure 5-5 Low Pass Waviness: Dwell Time vs Material Removal Depth

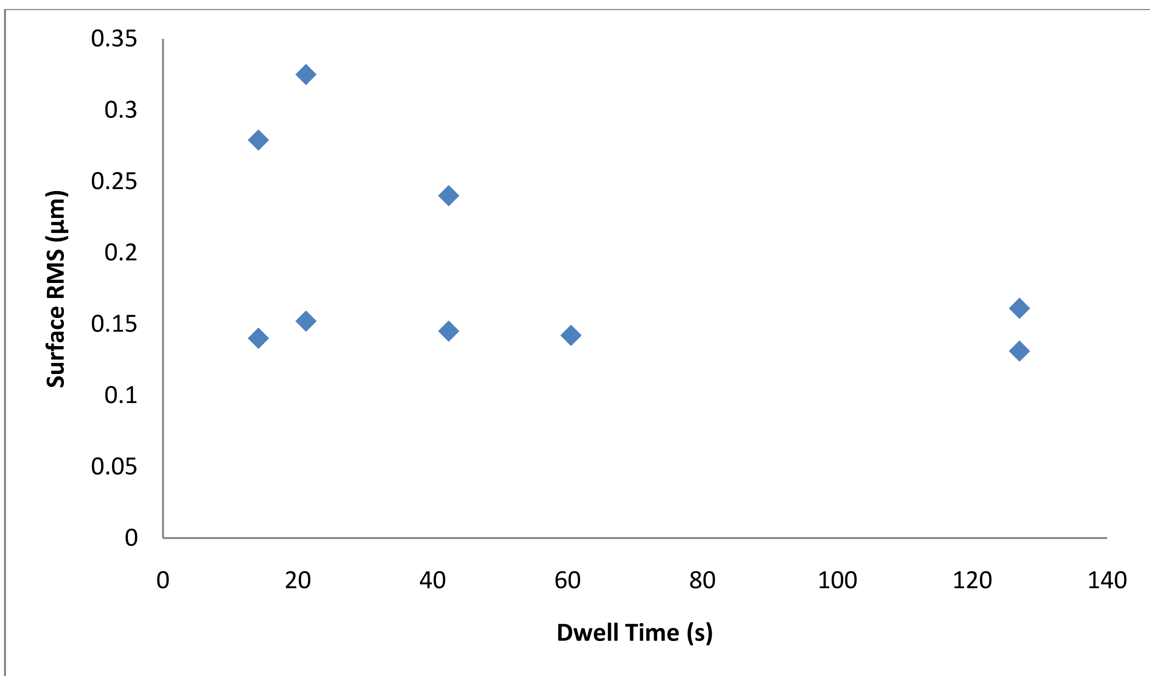

Figure 5-6 High Pass Roughness: Dwell Time vs Material Removal Depth

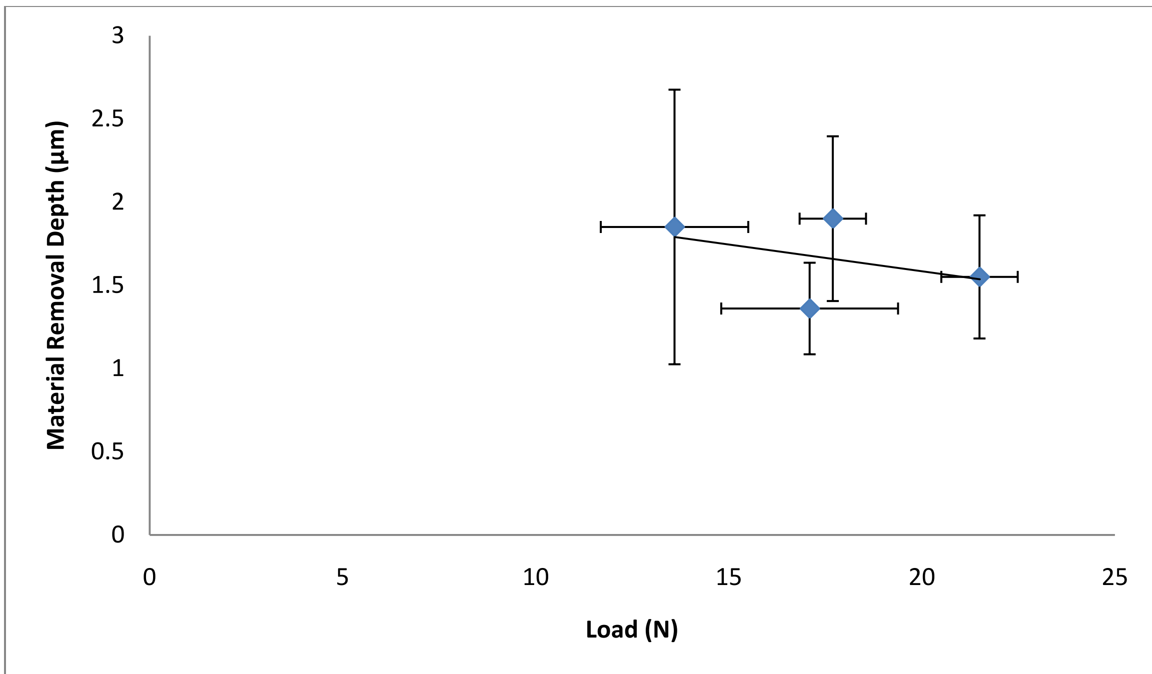

Figure 5-7 50nm Silica Slurry - Load vs Material Removal Depth

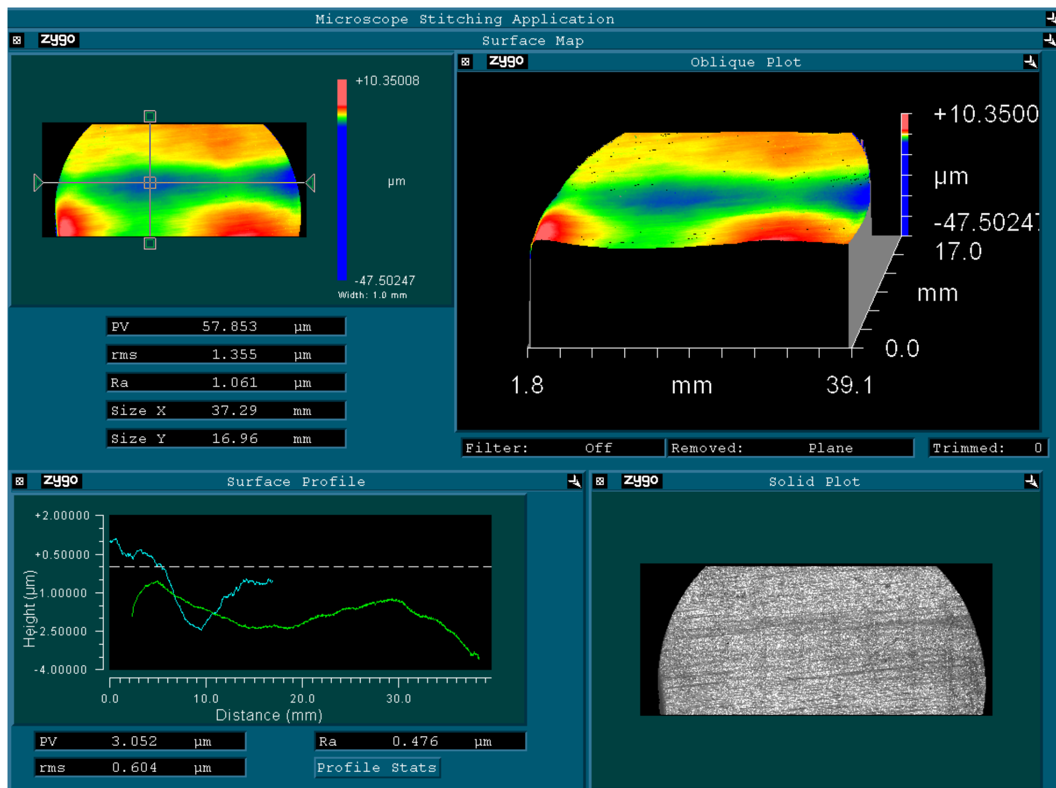

Figure 5-8 Zygo Results for 50nm Silica Slurry @ 13.6N

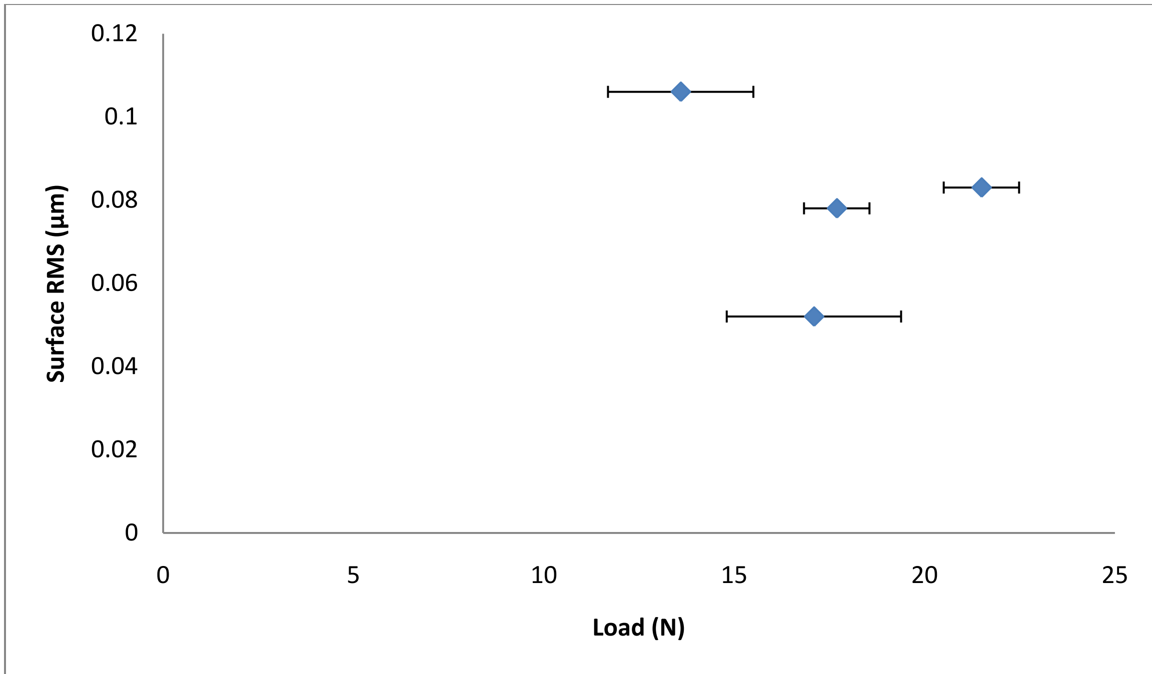

Figure 5-9 Low Pass Waviness: 50nm Silica Slurry - Load vs Material Removal Depth

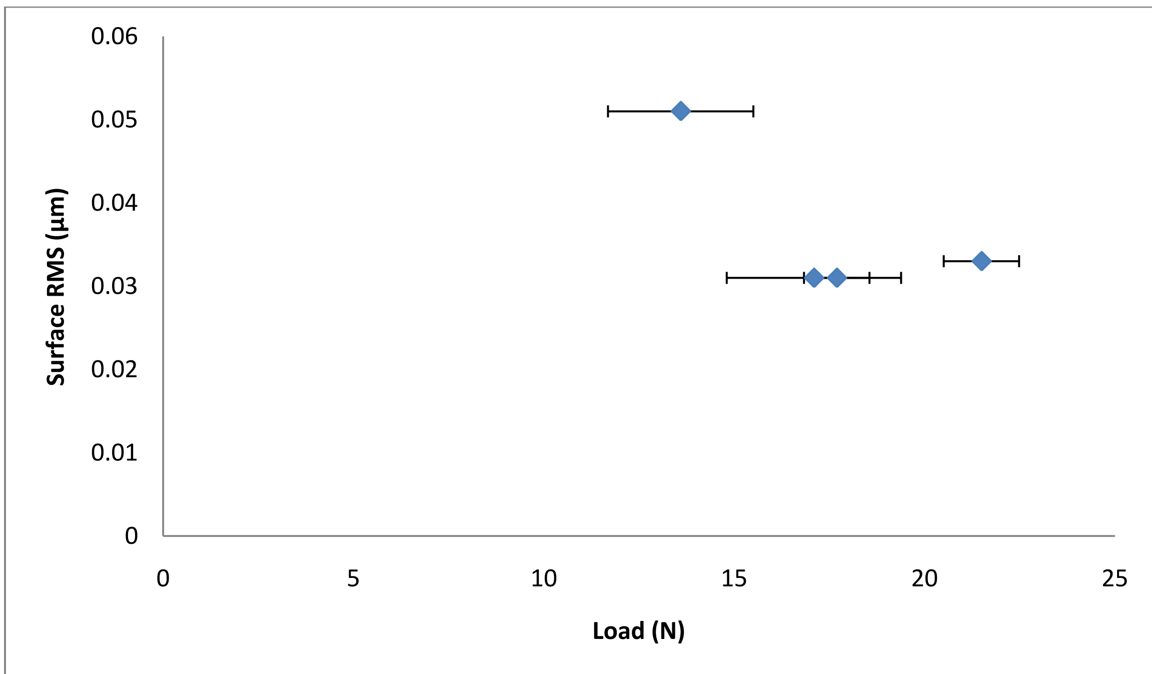

Figure 5-10 High Pass Roughness: 50nm Silica Slurry - Load vs Material Removal Depth

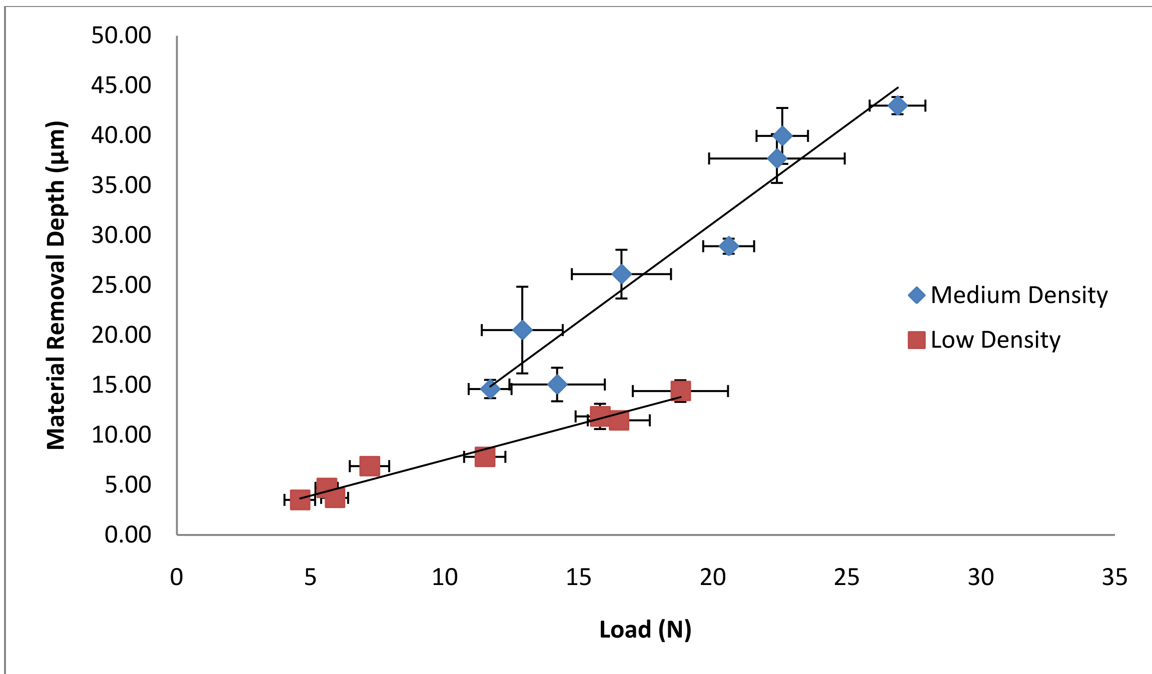

Figure 5-11 Medium Density Wheel - Load vs Material Removal Depth

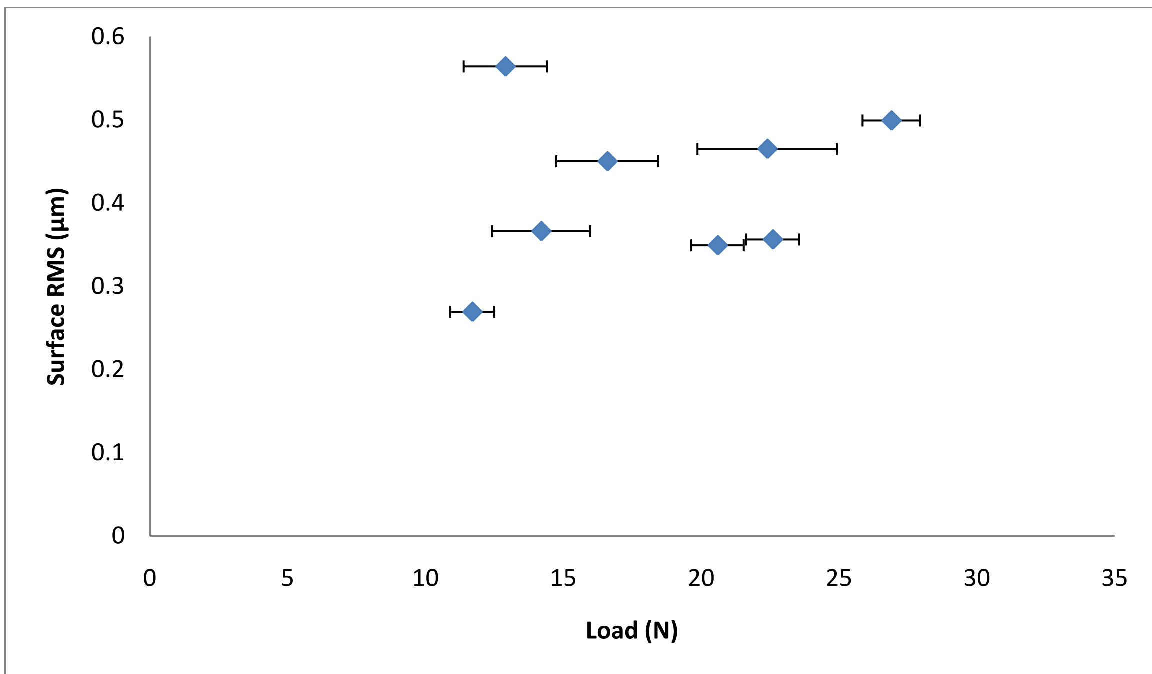

Figure 5-12 Low Pass Waviness: Medium Density Wheel - Load vs Material Removal Depth

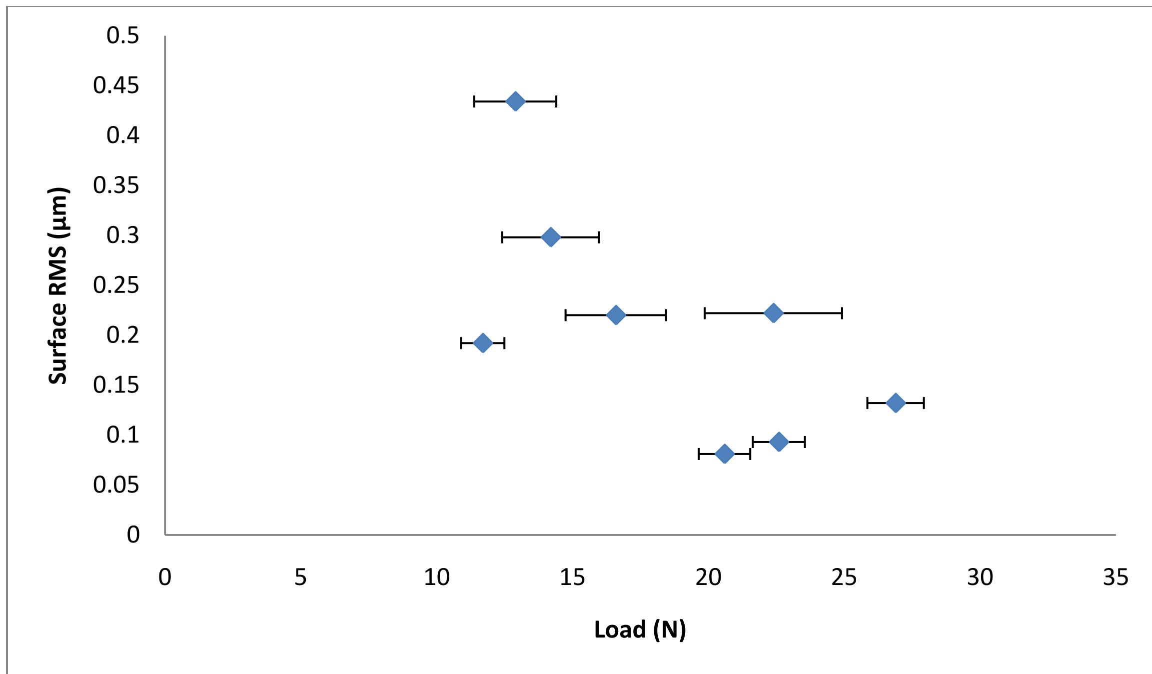

Figure 5-13 High Pass Roughness: Medium Density Wheel - Load vs Material Removal Depth

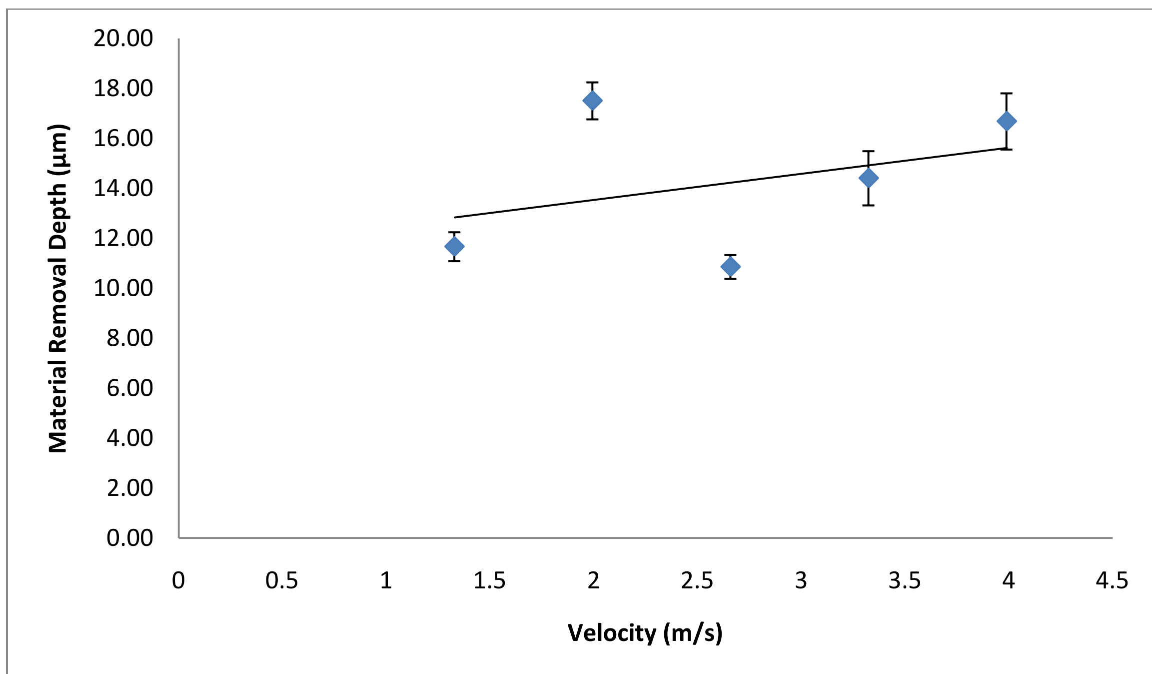

Figure 5-14 Relative Velocity vs Material Removal Depth

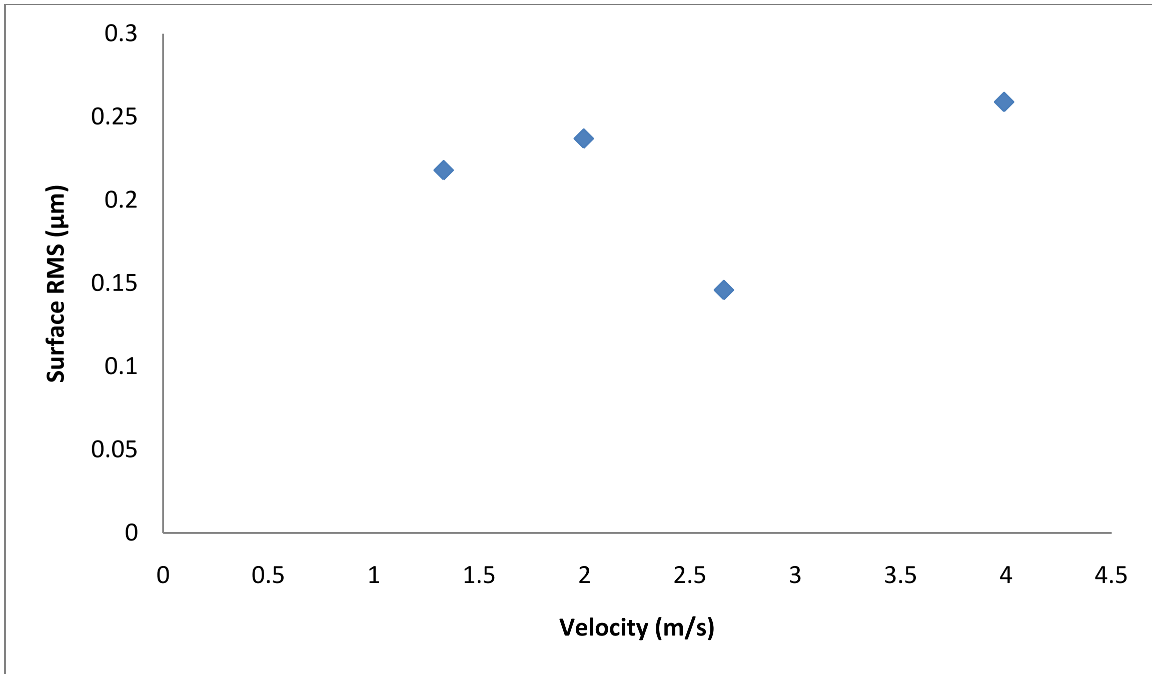

Figure 5-15 Low Pass Waviness: Relative Velocity vs Material Removal Depth

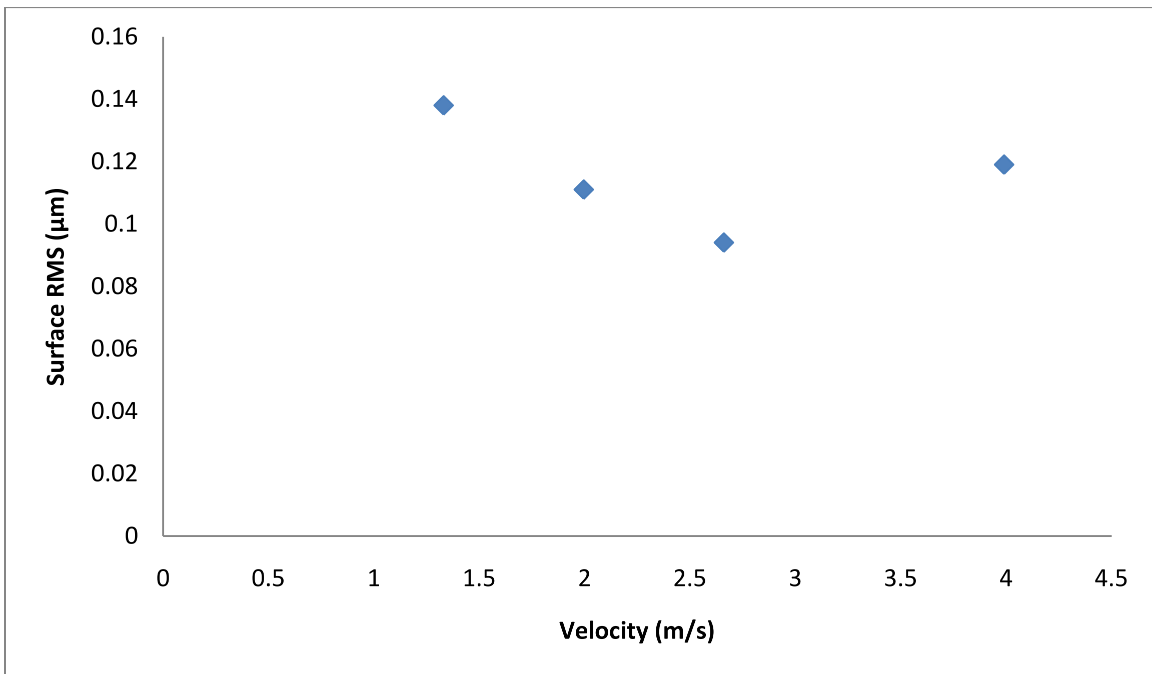

Figure 5-16 High Pass Roughness: Relative Velocity vs Material Removal Depth

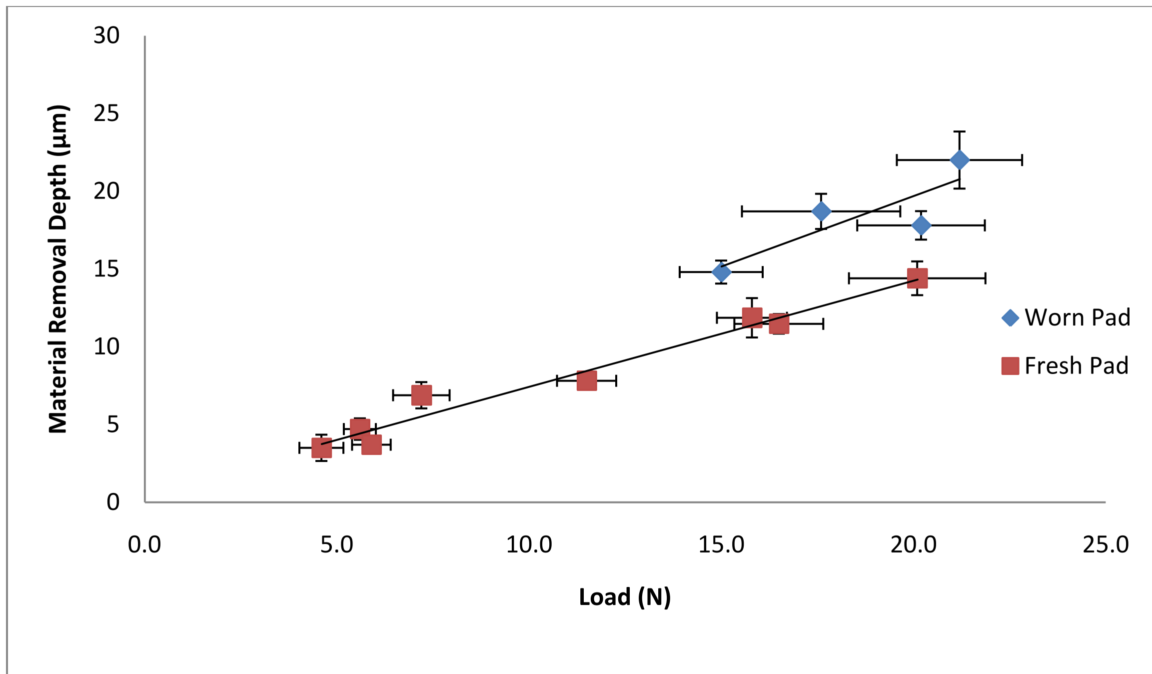

Figure 5-17 Worn Pad - Load vs Material Removal Depth

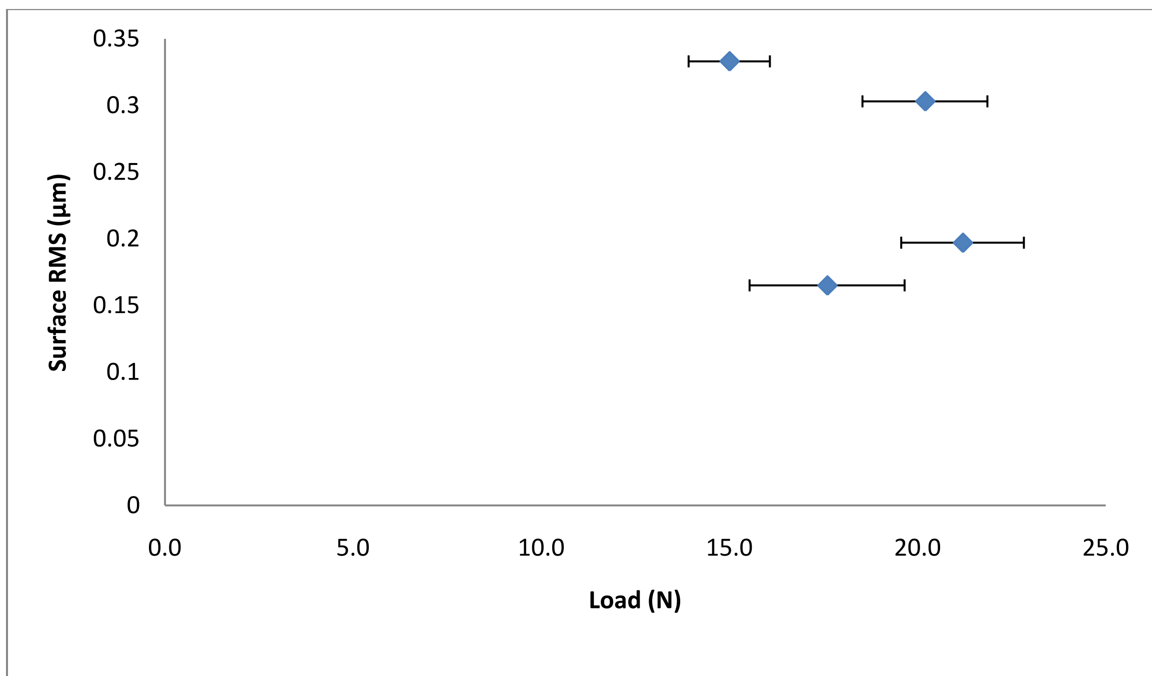

Figure 5-18 Low Pass Waviness: Worn Pad - Load vs Material Removal Depth

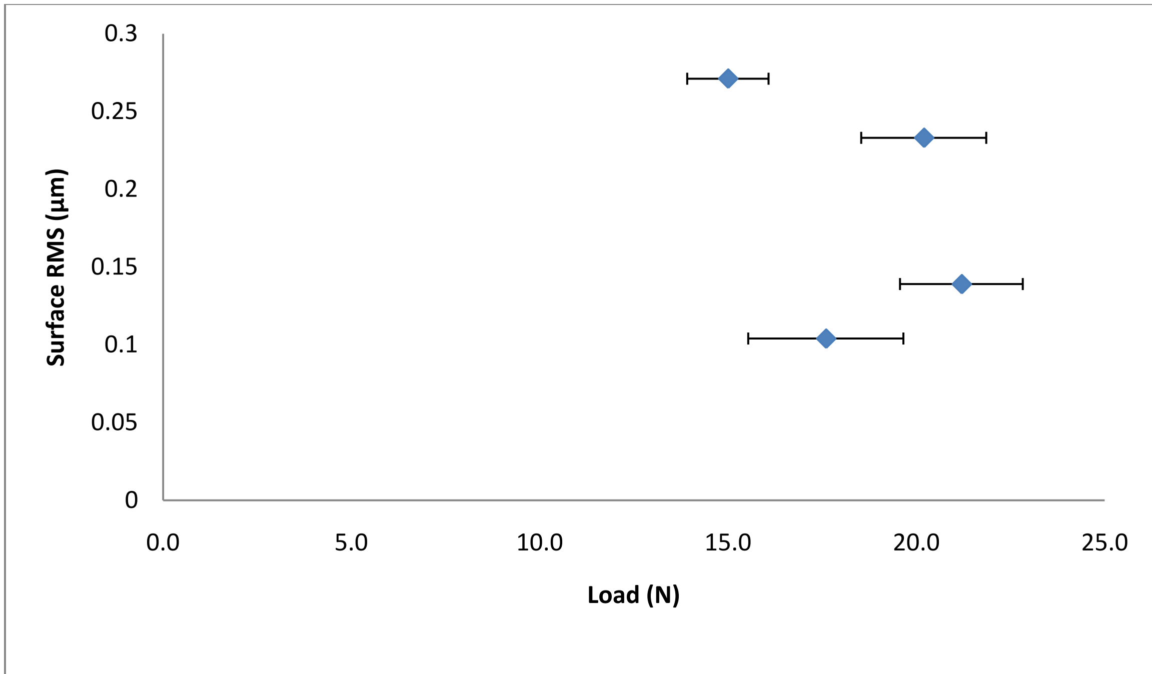

Figure 5-19 High Pass Roughness: Worn Pad - Load vs Material Removal Depth

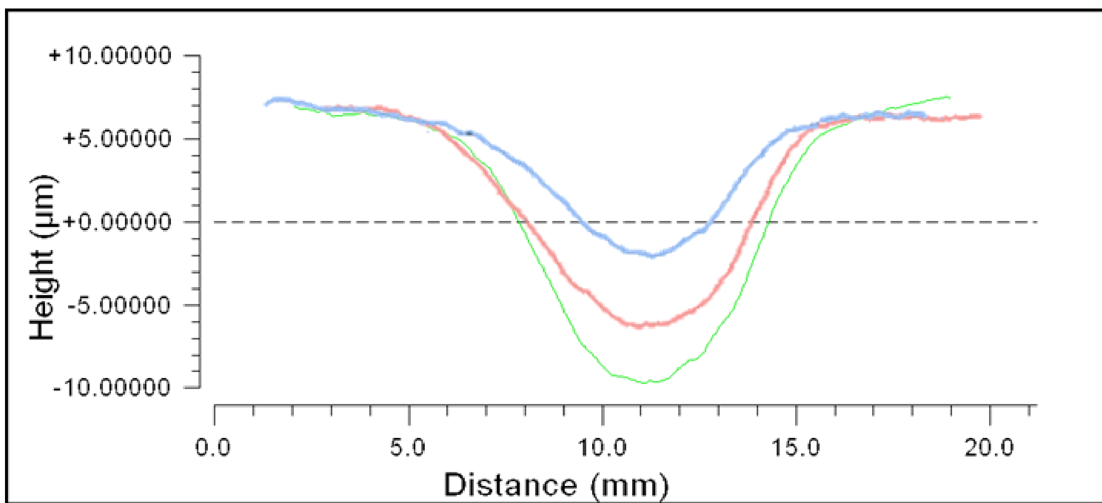

Figure 5-20 Profile Comparison of Load w/ Low Density Wheels

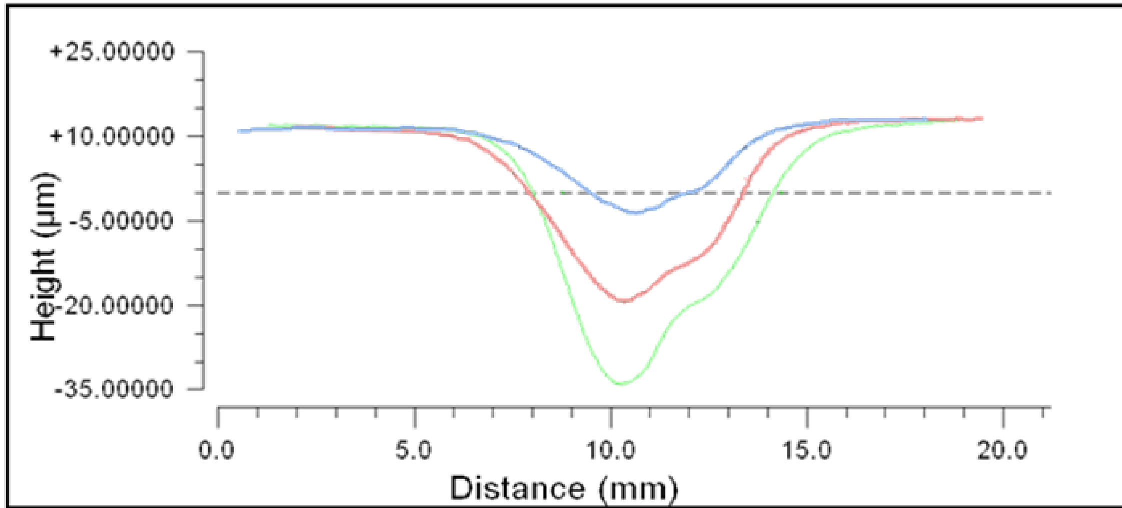

Hard Pad @Load 11.7, 20.6, 26.9 (N) @ Depth 14.6, 28.9, 43.0 (um)

Figure 5-21 Profile Comparison of Load w/ Medium Density Wheels

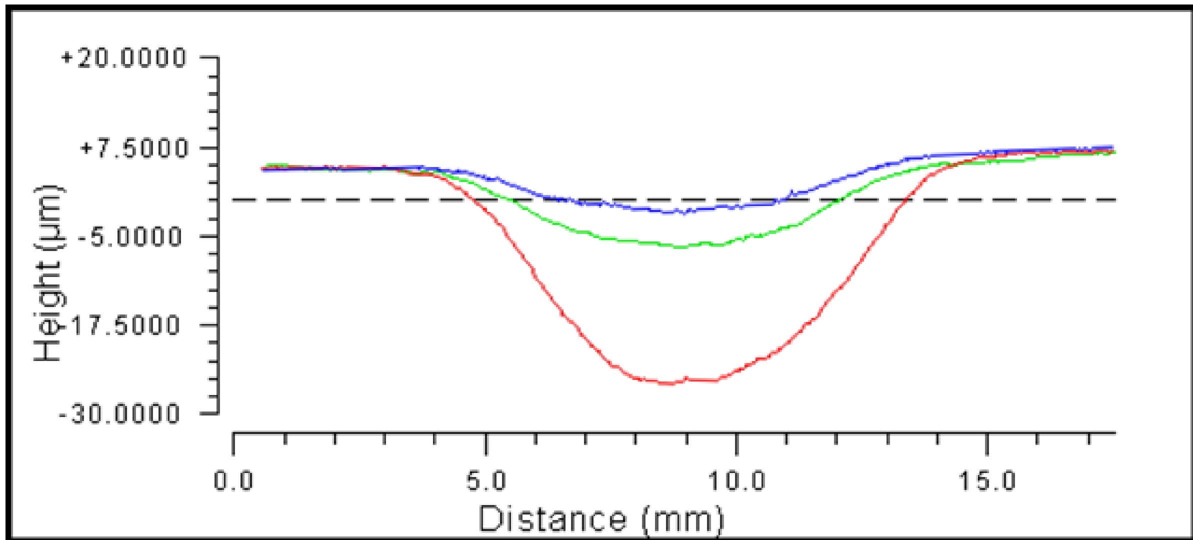

Dwell Time 21, 42, 127 (s) @ depth 6.5, 10.4, 30.2 (um)

Figure 5-22 Profile Comparison of Dwell Time

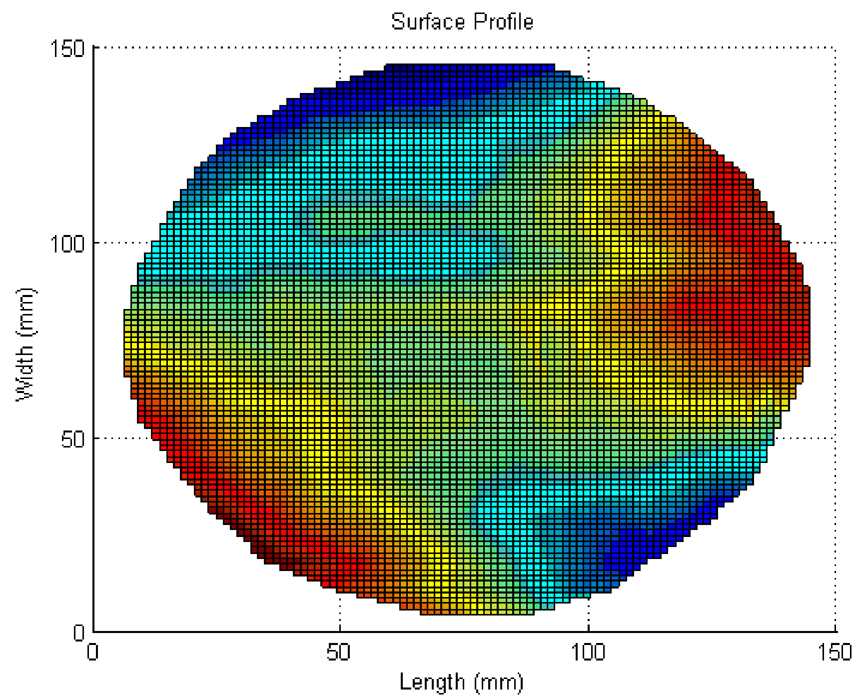

Figure 5-23 Wafer Waviness: Top Down View

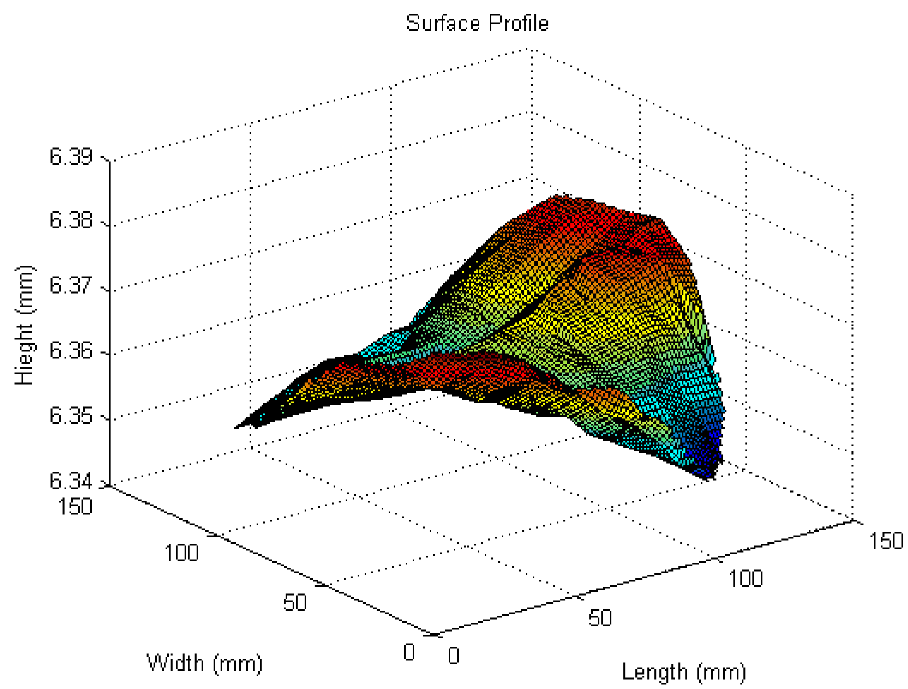

Figure 5-24 Wafer Waviness: Isometric View

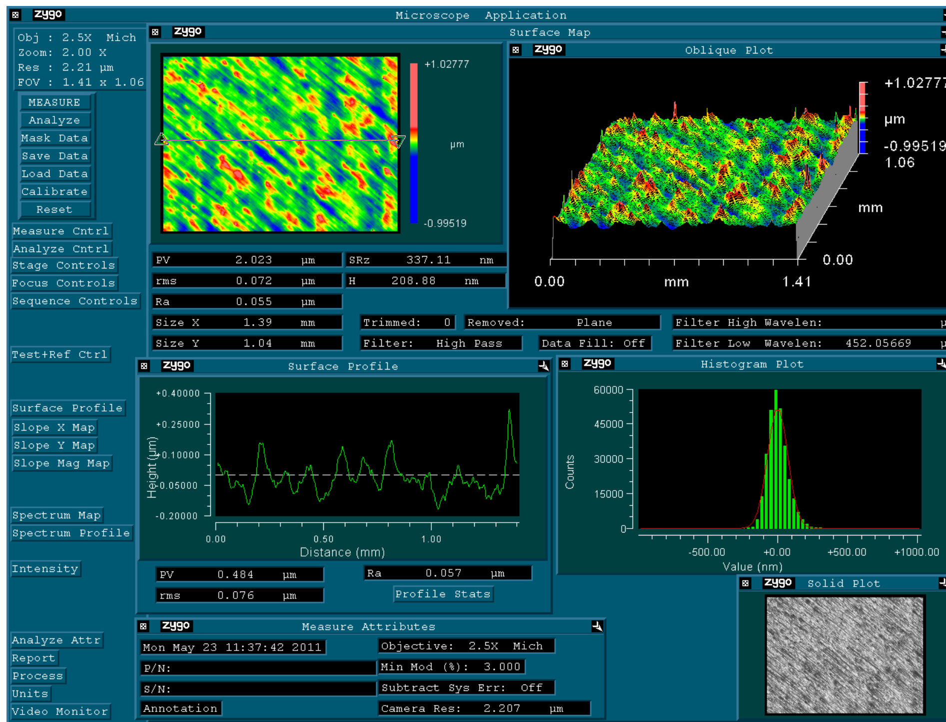

Figure 5-25 High Pass Roughness: 6” Polished Wafer

CHAPTER 6 CONCLUSION

The process parameters and consumables used in the prototype CMPG machine have been parameterized in an experimental study of their effect on MRR. Many of the results of the study conformed to the expectations predicted by standard CMP processes. The relationship between MRR & load, and MRR & dwell time had the expected directly proportional relationship. A few tests yielded inconclusive results however, due to insufficiently precise testing methodology. The tests using a low MRR slurry that used a 50nm Silica abrasive had MRR vs load trend that did not conform to expectations. The deviation in this case was suspected to be a result of test wafers that are not planarized sufficiently to detect the variation in material removal depth created by the low MRR slurry. Additional tests are required with an adequately planarized wafer to determine the relationship between MRR and load in the presence of a low MRR slurry. The tests that demonstrated an independent relationship between relative velocity and material removal depth were also unexpected. It is suspected that the relationship is not due to a departure from the mechanics of standard CMP. Rather, a condition of slurry starvation is presumed which prevents an increase in velocity from increasing the MRR. Further tests are needed in a slurry saturated environment before a relationship between relative velocity and material removal depth can be reached. The tests that used a medium density polishing wheel and a worn low density polishing wheels illustrated the effect that stiffness has on MRR. Contrary to standard CMP which generally has a lower MRR the higher the pad stiffness, the tests showed an increase in material removal depth when a polishing wheel with a greater bulk stiffness was used. It is suspected

this difference between standard CMP and the results of the prototype CMPG machine are a result of the use of fibrous polishing media rather than cellular polishing media as is standard in commercial CMP machines.

The lack of a discernable relationship between waviness or roughness and any of the test variables is likely a consequence of unrepeatability. Though testing conditions are held within a certain window, that window is still not small enough to reveal the relationship between roughness and waviness and is instead hidden behind the intractable variations between tests.

BIBLIOGRAPHY

Adams J. Smith E., Schultz S. Oscillating Orbital Polisher and Method [Patent] : 6,500,055 . - USA, Dec 31, 2002.

Banerjee G. Sundaram K., Desai V., Obeng Y. Chemical Mechanical Polishing 9 in ECS Transactions [Journal]. - [s.l.] : , Volume 13, Issue 4, The Electrochemical Society (ISBN 9781566776295), 2008. - 4 : Vol. 13. - ISBN 9781566776295.

Basim GB Brown SC, Vakarelski IU, Moudgil BM Strategies for optimal chemical mechanical polishing (CMP) slurry design [Journal]. - New York : MARCEL DEKKER INC, 2003. - 3-4 : Vol. 24. - ISSN 0193-2691 .

Bastawros A. F. Chandra A., Guo Y., Yan, B. , Pad Effects on Material Removal Rate in Chemical Mechanical Planarization [Article] // Journal of Electronic Materials. - 2002. - Vols. 31 no. 10, pp. 1022-1031..

Bastawros A.-F., Chandra, A. and Guo, Y. The Role of Surface Morphology and Mechanical Properties on the Material Removal Rate in CMP [Conference]. - [s.l.] : Proc. CMP-MIC 2003, 2003.

Bibby T. Holland K. Equipment [Article] // Semiconductors and Semimetals. - 2000. - Vol. 63.

Bifano T. Dow T., Scattergood R. Ductile Regime Grinding: A New Techonologuy for Machining Brittle Materials [Journal]. - [s.l.] : Journal of Engineering for Industry, 1991. - Vol. 113.

Bonner B. Mcreynolds P., Menk G., Iyer A., Prabhu G., Rondum E., Jackson R., Leung G. Materials for chemical mechanical polishing [Patent] : 7429210. - USA, 09 30, 2008.

Brown N. J. Some speculations on the mechanisms of abrasive grinding and polishing [Article] // Precision Engineering. - Livermore : Butterworth & CO, 1987. - 3 : Vol. 9.

Chandra A. K. Wang, Y. Huang, G. Subhash, M. H. Miller, W. Qu Role of Unloading in Machining of [Journal]. - [s.l.] : Journal of Manufacturing Science and Engineering, 2000. - Vol. 122.

Chandra A. P. Karra, A.F. Bastawros, R. Biswas, P.J. Sherman, S. Armini, D.A. Lucca Prediction of scratch generation in chemical mechanical planarization [Journal]. - [s.l.] : CIRP Annals - Manufacturing Technology, 2008. - Vol. 57.

Chandra A., Bastawros, A. Role of Forming in micro- and nano-scale material removal mechanisms during surface machining of ductile materials [Conference]. - [s.l.] : Proceedings of NUMIFORM, 2004.

Che W., Bastawros, A. –F, Chandra, A. Synergy between Chemical Dissolution and Mechanical Abrasion during Chemical Mechanical Polishing of Copper [Journal]. - [s.l.] : Mat. Res. Soc. Proc. , 2005 . - Vols. 867: 275-280..

Cronkhite P. Voege R., Poletti J. Apparatus and Process for Polishing Semiconductor or Similar Materials [Patent] : 3,708,921. - USA, Jan 9, 1973.

Dyer Timothy Chemical Mechanical Polishing [Book Section] // Semiconfuctor Manufacturing Handbook / book auth. Geng Hwaiyu. - [s.l.] : McGraw-Hill, 2005.

Evans C.J. Paul E., Dornfeld D., Lucca D.A., Byrne G., Tricard M., Klocke F., Dambon O., Mullany B.A Material removal mechanisms in lapping and polishing [Article] // Annals of the CIRP. - 2003. - Vols. 52/2:611-634..

Goetz Douglas P. Fixed abrasive article for use in modifying a semiconductor wafer [Patent] : 6632129 . - USA, 02 15, 2001.

INTERNATIONAL ROADMAP COMMITTEE INTERNATIONAL TECHNOLOGY ROADMAP FOR SEMICONDUCTORS [Report]. - 2010.

Kadavasal M. A. Chandra, A. Bastawros, S. Eamkajornsiri Yield improvement via minimisation of step height non-uniformity in chemical mechanical planarisation (CMP) with pressure and velocity as control variables [Journal]. - [s.l.] : Manufacturing Technology and Management, 2005. - Vol. 7.

Komanduri R. On material removal mechanisms in finishing of advanced ceramics and glasses [Article] // Annals of the CIRP. - 1996. - Vols. 45:509-514.

Komulski M. Chemical properties of material surfaces [Journal]. - New York : [s.n.], 2001.

Kondo S. Sakuma N., Homma Y., Goto Y., Ohashi N., Yamaguchi H., Owada N. Complete-abrasive-free process for copper damascene interconnection [Conference]. - Burlingame : IEEE 2000 International, 2000. - ISBN 0780363272.

Krusell W. Travis G., Engdahl E., Bagley J. Linear Reciprocating Disposable Belt Polishing Method and Apparatus [Patent] : 0123298. - USA, Sep 5, 2002.

LANDIS H BURKE P, COTE W, HILL W, HOFFMAN C, KAANTA C, KOBURGER C, LANGE W, LEACH M, LUCE S INTEGRATION OF CHEMICAL MECHANICAL POLISHING INTO CMOS INTEGRATED-CIRCUIT MANUFACTURING [Conference]. - SAN DIEGO : ELSEVIER SCIENCE SA LAUSANNE, 1992. - ISSN 0040-6090 .

LANDIS H BURKE P, COTE W, HILL W, HOFFMAN C, KAANTA C, KOBURGER C, LANGE W, LEACH M, LUCE S INTEGRATION OF CHEMICAL MECHANICAL POLISHING INTO CMOS INTEGRATED-CIRCUIT MANUFACTURING [Journal]. - San Diego : ELSEVIER SCIENCE SA LAUSANNE, 1992. - 1-2 : Vol. 220. - ISSN 0040-6090 .

Lee K. Lee Y., Kang S. Method and Apparatus for Chemical Mechanical Polishing [Patent] : 6315641. - USA, 12 31, 2001.

Li Y. Microelectronic applications of chemical mechanical planarization [Book]. - [s.l.] : Wiley-Interscience, 2007. - ISBN 0471719196.

Lin M Y., Lindsay, H.M., Weitz, D.A., Klein, R., Ball R.C., Meakin, P. , Universal diffusion-limited colloid aggregation [Journal]. - [s.l.] : Journal of Physics: Condensed Matter, 1990. - Vols. 2:3093-3113..

Lin M Y., Lindsay, H.M., Weitz, D.A., Klein, R., Ball R.C., Meakin, P. Universality of Fractal Aggregates as Probed by Light Scattering [Article] // Proceedings of the Royal Society of London . - , 1989,. - Vols. 423/1864:71-87. .

Luo J., Dornfeld, D. Effects of abrasive size distribution in chemical mechanical planarization: modeling and verification [Journal]. - [s.l.] : IEEE Trans. Semiconductor Manufacturing, 2003. - Vols. 16/3:469 - 476..

Moinpour Mansour Current and future challenges in CMP materials [Book Section] // Microelectronic Applications of Chemical mechanical Planarization / book auth. Li Yuzhuo. - New Jersey : John Wiley & Sons, 2008.

Oliver M R Chemical-mechanical planarization of semiconductor materials [Book]. - Berlin : Springer-Verlag, 2004.

Pant A. Young D., Meyer A., Volodarsky K., Weldon D. Control of Chemical-Mechanical Polishing Rate Across a Substrate Surface [Patent] : 5,800,248. - USA, Sep 1, 1998.

Qu W. K. Wang, M.H. Miller*, Y. Huang, A. Chandra Using vibration-assisted grinding to reduce subsurface damage [Journal]. - [s.l.] : Precision Engineering, 2000. - Vol. 24.

Regh J. Silvey G. Method for Polishing a Silicon Surface [Patent] : 3,615,955. - USA, Oct 26, 1971.

Saka N., Eusner, T. and Chun, J. H. Scratching by pad asperities in chemical-mechanical polishing [Journal]. - [s.l.] : Annals of CIRP, 2010. - Vols. 60, 1, pp. 329-332..

Shendon N. Chemical Mechanical Polishing Apparatus with orbital Polishing [Patent] : 5,899,800. - 1999, May 4, 1999.

Shon-Roy L CMP: Market trends and technology [Article] // Solid State Technology. - 2000. - 6 : Vol. 43.

Somekh S. Chemical Mechanical Polishing with Multiple Polishing Pads [Patent] : 5,897,426. - USA, Apr 27, 1999.

Steigerwald J. M. S. P. Murarka, R. J. Gutmann and D. J. Duquette Chemical processes in the chemical mechanical polishing of copper [Journal]. - Troy : ELSEVIER SCIENCE SA LAUSANNE, 2000. - 3 : Vol. 41. - ISSN 0254-0584.

Steigerwald J. Murarka S., Gutmann R. Chemical mechanical planarization of microelectronic materials [Book]. - [s.l.] : Wiley-VCH, 1997. - ISBN 0471138274.

Torbert W. Struven K., Lorenzini R., Bonaora A. Floating Subcarriers for Wafer Polishing Apparatus [Patent] : 4,918,870. - USA, APr 24, 1990.

Tucker Thomas Equipment Used in CMP Processes [Book Section] // Chemical Mechanical Planarization of Semiconductor Materials / book auth. M. Oliver. - Berlin : Springer-Verlag, 2004.

Velden P. van der Chemical mechanical polishing with fixed abrasives using different subpads to optimize wafer uniformity [Journal] // Microelectronic Engineering. - Eindhoven : Elsevier, 2000. - Vol. 50.

Wang C. X., Sherman, P., Chandra, A. Pad Surface Roughness and Slurry Particle Size Distribution Effects on Material Removal Rate in Chemical Mechanical Planarization (CMP) [Article] // Int. J. Manufacturing Technology and Management. - 2005. - Vols. 7(5-6), p 504-529..

Yoshio A. CMP Technology For ULSI Interconnections [Conference]. - San Francisco : SEMICON West, 2000. - ISBN 1892568500.

Zantye P. Kumar A., Sikder A.K. Chemical mechanical planarization for microelectronics applications [Journal]. - [s.l.] : Materials Science and Engineering, 2004. - Vol. 49.

APPENDIX

Table 1 Results Data

Load	Load (N)	Relative Velocity (m/s)	Dwell Time (s)	Material Removal Depth (um)	Pad Type	Slurry	Waviness (um)	Roughness (um)
	4.60	3.32	60.48	4.00	Low Density	1um Alumina	0.143	0.057
	5.60	3.32	60.48	4.75	Low Density	1um Alumina	0.182	0.135
	6.30	3.32	60.48	3.70	Low Density	1um Alumina	0.256	0.205
	7.10	3.32	60.48	8.20	Low Density	1um Alumina	0.153	0.119
	11.50	3.32	60.48	8.80	Low Density	1um Alumina	0.235	0.188
	15.80	3.32	60.48	13.00	Low Density	1um Alumina	0.351	0.248
	16.50	3.32	60.48	12.25	Low Density	1um Alumina	0.175	0.144
	20.10	3.32	60.48	15.00	Low Density	1um Alumina	0.178	0.142
Dwell Time	Load (N)	Relative Velocity (m/s)	Dwell Time (s)	Material Removal Depth (um)	Pad Type	Slurry	Waviness (um)	Roughness (um)
	22.20	3.32	14.11	4.30	Low Density	1um Alumina	0.177	0.14
	28.50	3.32	14.11	4.50	Low Density	1um Alumina	0.283	0.279
	21.80	3.32	21.17	7.25	Low Density	1um Alumina	0.188	0.152
	27.40	3.32	21.17	7.30	Low Density	1um Alumina	0.355	0.325
	22.30	3.32	42.33	11.00	Low Density	1um Alumina	0.191	0.145
	18.50	3.32	42.33	15.50	Low Density	1um Alumina	0.366	0.24
	20.10	3.32	60.48	15.00	Low Density	1um Alumina	0.178	0.142
	22.70	3.32	127.00	32.00	Low Density	1um Alumina	0.221	0.161
	21.30	3.32	127.00	42.00	Low Density	1um Alumina	0.328	0.131
05 Grit	Load (N)	Relative Velocity (m/s)	Dwell Time (s)	Material Removal Depth (um)	Pad Type	Slurry	Waviness (um)	Roughness (um)
	13.60	3.32	60.48	1.85	Low Density	.05 Silica	0.106	0.051
	17.70	3.32	60.48	1.90	Low Density	.05 Silica	0.052	0.031
	17.80	3.32	60.48	1.36	Low Density	.05 Silica	0.078	0.031
	22.30	3.32	60.48	1.55	Low Density	.05 Silica	0.083	0.033
Medium Density	Load (N)	Relative Velocity (m/s)	Dwell Time (s)	Material Removal Depth (um)	Pad Density	Slurry	Waviness (um)	Roughness (um)
	11.70	3.32	60.48	15.30	Medium Density	1um Alumina	0.269	0.192
	12.90	3.32	60.48	24.60	Medium Density	1um Alumina	0.564	0.434
	14.20	3.32	60.48	13.80	Medium Density	1um Alumina	0.366	0.298
	16.60	3.32	60.48	27.90	Medium Density	1um Alumina	0.45	0.22
	20.60	3.32	60.48	29.30	Medium Density	1um Alumina	0.349	0.081
	22.40	3.32	60.48	39.10	Medium Density	1um Alumina	0.465	0.222
	22.60	3.32	60.48	42.20	Medium Density	1um Alumina	0.356	0.093
	26.90	3.32	60.48	44.10	Medium Density	1um Alumina	0.499	0.132
Velocity	Load (N)	Relative Velocity (m/s)	Dwell Time (s)	Material Removal Depth (um)	Pad Type	Slurry	Waviness (um)	Roughness (um)
	19.10	1.33	60.48	12.00	Low Density	1um Alumina	0.218	0.138
	19.20	1.99	60.48	17.00	Low Density	1um Alumina	0.237	0.111
	20.90	2.66	60.48	11.00	Low Density	1um Alumina	0.146	0.094
	20.10	3.32	60.48	15.00	Low Density	1um Alumina	0.178	0.142
	19.90	3.99	60.48	16.00	Low Density	1um Alumina	0.259	0.119
Worn Pad	Load (N)	Relative Velocity (m/s)	Dwell Time (s)	Material Removal Depth (um)	Pad Type	Slurry	Waviness (um)	Roughness (um)
725s								
	15.0	3.32	60.48	14.80	Worn - Low Density	1um Alumina	0.333	0.271
	17.6	3.32	60.48	18.70	Worn - Low Density	1um Alumina	0.165	0.104
	20.2	3.32	60.48	17.80	Worn - Low Density	1um Alumina	0.303	0.233
	21.2	3.32	60.48	22.00	Worn - Low Density	1um Alumina	0.197	0.139
6" Wafer	Load (N)	Relative Velocity (m/s)	Dwell Time (s)	Material Removal Depth (um)	Pad Type	Slurry	Waviness (um)	Roughness (um)
	14.00	3.32	7 to 14	N/A	Medium Density	1um Alumina	N/A	0.0696

MATLAB CODE - Load Cell Data Analyzer

```
clc;
clear;
close all;

data = load('2011_03_30__L17_f021_G1_M-1.txt');

time = data(:,1);
dur = time(end)-time(1);    %test duration (s)
L = length(time);           %number of Cycles
samptime = dur/L;           %Sampling Cycle Time (s)
freq = round(1/samptime);   %Sampling Cycle frequency
fwind = 1;                  %front, back, and size of cycle window to analyze
bwind = L;
%fwind = round(freq*(157-time(1)));
%bwind = round(freq*(182-time(1)));
swind = bwind-fwind+1;
tim = time(fwind:bwind);
lateral = data(fwind:bwind,2);
vertical = data(fwind:bwind,3);
volt1 = data(fwind:bwind,4 : 6);
volt2 = data(fwind:bwind,7 : 9);
unit = 49;              %use to convert volts to either lbs(1:11) or kg(1:5)
offs = unit*min(min(min(volt1,volt2)));  %amount force values are offset by

forc1 = unit*volt1(:,2)-offs;              %a single unfiltered sample from each cycle (lbs)
forc2 = unit*volt2(:,2)-offs;
aveforc1 = unit*mean(volt1,2)-offs;    %all samples within a cycle averaged together (lbs)
aveforc2 = unit*mean(volt2,2)-offs;

%N = round(freq/2);
N = 100;
a=1;
b = 1/N*ones(N,1);
filtforc1 = filter(b,a,aveforc1);       %running average of N cycles
filtforc2 = filter(b,a,aveforc2);
filtforc3 = filter(b,a,forc1);
filtforc4 = filter(b,a,forc2);

%%

NFFT = 2^nextpow2(swind); % Next power of 2 from length of y
f = freq/2*linspace(0,1,NFFT/2+1);
fftforc1 = fft(forc1,NFFT)/swind;
fftforc2 = fft(forc2,NFFT)/swind;

figure(6);
% Plot single-sided amplitude spectrum.
plot(f,2*abs(fftforc2(1:NFFT/2+1)))
title('Single-Sided Amplitude Spectrum of Force 2 y(t)')
xlabel('Frequency (Hz)')
```

```
ylabel('|Y(f)|')
axis([0 f(end) 0 1])

figure(5);
% Plot single-sided amplitude spectrum.
plot(f,2*abs(fftforc1(1:NFFT/2+1)))
title('Single-Sided Amplitude Spectrum of Force 1 y(t)')
xlabel('Frequency (Hz)')
ylabel('|Y(f)|')
axis([0 f(end) 0 1])

%%

figure(4);
plot(tim,aveforc1-aveforc2,'b');
hold on
plot(tim,filtforc1-filtforc2, 'r');
title('Load Cell Force Differential (Data-b & RunAve-r)');
xlabel('Time (s)')
ylabel('Load (N)')

%%

figure(3);
plotyy(tim,filtforc1,tim,vertical);
hold on
plot(tim,filtforc2, 'r');
title('Running Average (1b&2r) and Vertical Actuator (g)');
axis auto
%axis([0 tim(end) 0 1.25*max(max(max(filtforc3,filtforc4)))])
xlabel('Time (s)')
ylabel('Load (N)')

figure(2);
plot(tim,aveforc1,'b');
hold on
plot(tim,aveforc2,'r');
hold on
title('Force Data (1b & 2r)');
xlabel('Time (s)')
ylabel('Load (N)')

figure(1);
plot(tim,aveforc1,'b');
hold on
plot(tim,aveforc2,'r');
hold on
plot(tim,filtforc1, 'y');
hold on
plot(tim,filtforc2, 'g');
title('Force Data (1b & 2r) and Running Average (1y&2g)');
xlabel('Time (s)')
ylabel('Load (N)')
```

```
%%

a = 0;
%a = round(25*freq);
b = 2.2;
c = 30;
load1 = mean(aveforc1(round(L/b)-c*freq:round(L/b)+c*freq))-mean(aveforc1(end-c*freq-a:end-a))
load2 = mean(aveforc2(round(L/b)-c*freq:round(L/b)+c*freq))-mean(aveforc2(end-c*freq-a:end-a))

x = 30;
range1 = max(filtforc1(round(L/b)-x*freq:round(L/b)+x*freq))-min(filtforc1(round(L/b)-
x*freq:round(L/b)+x*freq))
range2 = max(filtforc2(round(L/b)-x*freq:round(L/b)+x*freq))-min(filtforc2(round(L/b)-
x*freq:round(L/b)+x*freq))

y = 30;
std_filtforc1 = std(filtforc1(round(L/b)-y*freq:round(L/b)+y*freq))
std_filtforc2 = std(filtforc2(round(L/b)-y*freq:round(L/b)+y*freq))

std_aveforc1 = std(aveforc1(round(L/b)-y*freq:round(L/b)+y*freq))
std_aveforc2 = std(aveforc2(round(L/b)-y*freq:round(L/b)+y*freq))

median = L/(b*freq)
```

ACKNOWLEDGEMENTS

I would like to take this opportunity thank my major professor Dr. Chandra. I am genuinely appreciative of the opportunity to prove myself as an undergraduate and the encouragement to apply to graduate school. I'd like to thank both Dr. Chandra and Dr. Bastawros for their support and guidance through graduate school. My development as an engineer could not have turned out as well as it has without the patience and sage advice they have provided me in my studies.

I would like to thank Dr. Kim for serving on my committee. I would also like to thank Dr. Karra for the mentoring and guidance he provided at the beginning of my graduate studies at Iowa State University.